

**POLITECNICO DI TORINO**

Corso di Laurea Magistrale in Ingegneria Aerospaziale



Tesi di Laurea Magistrale

**OPTIMAL POWER PARTITIONING BETWEEN  
ELECTRIC THRUSTERS FOR SPACE  
TRAJECTORIES**

*Relatore*

Prof. Lorenzo Casalino

*Candidato*  
Giacomo Alò

Aprile 2020

OPTIMAL POWER PARTITIONING BETWEEN  
ELECTRIC THRUSTERS FOR SPACE  
TRAJECTORIES

Giacomo Alò

Anno Accademico 2018-2019



## **Abstract**

Subject of this thesis is the design of a space robotic mission to the asteroid 433 Eros. The mission aims to grab a boulder from its surface and transport it inside the Earth's influence sphere. This work was inspired by NASA's Asteroid Redirect Mission (ARM), which was cancelled in 2017 due to lack of funding, and whose purpose was to transfer a boulder from the surface of a Near-Earth asteroid (NEA) to a stable lunar orbit, where it could be further analyzed both by robotic probes and by a future manned mission. The propulsion system used for the theorized mission consists of three autonomous ion thrusters fully adjustable in magnitude and direction of thrust. Furthermore, during the return flight an Earth gravity assist is used to increase the mass of boulder that the spacecraft can transport towards Earth. The following chapters will analyze the interplanetary phase of this mission and, specifically, an optimization of the interplanetary trajectories will be carried out. An indirect method will be used to formulate the possible optimal combinations of the powers of the three engines, where, in the context of electric propulsion, the thrust and flow rate of the propellant are linked by a cubic dependence on the input power. The trends of the power, the thrust and the specific impulse of the optimal case will be compared with the case in which the power is distributed in such a way as to have a thruster always at maximum power and with the case in which the power is distributed uniformly. Finally, the results obtained from the asteroid Eros (Near-Earth asteroid) will be compared with those obtained from the sub-kilometer asteroid "2008ev5".

# Contents

<b>List of Figures</b>	3
<b>List of Tables</b>	5
<b>1 Introduction</b>	6
<b>2 Spaceflight Syllabus</b>	8
2.1 Two-Body Problem . . . . .	8
2.2 Orbital Elements . . . . .	8
<b>3 Space Propulsion</b>	12
3.1 Generalities of Space Propulsion . . . . .	12
3.2 Propulsion System Performance . . . . .	15
3.2.1 Total Impulse . . . . .	15
3.2.2 Specific Impulse . . . . .	15
3.3 Rocket Equation . . . . .	16
3.4 Velocity Losses . . . . .	18
<b>4 Electric Propulsion</b>	20
4.1 Solar Electric Propulsion (SEP) . . . . .	24
4.1.1 Solar Arrays . . . . .	25
4.1.2 Hall Thrusters . . . . .	27
4.1.3 Key Facts . . . . .	28
<b>5 Indirect Optimization of Low-Thrust Trajectory</b>	29
5.1 Optimal Control Theory . . . . .	29
5.2 Boundary Value Problem (BVP) . . . . .	34
<b>6 Statement of the Problem</b>	40
<b>7 Optimization of the segments</b>	43
7.1 Optimal Case . . . . .	46
7.1.1 Three Thrusters On . . . . .	46

7.1.2	Two Thrusters On . . . . .	48
7.1.3	One Thruster On . . . . .	48
7.1.4	Operating Modes . . . . .	49
7.2	Thrustmax Case . . . . .	49
7.3	Thrustuni Case . . . . .	50
7.3.1	Maximum number of thrusters . . . . .	50
7.3.2	Minimum number of thrusters . . . . .	51
<b>8</b>	<b>433 Eros Asteroid</b>	<b>52</b>
8.1	Eros Results . . . . .	52
8.1.1	Outbound Flight . . . . .	53
8.1.2	Inbound Flight . . . . .	66
<b>9</b>	<b>2008EV5 Asteroid</b>	<b>78</b>
9.1	2008EV5 Results . . . . .	78
9.1.1	Outbound Flight . . . . .	78
9.1.2	Inbound Flight . . . . .	86
<b>10</b>	<b>Conclusions</b>	<b>93</b>
<b>A</b>	<b>Spherical Coordinate System</b>	<b>94</b>
<b>B</b>	<b>The Patched-Conic Approximation</b>	<b>99</b>
<b>C</b>	<b>Vector and Matrix Calculation</b>	<b>100</b>
	<b>Bibliography</b>	<b>102</b>

# List of Figures

2.1	Keplerian elements . . . . .	10
3.1	Isolated system . . . . .	12
3.2	Spacecraft + propellant system . . . . .	13
3.3	Geometry . . . . .	14
3.4	Typical Characteristic Velocities . . . . .	17
3.5	Forces vectors . . . . .	18
4.1	Chemical propulsion . . . . .	20
4.2	Typical values of specific impulse of chemical propulsion . . . . .	21
4.3	Electrothermal propulsion . . . . .	22
4.4	Comparison between specific impulse and thrust for both chemical and electric propulsion . . . . .	24
4.5	Two solar arrays designs . . . . .	25
4.6	MegaFlex Solar Array on SEP vehicle . . . . .	26
4.7	Mega-ROSA Solar Array on SEP vehicle . . . . .	27
4.8	Blue ion beam of a Hall Thruster . . . . .	28
6.1	Thruster performance as a function of input power . . . . .	42
7.1	Generic behavior of function $f$ . . . . .	44
8.1	Number of active thrusters during the mission . . . . .	54
8.2	Power partitioning between thrusters . . . . .	56
8.3	Behavior of the thrust during the mission . . . . .	58
8.4	Comparison of the thrust for the different cases . . . . .	59
8.5	Comparison of the effective exhaust velocity for the different cases . . . . .	60
8.6	Comparison of the specific impulse for the different cases . . . . .	60
8.7	Comparison between the thrust and the specific impulse during the mission for the different cases . . . . .	61
8.8	2D Trajectory . . . . .	63
8.9	Thrust vectors along trajectory . . . . .	64

8.10	How inclination of the trajectory and angle $\phi$ vary during the mission for <i>optimal</i> case . . . . .	65
8.11	3D Trajectory . . . . .	65
8.12	Number of active thrusters during the mission . . . . .	67
8.13	Power partitioning between thrusters . . . . .	68
8.14	Behavior of the thrust during the mission . . . . .	70
8.15	Comparison of the thrust for the different cases . . . . .	71
8.16	Comparison of the effective exhaust velocity for the different cases . . . . .	71
8.17	Comparison of the specific impulse for the different cases . . . . .	72
8.18	Comparison between the thrust and the specific impulse during the mission for the different cases . . . . .	73
8.19	2D Trajectory . . . . .	75
8.20	Thrust vectors along trajectory . . . . .	76
8.21	How inclination of the trajectory and angle $\phi$ vary during the mission for <i>optimal</i> case . . . . .	77
8.22	3D Trajectory . . . . .	77
9.1	Number of active thrusters during the mission . . . . .	79
9.2	Power partitioning between thrusters . . . . .	80
9.3	Comparison of the thrust for the different cases . . . . .	81
9.4	Comparison of the specific impulse for the different cases . . . . .	81
9.5	Comparison between the thrust and the specific impulse during the mission for the different cases . . . . .	82
9.6	2D Trajectory . . . . .	83
9.7	Thrust vectors along trajectory . . . . .	84
9.8	How inclination of the trajectory and angle $\phi$ vary during the mission for <i>optimal</i> case . . . . .	85
9.9	3D Trajectory . . . . .	85
9.10	Number of active thrusters during the mission . . . . .	86
9.11	Power partitioning between thrusters . . . . .	87
9.12	Comparison of the thrust for the different cases . . . . .	88
9.13	Comparison of the specific impulse for the different cases . . . . .	88
9.14	Comparison between the thrust and the specific impulse during the mission for the different cases . . . . .	89
9.15	2D Trajectory . . . . .	91
9.16	How inclination of the trajectory and angle $\phi$ vary during the mission for <i>optimal</i> case . . . . .	92
9.17	3D Trajectory . . . . .	92
A.1	Spherical coordinates . . . . .	98

# List of Tables

7.1	Operating Modes (0, 1 and 2 thrusters on) . . . . .	49
7.2	Operating Modes (3 thrusters on) . . . . .	49
7.3	Operating Modes for <i>Thrustmax</i> Case (1, 2 and 3 thrusters on) . . . . .	50
7.4	Operating Modes for <i>Thrustuni</i> Case with maximum number of thrusters (1, 2 and 3 thrusters on) . . . . .	51
7.5	Operating Modes for <i>Thrustuni</i> Case with minimum number of thrusters (1, 2 and 3 thrusters on) . . . . .	51
8.1	Orbital elements of 433 Eros at the epoch 27 April 2019 (JD 2458600.5) [2] . . . . .	52
8.2	Results of indirect optimization . . . . .	74
9.1	Orbital elements of 2008 EV5 at the epoch 27 April 2019 (JD 2458600.5) [2] . . . . .	78
9.2	Results of indirect optimization . . . . .	90

# Chapter 1

## Introduction

Electric propulsion (EP) can boost the performance of interplanetary missions due to the low propellant consumption in comparison to chemical propulsion.

The optimization of an interplanetary trajectory is essential to satisfy all the scientific and technical requirements of a space mission. Space trajectories are typically controlled by the thrust vector. Optimization consists of finding the optimal control law for thrust magnitude and direction to maximize a specified performance index, while fulfilling the boundary conditions that characterize the mission. In the considered case, the optimization problem consists of finding the optimal power partitioning among the thrusters, the corresponding thrust magnitude and the optimal thrust direction. In preliminary analysis, the patched-conic approximation is adopted and two-body problem equations are commonly used to describe the interplanetary flight; this assumption is maintained here. Cubic relations are assumed for thrust and propellant flow rate as a function of input power. Each engine can either be turned off or operate between minimum and maximum input power limits. In addition, the total power cannot exceed the available power, which varies inversely with the distance from the Sun.

Numerical methods for trajectory optimization can be in general classified into three main groups: indirect methods, direct methods, and evolutionary algorithms. This thesis is focused in particular on the first group.

Indirect methods are based on the theory of optimal control and solve the optimization problem by defining and solving a boundary value problem. The theory of optimal control provides differential equations for the adjoint variables and boundary conditions for optimality. The optimal controls must maximize the Hamiltonian at any given point along the trajectory, in agreement with Pontryagin's maximum principle. The Hamiltonian is also a cubic function of the engine input powers and a detailed function analysis is presented to find the partitioning combinations that correspond to local maxima. It is then easy to compare them and select, at any trajectory point, the global optimum.

The asteroid (433) Eros is chosen as target in order to provide a wide variation in power available for thrusting, as opposed to primary ARM asteroids with more Earth-like orbits.

An Earth gravity assist in the return leg is used to improve performance. In order to simplify the optimization process, a different analysis is carried out separately for the outbound and inbound flights: for the outbound flight the aim is to minimize the propellant consumption with a fixed initial mass of propellant and dry mass, while, for the inbound flight, the performance index to be maximized is the initial mass (i.e. the total mass of the spacecraft departing from the asteroid, so the mass of grabbed boulder), using the real amount of propellant left from the outbound flight.

# Chapter 2

## Spaceflight Syllabus

### 2.1 Two-Body Problem

In classical mechanics, the two-body problem is to predict the motion of two massive objects which are abstractly viewed as point particles. The problem assumes that the two objects interact only with one another; the only force affecting each object arises from the other one, and all other objects are ignored.

The most prominent case of the classical two-body problem is the gravitational case, arising in astronomy for predicting the orbits (or escapes from orbit) of objects such as satellites, planets, and stars.

Two-body problem equations describe motion of point mass  $m$  with respect to the main body:

$$\frac{d\mathbf{r}}{dt} = \mathbf{V} \quad (2.1)$$

$$\frac{d\mathbf{V}}{dt} = \mathbf{g} + \frac{\mathbf{T}}{m} + \frac{\mathbf{D}}{m} + \frac{\mathbf{L}}{m} \quad (2.2)$$

$$\frac{dm}{dt} = -\frac{T}{c} \quad (2.3)$$

where  $\mathbf{r}$  is the position vector,  $\mathbf{V}$  the velocity vector,  $\mathbf{g} = -\mu\mathbf{r}/r^3$  the gravity acceleration,  $\mathbf{T}$  the thrust,  $\mathbf{D}$  the drag,  $\mathbf{L}$  the lift and  $c$  the effective exhaust velocity.

### 2.2 Orbital Elements

In physics, an orbit is the gravitationally curved trajectory of an object, such as the trajectory of a planet around a star or a natural satellite around a planet. Normally, orbit refers to a regularly repeating trajectory, although it may also refer to a non-repeating

trajectory. To a close approximation, planets and satellites follow elliptic orbits, with the central mass being orbited at a focal point of the ellipse, as described by Kepler's laws of planetary motion. In the absence of other forces than gravity, the mass  $m$  follows a conic trajectory which depends on the initial conditions.

The conic trajectory of body is given by:

$$r = \frac{p}{1 + e \cos \nu} \quad (2.4)$$

where  $p$  is a geometrical constant of the conic called the "parameter" or "semilatus rectum",  $e$  is the eccentricity,  $\nu$  is the "true anomaly" (angle between  $r$  and the point on the conic nearest the focus).

According to the eccentricity value, the geometric shape of the trajectory changes: it is possible to have a circle if  $e = 0$ , an ellipse if  $0 < e < 1$ , a parabola if  $e = 1$ , an hyperbola if  $e > 1$ .

There are two *constants of motion*: energy  $\epsilon = V^2/2 - \mu/r$ ; angular momentum  $\mathbf{h} = \mathbf{r} \times \mathbf{V}$  (the trajectory lies on a plane perpendicular to  $\mathbf{h}$ ).

The trajectory shape and orientation, and the position of the spacecraft at a given time are describes by six *Keplerian elements*.

Two elements define the shape and size of the ellipse:

- Semimajor axis  $a = -\mu/(2\epsilon)$ : the sum of the periapsis and apoapsis distances divided by two. For classic two-body orbits, the semimajor axis is the distance between the centers of the bodies, not the distance of the bodies from the center of mass. Use  $p = h^2/\mu$  in case of a parabola, when  $a$  is not defined;
- Eccentricity  $e = \sqrt{1 + 2\epsilon(h/\mu)^2}$ : shape of the ellipse, describing how much it is elongated compared to a circle (not marked in diagram). Also, the eccentricity vector  $\mathbf{e} = [(V^2 - \mu/r)\mathbf{r} - (\mathbf{r} \cdot \mathbf{V})\mathbf{V}]/\mu$  can be defined.

Two elements define the orientation of the orbital plane in which the ellipse is embedded:

- Inclination (angle between the orbit plane and the reference plane):  $i = \cos^{-1}(h_k/h)$  ( $h_k$  is the component along the axis perpendicular to the reference plane). This angle is defined between  $0^\circ$  and  $180^\circ$ ;
- Right ascension of ascending node (angle between line of nodes, pointing towards ascending nodes, and reference direction  $\mathbf{I}$ ):  $\Omega = \cos^{-1}(n_I/n)$  (line of nodes vector  $\mathbf{n} = \mathbf{K} \times \mathbf{h}$ ,  $n_I$  is the component along  $\mathbf{I}$ ). Change sign when  $n_J < 0$ .

The remaining two elements define the orientation of the conic in the orbital plane:

- Argument of periapsis (angle between line of nodes and eccentricity vector):  $\omega = \cos^{-1}[\mathbf{n} \cdot \mathbf{e}/(en)]$ . Change sign when  $e_K < 0$ ;

- True anomaly (angle between eccentricity and position vectors at a specific time):  
 $\nu = \cos^{-1}[\mathbf{e} \cdot \mathbf{r}/(er)]$ . Change sign when  $\mathbf{r} \cdot \mathbf{V} < 0$ .

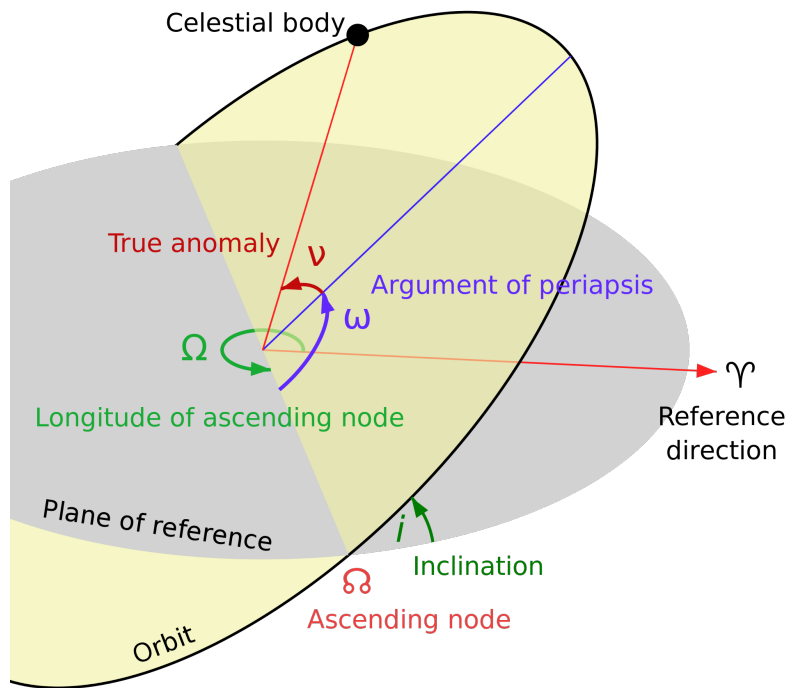


Figure 2.1: Keplerian elements

The intersection of the orbital plane with the  $xy$ -plane is called *line of nodes*. This line intersects the orbit at two points. At the *ascending node* the  $z$ -coordinate of body changes from negative to positive. The other intersection constitutes the *descending node*.

Apart from these classical orbital elements, other orbital elements are sometimes used as they may be more appropriate for certain problems, or because some classical elements become ill-determined when  $e$  and/or  $i$  approach zero. In the case  $e = 0$ , the periapsis  $\omega$  is not determined, and the position in the orbit should be measured from the ascending node. In the case  $i = 0$ , the ascending node  $\Omega$  is not determined. For this, the *Equinoctial elements* are introduced:

$$p = a(1 - e^2) \tag{2.5}$$

$$f = e \cos(\omega + \Omega) \tag{2.6}$$

$$g = e \sin(\omega + \Omega) \tag{2.7}$$

$$h = \tan(i/2) \cos \Omega \tag{2.8}$$

$$k = \tan(i/2) \sin \Omega \tag{2.9}$$

$$L = \Omega + \omega + \nu \tag{2.10}$$

where  $p$  is the semiparamiter and  $L$  is the true longitude.

Relationship between classical and modified equinoctial orbital elements:

- Semimajor axis:  $a = p/(1 - f^2 - g^2)$
- Orbital eccentricity:  $e = \sqrt{f^2 + g^2}$
- Orbital inclination:  $i = 2 \tan^{-1} \left( \sqrt{h^2 + k^2} \right)$
- Argument of periapsis:  $\omega = \tan^{-1} (g/f) - \tan^{-1} (k/h)$
- Right ascension of the ascending node:  $\Omega = \tan^{-1} (k/h)$
- True anomaly:  $\nu = L - (\Omega + \omega)$

# Chapter 3

## Space Propulsion

### 3.1 Generalities of Space Propulsion

Compared to atmospheric propulsion, in space propulsion there is not something to exchange momentum to obtain thrust. For this there is a need to bring propellant on board and the aim is to reduce its consumption as much as possible. Two types of propulsion can be defined:

- Primary propulsion: it is the type of propulsion that allows to change orbit;
- Auxiliary propulsion: this is the type of propulsion that allows to stay in a specific orbit, intervening against any external disturbances.

Consider an isolated system, which represents for example a rocket, with a certain mass  $m$  and a speed  $V$ :

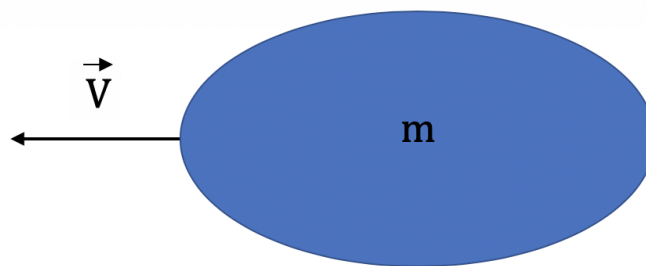


Figure 3.1: Isolated system

After a time interval  $dt$ , suppose that a mass of propellant  $dm_p$  is hurled along a certain direction with a speed  $c - v$ :

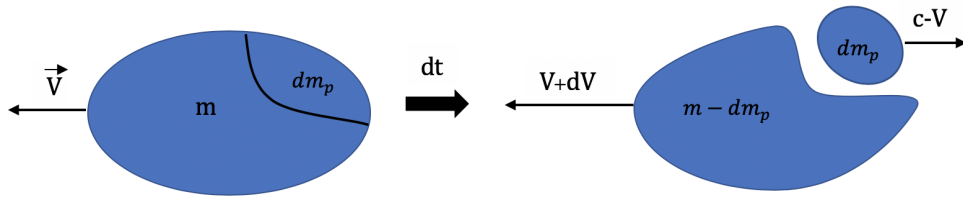


Figure 3.2: Spacecraft + propellant system

where  $c$  is the exhaust velocity with respect to the system.

Looking at the "spacecraft + propellant" system, this is an isolated system, so the total momentum at time  $t$  must be equal to the total momentum at time  $t + dt$ :

$$mV = (m - dm_p)(V + dV) - dm_p(c - V) \quad (3.1)$$

Simplifying, neglecting the higher order infinitesimals, we obtain:

$$mdV = dm_p c \quad (3.2)$$

$$dV = \frac{dm_p}{m} c \quad (3.3)$$

The peculiarity of the space propulsion is that the propellant is consumed in a continuous way, so we pass from the discrete system to the continuous system:

$$dV = \frac{dV}{dt} dt \quad (3.4)$$

$$dm_p = \frac{dm_p}{dt} dt = \dot{m}_p dt \quad (3.5)$$

where  $\dot{m}_p$  is the propellant mass flow.

Taking the equation (3.2) and dividing it by  $dt$ , for a continuous system we have:

$$m \frac{dV}{dt} = \dot{m}_p c = T \quad (3.6)$$

where  $T$  is the thrust.

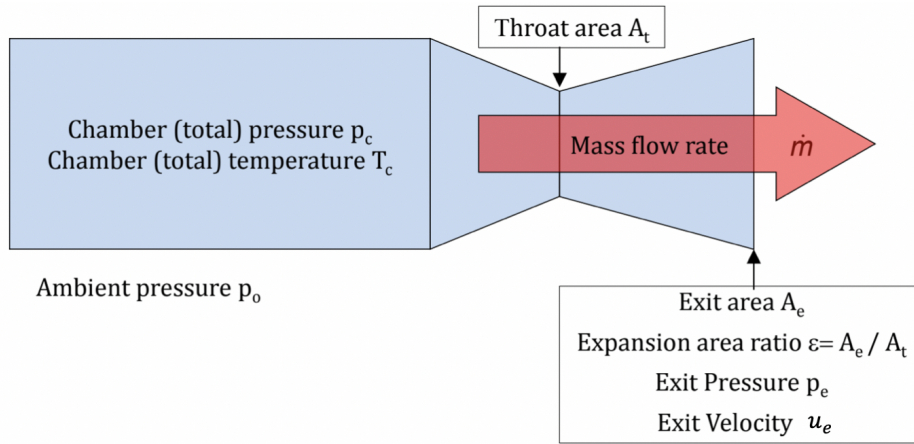


Figure 3.3: Geometry

By indicating with  $u_e$  the gas velocity at the outlet section, a further formula for thrust is obtained:

$$T = \dot{m}_p u_e + A_e (p_e - p_0) \quad (3.7)$$

But in the space  $p_0 = 0$ , so:

$$T = \dot{m}_p u_e + A_e p_e \quad (3.8)$$

So to obtain the maximum thrust it would be necessary to have an adapted nozzle ( $p_e = p_0 = 0$ ) but, given the high expansion ratios, it is possible to obtain a  $p_e \simeq 0$ . The *effective exhaust velocity*  $c$  is defined:

$$c = \frac{T}{\dot{m}_p} \implies c \simeq u_e \quad (3.9)$$

The equation that will be used will therefore be the (3.6).

The propellant must be accelerated with respect to the system, so it must be supplied with kinetic energy. This energy that must be supplied to the propellant is called *kinetic power* and is equal to:

$$P_K = \frac{1}{2} \dot{m}_p c^2 \quad (3.10)$$

To have thrust, therefore, you need an energy source, and the various types of propulsion differ from the type of source: to have chemical propulsion, energy derives from a chemical reaction; to obtain electric propulsion, energy is taken from an electric generator or a solar panel; to obtain nuclear propulsion, energy is taken from a nuclear generator.

## 3.2 Propulsion System Performance

### 3.2.1 Total Impulse

The *total impulse* is a measure, not very precise, of the propulsion effect:

$$I_t = \int_0^{t_f} T dt = T \Delta t, \quad T = \text{const.} \quad (3.11)$$

but, from the equation (3.6):

$$T dt = m dV$$

so we obtain:

$$I_t = m_{avg} \Delta V \quad (3.12)$$

where  $m_{avg}$  is the average mass of the mission.

Generally, for auxiliary propulsion, the amount of propellant used is much smaller than the mass of the system, so it can be assumed that the mass remains constant. Therefore:

$$I_t = m \Delta V \quad (3.13)$$

### 3.2.2 Specific Impulse

The expense, expressed in terms of kilos of propellant that I have to store, will be:

$$m_p = \int_0^t \dot{m}_p dt = \dot{m}_p \Delta t, \quad \dot{m}_p = \text{const} \quad (3.14)$$

The *specific impulse* is defined as follows:

$$I_{sp} = \frac{I_t}{\text{propellant weight on Earth}} = \frac{I_t}{m_p g_0} \quad (3.15)$$

where  $g_0$  is the gravity acceleration on Earth surface.

If we consider a fairly small time within which  $T$  and  $\dot{m}_p$  are constant, we obtain:

$$I_{sp} = \frac{T}{\dot{m}_p g_0} = \frac{c}{g_0} \quad [s] \quad (3.16)$$

Fixed the total impulse:

$$m_p \propto \frac{1}{I_{sp}} \quad (3.17)$$

so the bigger the specific impulse and the smaller the quantity of propellant that will serve for the mission.

Note that dimensionally the specific impulse is a time [s]. This is explained by considering a rocket engine on the ground, which to start, at zero instant, has a thrust equal to the weight  $T = mg_0$ . The expelled flow rate is considered constant and equal to  $\dot{m} = m/t_b$ , where  $t_b$  is the operating time (burning). Substituting in the thrust one obtains  $T = \dot{m}t_b g_0$  from which  $t_b = T/(\dot{m}g_0) = I_{sp}$ . The specific impulse therefore coincides with the operating time of this object.

### 3.3 Rocket Equation

Speed variation is evaluated:

$$dV = \frac{T}{m} dt \quad (3.18)$$

$$\Delta V = \int_0^{t_f} dV = \int_0^{t_f} \frac{\dot{m}_p c}{m} dt \quad (3.19)$$

The  $\Delta V$  does not indicate the simple variation of speed, but that which the engine would give in the absence of other forces and with thrust aligned with the speed. By definition of flow rate:

$$\frac{dm}{dt} = -\dot{m}_p \quad (3.20)$$

By replacing and changing the integration variable:

$$\Delta V = \int_{m_0}^{m_f} -\frac{c}{m} dm = c \ln \frac{m_0}{m_f}, \quad c = \text{cost}. \quad (3.21)$$

This equation represents the *Rocket Equation*, and is the most important equation of space propulsion. For each mission it is possible to calculate the minimum  $\Delta V$  that must be achieved if you really want to carry out that mission. Once the mission to be achieved is defined, the specific impulse of the propulsion system is fixed, the ratio between the final mass and the initial mass is obtained:

$$\frac{m_f}{m_0} = e^{-\frac{\Delta V}{c}} \quad (3.22)$$

If you want to have significant final masses, you must have values of  $c$  at least equal to the  $\Delta V$  you want to achieve, or if you can also have larger or much larger values.

Mission	$\Delta V$ , km/s
LEO insertion	10
1 year station keeping	0.5
LEO-GEO (impulsive)	3.5
LEO-GEO (spiral)	6
Earth escape (impulsive)	3.2
Earth escape (spiral)	8
Earth-Mars (impulsive)	5.5
Earth-Mars (spiral)	6
Earth-Jupiter (spiral)	16.7
Earth-Alpha Centauri	30000

Figure 3.4: Typical Characteristic Velocities

### 3.4 Velocity Losses

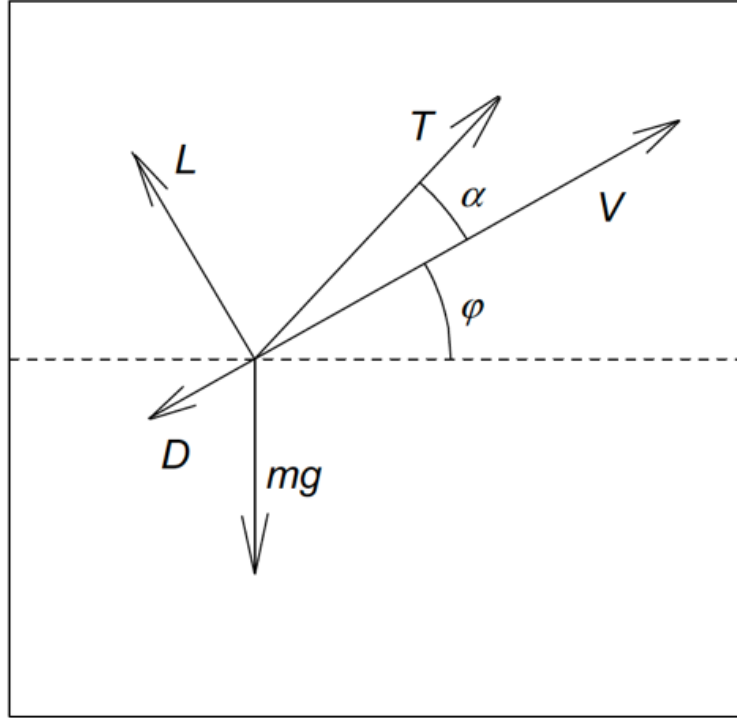


Figure 3.5: Forces vectors

The angle  $\varphi$  is called *Flight Path Angle*.

Assuming we neglect lift, we have the following vector equation:

$$m \frac{dV}{dt} = T + D + mg \quad (3.23)$$

Projecting the various vectors along the direction of  $V$ :

$$\frac{dV}{dt} = \frac{T}{m} \cos \alpha - D - g \sin \varphi = \frac{T}{m} - \frac{T}{m} (1 - \cos \alpha) - \frac{D}{m} - g \sin \varphi \quad (3.24)$$

Integrating between the initial and the final instant:

$$V_f - V_0 = \Delta V - \int_0^{t_f} \frac{T}{m} (1 - \cos \alpha) dt - \int_0^{t_f} \frac{D}{m} dt - \int_0^{t_f} g \sin \varphi dt = \Delta V - \text{losses} \quad (3.25)$$

There are generally three types of losses:

- The term  $\int_0^{t_f} \frac{T}{m}(1 - \cos \alpha) dt$  represents the *misalignment losses*, which are canceled if  $\alpha = 0$ . However, it is generally advisable to introduce a certain  $\alpha$  (therefore losses due to misalignment) if this allows the other two losses to be reduced;
- The term  $\int_0^{t_f} \frac{D}{m} dt$  represents the *aerodynamic losses*, that is losses due to aerodynamic drag, which depend on density and speed;
- The term  $\int_0^{t_f} g \sin \varphi dt$  represents the *gravity losses*, which are the most significant. They are due to the fact that the body moves in a gravitational field, which attracts it, and tends to vary the speed.

Multiplying and dividing by  $V$ :

$$\int_0^{t_f} \frac{g}{V} V \sin \varphi dt \tag{3.26}$$

But the term  $V \sin \varphi$ , from the figure, represents the vertical component of speed, so:

$$\int_{r_0}^{r_f} \frac{g}{V} dr \tag{3.27}$$

It is noted that, at the same altitude, if you increase the speed you can reduce this term. So the optimal strategy is to accelerate as much as possible at the start, gain speed, and increase in altitude. Electric propulsion, which has very little thrusts, fails to do this.

# Chapter 4

## Electric Propulsion

Electric Propulsion (EP) is a class of space propulsion which makes use of electrical power to accelerate a propellant by different possible electrical and/or magnetic fields. The use of electrical power enhances the propulsive performances of the EP thrusters compared with conventional chemical thrusters. Unlike chemical systems, electric propulsion requires very little mass to accelerate a spacecraft. The propellant is ejected up to twenty times faster than from a classical chemical thruster and therefore the overall system is many times more mass efficient.

To fully understand the operation of an electric propulsion system, it is therefore necessary to understand the operation of the chemical propulsion.

There is a combustion chamber where propellant is injected, inside which an exothermic chemical reaction takes place (develops heat).

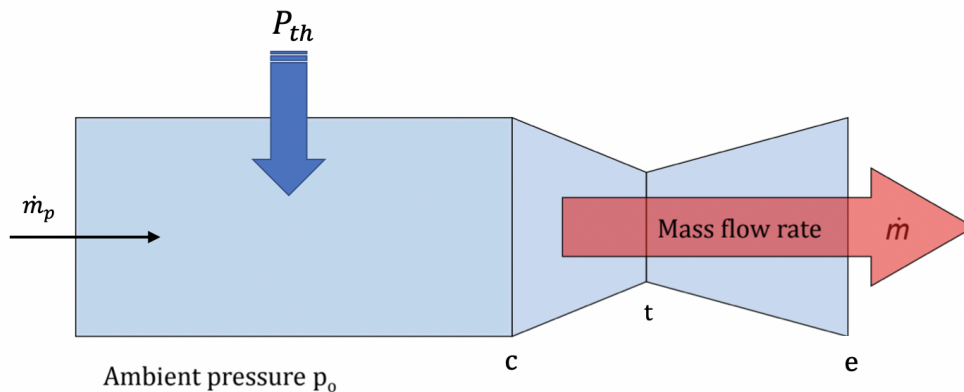


Figure 4.1: Chemical propulsion

Thanks to the thermal power generated, the flow heats up and is expanded into a nozzle.

From the first principle of thermodynamics, in stationary conditions and adopting an Eulerian point of view:

$$P_t = \dot{m}_p E_{ch} = \dot{m}_p \left( h_c + \frac{u_c^2}{2} - h_0 - \frac{u_0^2}{2} \right) \quad (4.1)$$

In the second section:

$$0 = \dot{m}_p \left( h_e + \frac{u_e^2}{2} - h_c - \frac{u_c^2}{2} \right) \quad (4.2)$$

As a first approximation it can be said that the propellant arrives cold in the combustion chamber,  $h_0 = 0$ ; the speed of the gases with which they enter the combustion chamber is very small,  $u_0 = 0$ ; the speed of the gases leaving the combustion chamber is very small (subsonic flow and large area),  $u_c = 0$ .

In space propulsion the expansion ratios are very large, so at the exit there could be a very small enthalpy,  $h_e = 0$ .

From equation (4.2) we thus obtain:

$$c \simeq u_e = \sqrt{2h_c} = \sqrt{2C_p T_c} = \sqrt{2E_{ch}} \quad (4.3)$$

This is why the specific impulse in chemical propulsion is limited, because it depends on the amount of energy that can be extracted from the propellant.

Propellants	State	Specific Impulse, s
LOX/LH2	L	400-450
LOX/RP-1	L	300-330
LOX/CH4	L	280-310
NTO/Hydrazine	L	280-310
NTO/MMH	L	280-310
NC/NG	S	200-250
AP/PBAN/Al	S	260-290

Figure 4.2: Typical values of specific impulse of chemical propulsion

So the chemical propulsion is capable of generating high thrusts, but has limited specific impulses. The other advantage is that only a combustion chamber is needed, but if the  $\Delta V$  becomes large, the consumption will also become higher.

Electric propulsion thrusters for spacecraft may be grouped into three families based on the type of force used to accelerate the ions of the plasma:

- *Electrothermal propulsion*: Electricity is used to heat: the acceleration is still of the thermofluid-dynamic type, that is, the hot fluid under pressure is accelerated in

a nozzle, as occurs in chemical rocket engines.

The electrothermal category groups the devices where electromagnetic fields are used to generate a plasma to increase the temperature of the bulk propellant. The thermal energy imparted to the propellant gas is then converted into kinetic energy by a nozzle of either solid material or magnetic fields. Low molecular weight gases (e.g. hydrogen, helium, ammonia) are preferred propellants for this kind of system. There are two types of electrothermal rocket engines: *resistojet*, in which the fluid is heated by an electrical resistance; *arcjet*, in which an electric arc is triggered inside the fluid (in the throat of the nozzle) which will function as a resistance.

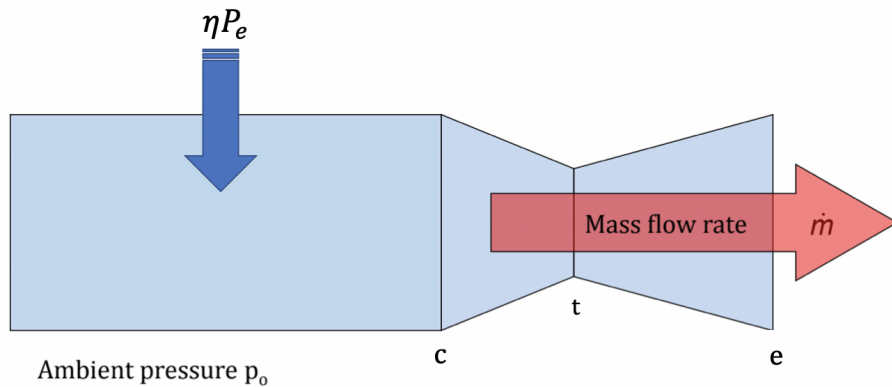


Figure 4.3: Electrothermal propulsion

An efficiency is added because, generally, it is not possible to transform all the electric power obtained from the solar panels (which is then transmitted to the propellant) into a Joule effect, and therefore into heat.

The problem with this type of propulsion is that a hot gas is produced, so there will be a limit on  $u_e$ :

$$u_e = \sqrt{2h_c} = \sqrt{2C_p T_c} = \sqrt{2 \frac{\eta P_e}{\dot{m}_p}} \implies \eta P_e = \dot{m}_p h_c = \dot{m}_p \frac{u_e^2}{2} \quad (4.4)$$

It is therefore noted that the electrothermal propulsion has more or less the same specific impulse values as the chemical propulsion.

- *Electrostatic propulsion*: If the acceleration is caused mainly by the Coulomb force (i.e. application of a static electric field in the direction of the acceleration) the device is considered electrostatic. A "neutralizer" must be present as spacecraft must not be electrically charged;

- *Electromagnetic propulsion*: If ions are accelerated either by the Lorentz force or by the effect of electromagnetic fields where the electric field is not in the direction of the acceleration, the device is considered electromagnetic.

Both in electrostatic and electromagnetic propulsion, a passage is eliminated: the propellant is accelerated directly by the electric power, without passing through a high temperature zone. This means that  $u_e$  can take any value, just increase  $P_e$  or decrease  $\dot{m}_p$ . This is the reason why you can have an unlimited specific impulse in electric propulsion.

$$\eta P_e = \dot{m}_p \frac{c^2}{2} = \frac{Tc}{2} \implies c = \sqrt{2 \frac{\eta P_e}{\dot{m}_p}} = 2 \frac{\eta P_e}{T} \quad (4.5)$$

But increasing the power  $P$  is not a viable way, because it depends on the size of the solar panels from which it is extracted, or in general it depends on the size and weight of the power generator. But also decreasing the  $\dot{m}_p$  is not convenient, in fact the thrust decreases and, for the same  $\Delta V$ , the mission time is longer.

It is assumed that the mass of the generator is proportional to the power:

$$m_{generator} = \alpha P_e \quad (4.6)$$

with  $\alpha$  parameter which depends on the type of generator.

The system can be viewed as:

$$m = m_{useful} + m_{propellant} + m_{generator} \quad (4.7)$$

If it is assumed to have neither propellant nor payload, the mass of the system will be equal to or slightly higher than that of the generator, so:

$$\frac{T}{m} < \frac{T}{m_{generator}} = \frac{T}{\alpha P_e} = \frac{T}{\alpha \frac{Tc}{2\eta}} = \frac{2\eta}{\alpha c} \quad (4.8)$$

This represents the maximum theoretical acceleration that can be had.

System	Specific Impulse, s	Thrust, N
Liquid monopropellant (CP)	200-250	0.01-100
Liquid bipropellant (CP)	300-450	$0.01-10^7$
Solid propellant (CP)	200-300	$1-10^6$
Hybrid propellant (CP)	250-350	$1-10^6$
Resistojets (EP)	200-350	0.2-0.3
Arcjets (EP)	400-1000	0.2-1
Ion thrusters (EP)	2000-5000	$<0.2$
Hall thrusters (EP)	1500-2000	$<2$
Pulsed plasma thrusters (EP)	600-2000	$<0.01$
MPD thrusters (EP)	2000-5000	$<2$

Figure 4.4: Comparison between specific impulse and thrust for both chemical and electric propulsion

In general, with electric propulsion it is possible to consume 10 times less but with much longer mission times.

The different applications which currently make or may make use of Electric Propulsion Systems in the future, are:

- LEO (e.g. Earth Observation, Earth Science, constellations)
- MEO (e.g. Navigation)
- GEO (e.g. Telecommunications)
- Space Transportation (e.g. launcher kick stages, space tugs)
- Space Science, Interplanetary, and Space exploration.

For these different types of missions and requirements, the technology is faced with operational challenges in order to be able to cope with different type of maneuvers, such as: electric transfer from GTO to GEO, station keeping, interorbital transfer, interplanetary cruise, continuous LEO operations (air-drag control), (extreme) fine and/or highly agile attitude control, Long-endurance missions, etc.

## 4.1 Solar Electric Propulsion (SEP)

*Solar electric propulsion* (SEP) refers to the combination of solar cells and electric thrusters to propel a spacecraft through outer space. This technology has been exploited in a variety of spacecraft by the European Space Agency, the Japanese Space

Agency, Indian Space Research Organisation and NASA. SEP has a significantly higher specific impulse than normal chemical rockets, thus requiring less propellant mass to be launched with a spacecraft and it has been evaluated for missions to Mars.

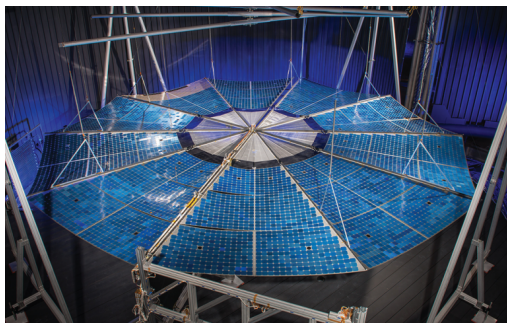
Solar electric propulsion combines solar panels on spacecraft and one or more electric thrusters, used in tandem. [9]

### 4.1.1 Solar Arrays

The SEP project began developing large, flexible, radiation-resistant solar arrays that can be stowed into small, lightweight, more cost-effective packages for launch. After launch, they unfurl to capture enough solar energy to provide the high levels of electrical power needed to enable high-powered solar electric propulsion.

The SEP project worked with ATK Aerospace and Deployable Space Systems Inc. to build and test two solar array designs: one that folds out like a fan (*ATK MegaFlex*) and another that rolls out like a window shade (*DSS ROSA*). Both use lightweight structures and flexible blanket technology and are durable enough to operate for long periods in Earth orbit or passing through the punishing space environment, including the Van Allen radiation belts.

Both arrays achieved all state-of-the-art-related goals including four times the radiation tolerance, 1.7 times the power per mass (kW/kg), four times the stowed volume efficiency, and over twenty times deployed strength. [10]



(a) *MegaFlex* Solar Array



(b) Roll Out Solar Arrays (*ROSA*)

Figure 4.5: Two solar arrays designs

Development of *MegaFlex* technology will leverage the mission-proven Ultraflex solar array design will be scaled up for power levels between 30-50 kW.

*MegaFlex* is an accordion fanfold flexible blanket solar array comprised of interconnected isosceles-triangular shaped lightweight substrates. When stowed, the solar array is configured as a flat-pack to produce a compact launch volume and high system frequency. The circular membrane structure, which contains radial spar elements, becomes tensioned similar to an umbrella, resulting in a highly efficient, strong and stiff structure. [11]

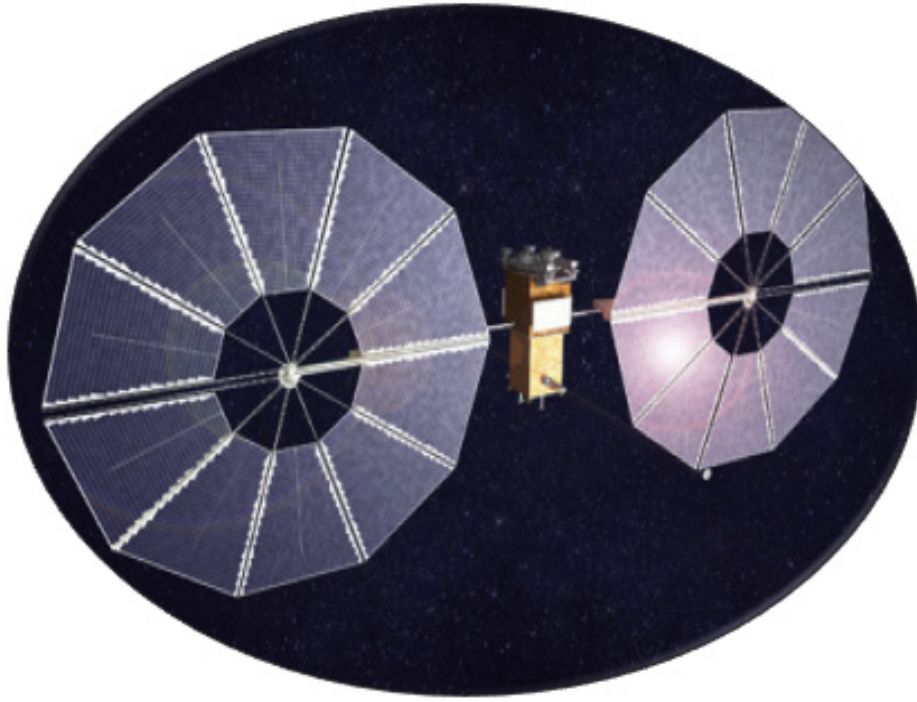


Figure 4.6: MegaFlex Solar Array on SEP vehicle

The *ROSA* technology (Roll-Out Solar Array) is a new/innovative mission-enabling solar array system that will offer maximum performance in key areas and affordability for future space missions. The Mega-ROSA architecture integrates multiple high-voltage elastically deployable ROSA modular "winglet" elements into a deployable backbone structure. It features a flex-blanket solar array configuration conducive to providing high power levels.

The technology is proposed to be lighter and less expensive than current solar array designs, offer compact stowed packaging and strength and stiffness that is conducive to providing power levels – from 60 kW to more than 300 kW and increase the solar array's deployed stiffness and strength, operation reliability, radiation tolerance, scalability, and high voltage operation capability. [11]

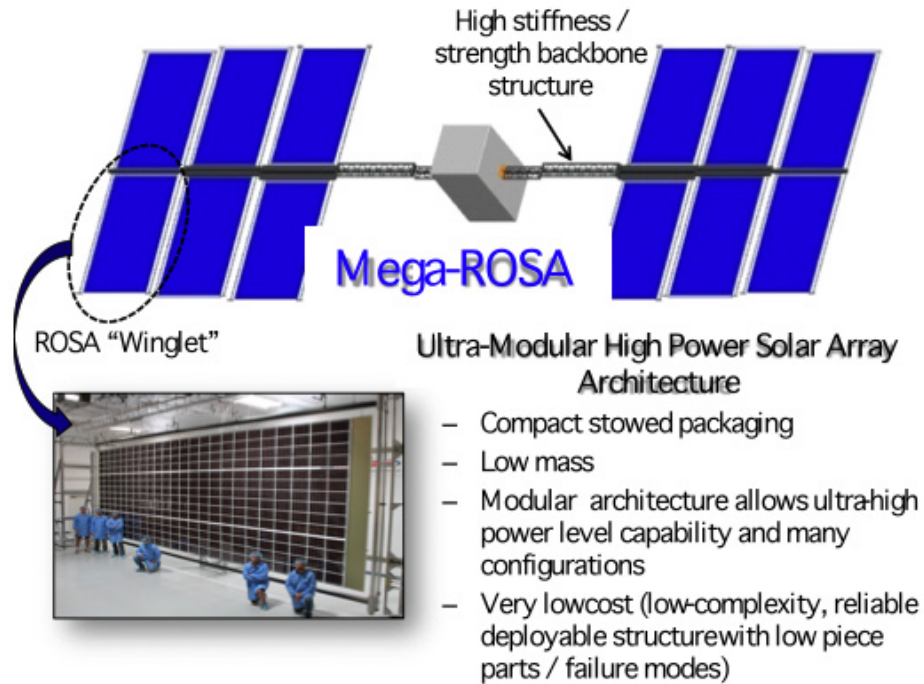


Figure 4.7: Mega-ROSA Solar Array on SEP vehicle

## 4.1.2 Hall Thrusters

The SEP project will use electrostatic Hall thrusters with advanced magnetic shielding instead of a rocket engine with conventional chemical propellant. With SEP, large solar cell arrays convert collected sunlight energy to electrical power. That energy is fed into exceptionally fuel-efficient thrusters that provide gentle but non-stop thrust throughout the mission.

The thruster traps electrons in a magnetic field and uses them to ionize the onboard propellant — in this case, the inert gas *xenon* (it has a low ionization energy and a heavy mass)— efficiently accelerated to generate thrust and then neutralized in the nozzle. Several Hall thrusters can be combined to increase the power of an SEP spacecraft. Such a system can be used to accelerate xenon ions to more than 65,000 mph and will provide enough force over a period of time to move cargo and perform orbital transfers. [10]



Figure 4.8: Blue ion beam of a Hall Thruster

### **4.1.3 Key Facts**

- Solar electric propulsion allows deep-space missions to carry more cargo and use smaller launch vehicles while reducing mission costs.
- The Solar Electric Propulsion project has developed solar arrays that are lighter, stronger, more compact, and less expensive than those currently available.
- Solar electric propulsion provides such high fuel economy that it reduces the amount of propellant required onboard vehicles for deep-space missions by as much as 90 percent.
- Solar electric propulsion will enable affordable human-crewed missions beyond low Earth orbit.

## Chapter 5

# Indirect Optimization of Low-Thrust Trajectory

An optimization problem consists in searching for the control law that maximize or minimize a particular *performance index*. Given the great influence that propellant consumption has on the costs of an orbital transfer (and those of putting the vehicle into orbit), it's essential to minimize the amount of propellant required for the maneuver or, equivalently, maximize the final mass of the vehicle, fixed the initial one. The optimal problem therefore consists in the research of the strategy that allows to realize the orbital transfer maximizing the mass at the end of the maneuver (or other performance indexes, such as the maximization of the payload). The analytical solution of a problem of this type, for an orbital transfer, can be found only for a few simple cases, given the simplifications that must be adopted. For the search of meaningful solutions, the optimal problem must therefore be solved by searching for approximate solutions or with numerical methods. Among the numerical methods, the indirect optimization techniques offer high numeric precision and an important theoretical content, and allow to obtain the optimal solution with a limited number of parameters and limited calculation times. In this chapter it's examined the optimal control theory, based on indirect optimization. For references on the vector and matrix calculation, refer to the Appendix.

### 5.1 Optimal Control Theory

The theory of optimal control, based on the principles of variational calculus, is here described in the form best suited to the optimization of spatial trajectories.

The generic system to which the optimal control theory is applied, is described by a vector of state variables  $\boldsymbol{x}$ . The differential equations that describe the evolution between the initial and final instants (*external contours*) are functions of  $\boldsymbol{x}$ , of the controls vector  $\boldsymbol{u}$  and of the independent variable  $t$  (time), and they have the generic form:

$$\frac{d\mathbf{x}}{dt} = \mathbf{f}(\mathbf{x}, \mathbf{u}, t) \quad (5.1)$$

In the particular case being examined, it is convenient to divide the trajectory into a number  $n$  of subintervals, or arcs, within each of which the variables are continuous. The  $j$ -th interval starts at time  $t_{(j-1)+}$  and ends at time  $t_{j-}$  and the values that the variables assume at its endpoints are  $\mathbf{x}_{(j-1)+}$  and  $\mathbf{x}_{j-}$ , where the signs - and + indicate the values assumed immediately before or after the point considered. In this way it is possible to take into account the possible discontinuities of the variables (for example the speed and the mass are discontinued at the end of an impulsive maneuver) and, at the limit, also of the time (in the case of a planet flyby) which apply to the junction points between the various arcs (*internal contours*). With this formulation it is also possible (and, as will be seen, convenient) to make the second member of the equations (5.1) assume different expressions depending on the sub-interval considered.

Mixed boundary conditions are also imposed, involving the values of the state variables and the independent variable (time) both at the external and internal boundaries. The conditions imposed are generally non-linear and are expressed as:

$$\chi(\mathbf{x}_{(j-1)+}, \mathbf{x}_{j-}, t_{(j-1)+}, t_{j-}) = 0 \quad j = 1, \dots, n \quad (5.2)$$

The optimal problem consists in the search for the extremal values (maximum or minimum relative) of a functional that, in its general form, is of the type:

$$J = \varphi(\mathbf{x}_{(j-1)+}, \mathbf{x}_{j-}, t_{(j-1)+}, t_{j-}) + \sum_j \int_{t_{(j-1)+}}^{t_{j-}} \Phi(\mathbf{x}(t), \mathbf{u}(t), t) dt \quad j = 1, \dots, n \quad (5.3)$$

The functional  $J$  is the sum of two terms: the function  $\varphi$ , dependent on the values assumed by the variables and the time to the contours (internal and external), and the integral, extended to the whole trajectory of the function  $\Phi$ , which depends on time and from the values assumed in each point by variables and controls. Note that with the introduction of appropriate auxiliary variables it is always possible to refer to the case  $\varphi = 0$  (Lagrange formulation) or  $\Phi = 0$  (Mayer formulation, here preferred).

It is useful to rewrite the functional introducing the Lagrange multipliers, constants  $\boldsymbol{\mu}$  associated with boundary conditions, and variables  $\boldsymbol{\lambda}$ , also called added variables, associated with the equations of state:

$$J^* = \varphi + \boldsymbol{\mu}^T \boldsymbol{\chi} + \sum_j \int_{t_{(j-1)+}}^{t_{j-}} \left( \Phi + \boldsymbol{\lambda}^T (\mathbf{f} - \dot{\mathbf{x}}) \right) dt \quad (5.4)$$

where the point  $\dot{\cdot}$  indicates the derivative respect to time.

The functionals  $J$  and  $J^*$  depend on the time  $t$ , on the state variables  $\mathbf{x}$  and on their derivatives  $\dot{\mathbf{x}}$  (in particular on the values that time and variables assume at the extremes of

each arc,  $t_j$  and  $\mathbf{x}_j$ ) and from the controls  $\mathbf{u}$ . Obviously, if boundary conditions and state equations are satisfied, the two functional, and therefore their extremal values, coincide. Integrating by parts to eliminate the dependence on the derivatives of the variables  $\dot{\mathbf{x}}$  we obtain:

$$J^* = \varphi + \boldsymbol{\mu}^T \boldsymbol{\chi} + \sum_j (\boldsymbol{\lambda}_{(j-1)+}^T \mathbf{x}_{(j-1)+} - \boldsymbol{\lambda}_{j-}^T \mathbf{x}_{j-}) + \sum_j \int_{t_{(j-1)+}}^{t_{j-}} (\Phi + \boldsymbol{\lambda}^T \mathbf{f} - \dot{\boldsymbol{\lambda}}^T \mathbf{x}) dt \quad j = 1, \dots, n \quad (5.5)$$

and differentiating we obtain the first variations of the functional  $\delta J^*$  (the square brackets indicate a matrix):

$$\begin{aligned} \delta J^* = & \left( -H_{(j-1)+} + \frac{\partial \varphi}{\partial t_{(j-1)+}} + \boldsymbol{\mu}^T \frac{\partial \boldsymbol{\chi}}{\partial t_{(j-1)+}} \right) \delta t_{(j-1)+} + \\ & + \left( H_{j-} + \frac{\partial \varphi}{\partial t_{j-}} + \boldsymbol{\mu}^T \frac{\partial \boldsymbol{\chi}}{\partial t_{j-}} \right) \delta t_{j-} + \\ & + \left( \boldsymbol{\lambda}_{(j-1)+}^T + \frac{\partial \varphi}{\partial \mathbf{x}_{(j-1)+}} + \boldsymbol{\mu}^T \left[ \frac{\partial \boldsymbol{\chi}}{\partial \mathbf{x}_{(j-1)+}} \right] \right) \delta \mathbf{x}_{(j-1)+} + \\ & + \left( \boldsymbol{\lambda}_{j-}^T + \frac{\partial \varphi}{\partial \mathbf{x}_{j-}} + \boldsymbol{\mu}^T \left[ \frac{\partial \boldsymbol{\chi}}{\partial \mathbf{x}_{j-}} \right] \right) \delta \mathbf{x}_{j-} + \\ & + \sum_j \int_{t_{(j-1)+}}^{t_j} \left( \left( \frac{\partial H}{\partial \mathbf{x}} + \dot{\boldsymbol{\lambda}}^T \right) \delta \mathbf{x} + \frac{\partial H}{\partial \mathbf{u}} \delta \mathbf{u} \right) dt \quad j = 1, \dots, n \end{aligned} \quad (5.6)$$

where the Hamiltonian  $H$  of the system was defined as:

$$H = \Phi + \boldsymbol{\lambda}^T \mathbf{f} \quad (5.7)$$

The (necessary) optimal condition prescribes the stationarity of the functional and, therefore, the annulment of its first variation for any choice of variations  $\delta \mathbf{x}$ ,  $\delta \mathbf{u}$ ,  $\delta \mathbf{x}_{(j-1)+}$ ,  $\delta \mathbf{x}_{j-}$ ,  $\delta t_{(j-1)+}$ ,  $\delta t_{j-}$  compatible with differential equations and boundary conditions. The introduction of added variables and constants allows, with an appropriate choice, to cancel at the same time the coefficient of each of the variations in expression (5.6), thus ensuring the stationarity of the functional expressed by the condition  $\delta J^* = 0$ .

By canceling the coefficients of  $\delta \mathbf{x}$  and  $\delta \mathbf{u}$  within the integral for each point of the trajectory we obtain, respectively, the Euler-Lagrange differential equations for the added variables:

$$\frac{d\boldsymbol{\lambda}}{dt} = - \left( \frac{\partial H}{\partial \mathbf{x}} \right)^T \quad (5.8)$$

and the algebraic equations for controls:

$$\left(\frac{\partial H}{\partial \mathbf{u}}\right)^T = 0 \quad (5.9)$$

It is interesting to note that the control laws (and as will be seen also the boundary conditions) are formally independent of the fact of searching for the maximum or minimum of  $J$ .

Particular attention must be paid if one of the controls is subject to a constraint, ie it must belong to a given *admissibility domain* (for example the thrust module must be between the minimum value 0 and the maximum value  $T_{max}$ ; the same applies to the coefficient of lift that has an upper limit  $C_{Lmax}$ ). The cases in which the constraint depends on time or state variables are not considered, but only those in which it is explicit and constant, as in the cases illustrated above. In the presence of such a constraint, the optimal value of the control at each point of the trajectory is that which, belonging to the admissibility domain, maximizes, if the maximums of  $J$  are sought, or minimizes, if the minimums are sought, the Hamiltonian (5.7) at that point (*Maximum principle of Pontryagin*). In practice there are two possibilities:

- the optimal value of the control is that provided by equation (5.9) if it falls within the admissibility domain and therefore the constraint does not intervene at that point (locally "unconstrained" control). In other words, if the value obtained is in the admissibility domain, then it is the optimal one;
- the optimal value is at the extremes of the domain, ie the control assumes the maximum or minimum value, if that provided by equation (5.9) does not fall within the admissibility domain ("constrained" control). In other words, if the value obtained does not falls within the admissibility domain, the optimal value is the maximum or minimum one (according to Pontryagin's principle).

A particular case occurs if the Hamiltonian is linear with respect to one of the controls subject to constraints, since in the corresponding equation (5.9) the control does not appear explicitly and therefore cannot be determined. In this case, there are still two possibilities (referring to the case where  $J$  should be maximized):

- If in the equation (5.7) the coefficient of the considered control is not zero, then  $H$  is maximized for the maximum value of the control if the coefficient is positive and minimum if it is negative (*bang-bang* control), according to the principle of maximum of Pontryagin. In other words, the optimal value is the maximum value of the control if the coefficient in  $H$  is positive; or the minimum value of the control if the coefficient in  $H$  is negative;
- if in the equation (5.7) the coefficient of the considered control is identically zero during a finite interval of time (*singular arc*), then it is necessary to impose the annulment of all the successive derivatives of the coefficient with respect to time,

until in one of them the control does not appear explicitly: the optimal control is therefore determined by setting equal to zero the last derivative. It is well known that the order of derivation necessary for the purpose is always even and its half indicates the order of the singular arc.

Regarding the missing boundary conditions, it is convenient to refer to the  $j$ -th contour, writing the conditions that derive from considering it as the final endpoint of the  $(j-1)$ -th subinterval or as the initial endpoint of the  $j$ -th subinterval; canceling in the order the coefficients of  $\delta \mathbf{x}_{j-}$ ,  $\delta \mathbf{x}_{j+}$ ,  $\delta t_{j-}$ ,  $\delta t_{j+}$  in the expression (1.6), we obtain:

$$-\boldsymbol{\lambda}_{j-}^T + \frac{\partial \varphi}{\partial \mathbf{x}_{j-}} + \boldsymbol{\mu}^T \left[ \frac{\partial \boldsymbol{\chi}}{\partial \mathbf{x}_{j-}} \right] = 0 \quad j = 1, \dots, n \quad (5.10)$$

$$\boldsymbol{\lambda}_{j+}^T + \frac{\partial \varphi}{\partial \mathbf{x}_{j+}} + \boldsymbol{\mu}^T \left[ \frac{\partial \boldsymbol{\chi}}{\partial \mathbf{x}_{j+}} \right] = 0 \quad j = 0, \dots, n-1 \quad (5.11)$$

$$H_{j-} + \frac{\partial \varphi}{\partial t_{j-}} + \boldsymbol{\mu}^T \frac{\partial \boldsymbol{\chi}}{\partial t_{j-}} = 0 \quad j = 1, \dots, n \quad (5.12)$$

$$-H_{j+} + \frac{\partial \varphi}{\partial t_{j+}} + \boldsymbol{\mu}^T \frac{\partial \boldsymbol{\chi}}{\partial t_{j+}} = 0 \quad j = 0, \dots, n-1 \quad (5.13)$$

where the subscripts  $j_-$  and  $j_+$  indicate the values assumed respectively immediately before and after the point  $j$  (it is necessary to distinguish as discontinuities may occur in the junction points between sub-intervals). Equations (5.10) and (5.12) have no meaning at the beginning of the trajectory ( $j = 0$ ), while equations (5.11) and (5.13) have no meaning at its end ( $j = n$ ).

Eliminating the added constants  $\boldsymbol{\mu}$  from the equations (5.10)  $\div$  (5.13) we have the boundary conditions of optimum:

$$\boldsymbol{\sigma}(\mathbf{x}_{(j-1)+}, \mathbf{x}_{j-}, \boldsymbol{\lambda}_{(j-1)+}, \boldsymbol{\lambda}_{j-}, t_{(j-1)+}, t_{j-}) = 0 \quad (5.14)$$

that, with the assigned conditions (5.2), they complete the differential system given by equations (5.1) and (5.8).

Considering a generic state variable  $x$ , if subjected to particular boundary conditions, equations (5.10) and (5.11) provide particular optimal conditions for the corresponding addition variable  $\lambda_x$ :

- if the state variable  $x$  is explicitly assigned to the initial  $t_0$  or final  $t_f$  instant, the corresponding added variable  $\lambda_{x,0}$  is free at that point;
- if the initial or final value of the state variable  $x$  does not appear neither in the function  $\varphi$  nor in the boundary conditions, the corresponding added variable  $\lambda_{x,0}$  is null at that point;

- if a state variable is continuous and free in an internal point  $i$  ( $\chi$  contains the equation  $x_{j+} = x_{j-}$ ), the corresponding added variable is also continuous at that point ( $\lambda_{x_{j+}} = \lambda_{x_{j-}}$ );
- if a state variable is continuous and explicitly assigned in an internal point ( $\chi$  contains the equations  $x_{j+} = x_{j-} = a$ ), the corresponding added variable has a "free" discontinuity at that point: that is, the value of  $\lambda_{x_{j+}}$  is independent of  $\lambda_{x_{j-}}$  and must be determined by the optimization procedure.

Similarly, if  $H$  does not explicitly depend on time, equations (5.12) and (5.13) also provide, in some cases, particular boundary conditions:

- if the initial time  $t_0$  (or the final time  $t_f$ ) does not appear explicitly neither in the boundary conditions nor in the function  $\varphi$  (ie is free), the Hamiltonian is null at the initial (or final) time ( $H_0 = 0$ );
- if the initial or final time is assigned, the Hamiltonian is there free;
- if the intermediate time  $t_j$  does not explicitly appear in the function  $\varphi$ , (the only condition in  $\chi$  that involves it is the continuity of time  $t_{j+} = t_{j-}$ ) (ie it is free and continuous) the Hamiltonian is continuous at point  $j$  ( $H_{j+} = H_{j-}$ );
- if the intermediate time  $t_j$  is explicitly assigned, (in  $\chi$  the equations  $t_{j+} = t_{j-} = a$  appear) the Hamiltonian has a "free" discontinuity at that point.

## 5.2 Boundary Value Problem (BVP)

The indirect method adopted for the optimization of orbital transfers involves the application of the optimal control theory to the system of equations (5.1) which has boundary conditions dependent on the type of orbits between which the transfer takes place. The theory of optimal control formulates a new system of differential equations (BVP) in which some of the initial values of the variables are unknown, as we saw in the previous chapter. The solution to this problem is to find which initial values allow, by numerically integrating the differential system, to satisfy all boundary conditions, both imposed and optimal.

We now describe the BVP resolution method and how the optimal problem is formulated so as to adapt to its characteristics.

As we saw in the previous chapter, the optimal control theory formulates the optimal problem as a mathematical problem subject to differential and algebraic constraints. Since some initial values of state variables and additions are unknown, the optimal problem translates into a differential boundary problem (BVP), with the differential equations (5.1) and (5.8), in which the controls are determined by the algebraic equations (5.9), supported by the boundary conditions imposed (5.2) and of optimum (5.14). The problem in question has some peculiarities:

- the integration interval is subdivided into sub-intervals in which the differential equations can have different expression;
- the duration of each sub-interval is generally unknown;
- the boundary conditions can be non-linear and involve the values of the variables both at the external and internal boundaries;
- the variables can be discontinuous to the internal contours and their value can be unknown after the discontinuity.

The main difficulty of indirect optimization techniques is precisely the solution of the boundary problem that emerge from their application: the method for its solution is therefore an indispensable tool and moreover there must be correspondence between its characteristics and those of the problem under consideration. The BVP solution is obtained by reducing it to a succession of initial values problems that is brought to convergence according to the Newton method.

To resolve the indeterminacy of the duration of each sub-interval, we resort, for the sole purpose of integration, to the replacement of the independent variable  $t$  with a new variable  $\varepsilon$  defined in the  $j$ -th sub-interval through the relation:

$$\varepsilon = j - 1 + \frac{t - t_{j-1}}{t_j - t_{j-1}} = j - 1 + \frac{t - t_{j-1}}{\tau_j} \quad (5.15)$$

where  $\tau_j$  is the duration (generally unknown) of the subinterval. In this way the internal and external contours are fixed, thanks to the introduction of the unknown parameters  $\tau_j$ , and correspond to consecutive integer values of the new independent variable  $\varepsilon$ .

For the description of the method, we refer to the generic system of equations given by (5.1) and (5.8) in which the controls have been replaced by expressions (5.9). There is therefore a differential problem in the variables, of state and additions, now no longer distinct,  $\mathbf{y} = (\mathbf{x}, \boldsymbol{\lambda})$ :

$$\frac{d\mathbf{y}}{dt} = \mathbf{f}^*(\mathbf{y}, t) \quad (5.16)$$

It must be taken into account that, in the problem under consideration, constant parameters also appear, such as the durations of the subintervals  $\tau_j$  or the values of the variables after a discontinuity: it is therefore useful to refer to a new vector  $\mathbf{z} = (\mathbf{y}, \mathbf{c})$  which contains the state and addition variables and the new vector  $\mathbf{c}$  of the constant parameters.

Applying the change of independent variable, the system of differential equations takes the form:

$$\frac{d\mathbf{z}}{d\varepsilon} = \mathbf{f}(\mathbf{z}, \varepsilon) \quad (5.17)$$

Explaining the second member of the equations (5.17), for state variables and additions we have:

$$\frac{d\mathbf{y}}{d\varepsilon} = \tau_j \frac{d\mathbf{y}}{dt} \quad (5.18)$$

while for the constant parameters we have, of course:

$$\frac{d\mathbf{c}}{d\varepsilon} = 0 \quad (5.19)$$

The boundary conditions are generically expressed, without distinguishing between imposed and optimal conditions, such as:

$$\Psi(\mathbf{s}) = 0 \quad (5.20)$$

where  $\mathbf{s}$  is a vector that contains values that the variables assume for each contour (internal or external)  $\varepsilon = 0, 1, \dots, n$ , and the unknown parameters.

$$\mathbf{s} = (\mathbf{y}_0, \mathbf{y}_1, \dots, \mathbf{y}_n, \mathbf{c}) \quad (5.21)$$

The initial values of some of the variables are generally unknown, and the search for the solution translates into determining, through an iterative procedure, which values they must assume to satisfy the equations (5.20). The procedure is described assuming that none of the initial values is known. The  $r$ -th iteration begins with the integration of the equations (5.17) with the initial values  $\mathbf{p}^r$  found at the end of the previous iteration. That is fixed:

$$\mathbf{z}(0) = \mathbf{p}^r \quad (5.22)$$

and we proceed to the integration of equations along the entire trajectory taking into account any discontinuities at the internal contours (to start the procedure, at the first iteration it is necessary to choose tentative values  $\mathbf{p}^1$ ). In each of the contours, the value of state variables is determined and, at the end of the integration, the error on boundary conditions  $\Psi^r$  is calculated at the  $r$ -th iteration.

A  $\Delta\mathbf{p}$  variation leads to varying the error on the boundary conditions of a quantity which, taking into account only terms of the first order, is equal to:

$$\Delta\Psi = \left[ \frac{\partial\Psi}{\partial\mathbf{p}} \right] \Delta\mathbf{p} \quad (5.23)$$

Having to cancel the error on boundary conditions (ie wanting to get  $\Delta\Psi = -\Psi^r$ ), at each iteration the initial values are corrected by a quantity:

$$\Delta\mathbf{p} = \mathbf{p}^{r+1} - \mathbf{p}^r = - \left[ \frac{\partial\Psi}{\partial\mathbf{p}} \right]^{-1} \Psi^r \quad (5.24)$$

until the boundary conditions (5.20) are verified with the desired precision. The matrix that appears in equation (5.24) is calculated as the product of two matrices:

$$\begin{bmatrix} \frac{\partial \Psi}{\partial \mathbf{p}} \end{bmatrix} = \begin{bmatrix} \frac{\partial \Psi}{\partial \mathbf{s}} \end{bmatrix} \begin{bmatrix} \frac{\partial \mathbf{s}}{\partial \mathbf{p}} \end{bmatrix} \quad (5.25)$$

where the first can be immediately obtained by deriving the boundary conditions from the quantities that appear there. The second matrix, which contains the derivatives of values of the variables to the contours with respect to the initial values, that is the values that are assumed to the contours ( $\varepsilon = 0, 1, \dots, n$ ) from the matrix:

$$\begin{bmatrix} \frac{\partial \mathbf{z}}{\partial \mathbf{p}} \end{bmatrix} = [\mathbf{g}(\varepsilon)] \quad (5.26)$$

is obtained by integrating the system of differential equations obtained by deriving the main system (5.17) with respect to each of the initial values:

$$[\dot{\mathbf{g}}] = \frac{d}{d\varepsilon} \begin{bmatrix} \frac{\partial \mathbf{z}}{\partial \mathbf{p}} \end{bmatrix} = \begin{bmatrix} \frac{\partial}{\partial \mathbf{p}} \left( \frac{d\mathbf{z}}{d\varepsilon} \right) \end{bmatrix} = \begin{bmatrix} \frac{\partial \mathbf{f}}{\partial \mathbf{p}} \end{bmatrix} \quad (5.27)$$

where the point  $\cdot$  now indicates the derivative with respect to the new independent variable  $\varepsilon$ . Explaining the Jacobian of the main system (5.17), equation (5.27) takes the form:

$$[\dot{\mathbf{g}}] = \begin{bmatrix} \frac{\partial \mathbf{f}}{\partial \mathbf{z}} \end{bmatrix} \begin{bmatrix} \frac{\partial \mathbf{z}}{\partial \mathbf{p}} \end{bmatrix} = \begin{bmatrix} \frac{\partial \mathbf{f}}{\partial \mathbf{z}} \end{bmatrix} [\mathbf{g}] \quad (5.28)$$

The initial values for the homogeneous system (5.28) are obtained by deriving the relation (5.22); the identical matrix is thus obtained:

$$[\mathbf{g}(0)] = \begin{bmatrix} \frac{\partial \mathbf{z}(0)}{\partial \mathbf{p}} \end{bmatrix} = [\mathbf{I}] \quad (5.29)$$

Note that with this method it is also possible to treat discontinuities in the variables. In fact, for a discontinuity in point  $i$ , it is sufficient to update both the vector of the variables  $\mathbf{z}$  and the matrix  $\mathbf{g}$  through the relation  $\mathbf{h}$  that binds the values of the variables before and after the discontinuity:

$$\mathbf{z}_{i+} = \mathbf{h}(\mathbf{z}_{i-}) \quad (5.30)$$

$$\begin{bmatrix} \mathbf{g}_{i+} \end{bmatrix} = \begin{bmatrix} \frac{\partial \mathbf{h}}{\partial \mathbf{z}} \end{bmatrix} \begin{bmatrix} \mathbf{g}_{i-} \end{bmatrix} \quad (5.31)$$

(for this reason, in defining the vector  $\mathbf{s}$  there is no distinction between the vectors  $\mathbf{y}_{i+}$  and  $\mathbf{y}_{i-}$ , as one is a known function, through  $\mathbf{h}$ , of the other and of the vector  $\mathbf{c}$ ). Obviously, if some of the initial values of the variables are known, the problem is simplified since the vector  $\mathbf{p}$  is reduced to the estimation of only the unknown components

of  $\mathbf{z}(0)$  and the vector  $\Psi$  to the non-explicit boundary conditions at the initial time. The matrix that appears in equation (5.24) can also be evaluated numerically: its  $i$ -th row is obtained by varying the  $i$ -th component of  $\mathbf{p}$  by a small quantity  $\Delta p$  (keeping the others fixed) and then integrating the equations (5.17). It is thus possible to calculate the variation of the boundary conditions  $\Delta\Psi(\Delta p)$  and, linearizing, obtain the corresponding row as  $\Delta\Psi^T/\Delta p$ . This procedure allows in some cases a simpler and faster solution of the BVP (suitable values for  $\Delta p$ , found empirically, are of the order of  $10^{-6} \div 10^{-7}$ ) but it is not always able to guarantee convergence: the determination of the matrix in equation (1.24) is in fact less accurate than its calculation through the solution of the system (5.28) and, given the great sensitivity of the problem, the numerical approximations introduced can compromise convergence.

A similar numeric procedure can also be used for the calculation of the Jacobian and the matrix  $[\partial\Psi/\partial s]$ : however, it was preferred to maintain the analytical evaluation and to use, in the setting of the codes, the values obtained numerically to verify, by comparison with those provided by the analytic expressions of the Jacobian and the matrix  $[\partial\Psi/\partial s]$ , the accuracy of these expressions.

The integration of all the differential equations, both for the main system (5.17) and for the homogeneous one (5.28), is performed with a variable step and order method based on the Adams formulas, as described by Shampine and Gordon [6].

In the examples that follow, the required precision is  $10^{-7}$  (that is, it is required that the maximum error  $E_{max} = \max_i(\Psi_i)$  on the boundary conditions be less than this value). The linearization introduced for the calculation of the  $\Delta\mathbf{p}$  correction given by equation (5.24), to be applied to the initial attempt values, introduces errors that can compromise convergence by increasing rather than decreasing the error on the boundary conditions. Some steps have therefore been taken to improve the procedure.

- In order not to stray too far from the solution, the correction made is actually a fraction of the one determined, that is:

$$\mathbf{p}^{r+1} = \mathbf{p}^r + K_1 \Delta\mathbf{p} \quad (5.32)$$

with  $K_1 = 0.1 \div 1$ , depending on whether the starting solution is relatively distant or close to the one sought.

- At each iteration, after the new vector of initial attempt values  $\mathbf{p}^{r+1}$  has been determined through (5.32) and the equations of motion are integrated, we compare the maximum error on boundary conditions  $E_{max}^{r+1}$  with that obtained at the previous iteration  $E_{max}^r$ : if the maximum error is less than a multiple of the previous one, ie if  $E_{max}^{r+1} < K_2 E_{max}^r$ , proceed with the new iteration. As to converge to the solution the error on the boundary conditions, in the first iterations, can increase, the value of  $K_2$  must be greater than the unit: a value of  $K_2 = 2 \div 3$  guarantees good results.
- If, on the other hand, the error in the new iteration is too large with respect to the previous one, we proceed to the bisection of the correction made, halving it: that

is, integrating the equations of motion with the attempt values:

$$\mathbf{p}^{r+1} = \mathbf{p}^r + K_1 \Delta \mathbf{p} / 2 \quad (5.33)$$

The comparison between the new maximum error obtained and that of the previous iteration is then repeated and, if necessary, also the bisection. A maximum number of 5 bisections has been set, after which the procedure stops, meaning that the solution of attempt chosen cannot lead to convergence.

# Chapter 6

## Statement of the Problem

In preliminary analysis, the patched-conic approximation is commonly adopted and the two-body problem equations are used to describe the motion of the point-mass spacecraft (with variable mass  $m$ ). For the presented case, only the heliocentric phases are considered and the state equations are the following:

$$\frac{d\mathbf{r}}{dt} = \mathbf{V} \quad (6.1)$$

$$\frac{d\mathbf{V}}{dt} = \mathbf{g} + \frac{\mathbf{T}}{m} \quad (6.2)$$

$$\frac{dm}{dt} = -q \quad (6.3)$$

where  $r$  is the position vector and  $\mathbf{V}$  the velocity vector.

A trajectory based on the *Asteroid Redirect Mission scenario* is considered. Asteroid (433) Eros is selected as the target to provide a wide variation of available power, as opposed to primary ARM asteroids (for example asteroid 2008EV5) with more Earth-like orbits. The mission purpose is to pick up a large boulder from Eros surface and deliver it to a stable orbit in the Earth-Moon system. The spacecraft leaves the Earth's sphere of influence on a specific date, dictated by the possibility of a lunar gravity assist to boost the escape mass.

The value of the spacecraft initial mass is assigned and it is equal to 10000 kg, of which 5000 kg is the mass of the available propellant. Escape velocity is fixed at  $1.4\text{km/s}$  ( $C3$  equals to  $2\text{km}^2/\text{s}^2$ ). After rendezvous, the spacecraft remains at Eros for 174 days and then starts the return flight with a pick-up mass that must be maximized. An Earth gravity assist in the return leg is used to improve the performance. Arrival date and arrival velocity  $C3$  ( $2\text{km}^2/\text{s}^2$ ) are here fixed. These previous values are chosen on the base of performance of the current technology.

Boundary conditions can be written as:

$$\mathbf{r}_0 = \mathbf{r}_E(t_0) \quad (6.4)$$

$$[\mathbf{v}_0 - \mathbf{v}_E(t_0)]^2 = C3_0 \quad (6.5)$$

$$m_0 = 10000kg \quad (6.6)$$

$$\mathbf{r}_1 = \mathbf{r}_A(t_1) \quad (6.7)$$

$$\mathbf{V}_1 = \mathbf{V}_A(t_1) \quad (6.8)$$

$$\mathbf{r}_2 = \mathbf{r}_A(t_2) \quad (6.9)$$

$$\mathbf{V}_2 = \mathbf{V}_A(t_2) \quad (6.10)$$

$$m_2 - m_1 = m_{boulder} \quad (6.11)$$

$$\mathbf{r}_{3-} = \mathbf{r}_{3+} = \mathbf{r}_E(t_3) \quad (6.12)$$

$$[\mathbf{V}_{3-} - \mathbf{V}_E(t_3)]^2 = [\mathbf{V}_{3+} - \mathbf{V}_E(t_3)]^2 \quad (6.13)$$

$$\mathbf{r}_f = \mathbf{r}_E(t_f) \quad (6.14)$$

$$[\mathbf{V}_f - \mathbf{V}_E(t_f)]^2 = C3_f \quad (6.15)$$

$$m_f = 5000kg \quad (6.16)$$

where subscripts 0, 1, 2, 3 and  $f$  refer to Earth departure, Eros arrival, Eros departure, Earth gravity assist (- just before, + just after) and Earth arrival, respectively. Subscripts  $E$  and  $A$  refer to Earth and target asteroid. The pick-up mass  $m_{boulder}$  is maximized.

Thrust magnitude and propellant mass flow rate of a thruster are related to its input power. As a consequence, the effective exhaust velocity (therefore the specific impulse) is also a function of the input power. Cubic relations are assumed here for thrust magnitude  $T$  and propellant mass flow rate  $q$ :

$$T = a_0 + a_1P + a_2P^2 + a_3P^3 \quad (6.17)$$

$$q = b_0 + b_1P + b_2P^2 + b_3P^3 \quad (6.18)$$

and the specific relationships applied in the example problems for this work are shown in Figure 6.1(a). Additionally, the engine specific impulse as a function of input power is illustrated in Figure 6.1(b), where  $I_{sp} = T/(qg_0)$ .

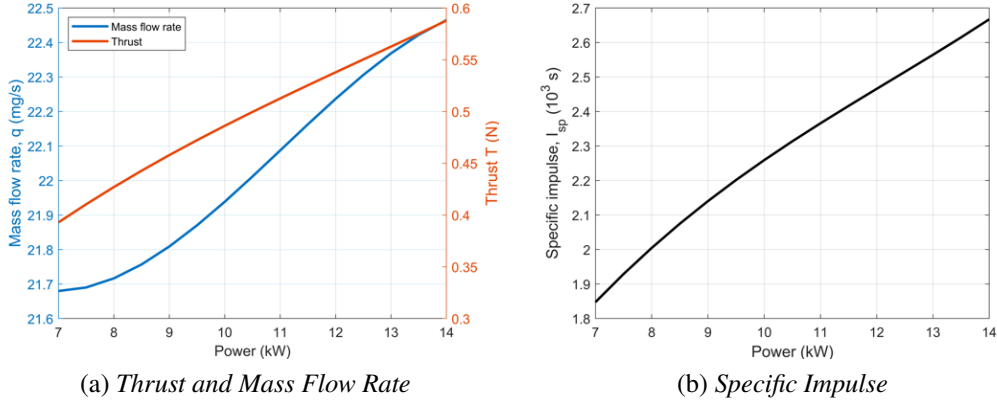


Figure 6.1: Thruster performance as a function of input power

As is shown in the previous graphs, each thruster works with a minimum input power of 7 kW and maximum input power of 13.95 kW. Three fully autonomous thrusters are considered for this mission. It is important to notice that the maximum value of specific impulse, namely the minimum propellant consumption, corresponds to the maximum input power. For this reason, in order to use the least amount of propellant, is fundamental to use the thrusters at maximum power for as long as possible.

The spacecraft has solar arrays that produce 47 kW of electric power at 1 AU (initial and final position of the mission), but 5 kW must be reserved for on board electronics. The array power is assumed to vary in an inverse relation with the squared distance from the sun and the available power for thrusting is  $P_a = 47/r^2 - 5kW$ , with  $r$  in AU. A 90% duty cycle is considered. Thrust magnitude and direction are the problem control variables. These propulsion assumptions are similar to those used in the development of the Asteroid Redirect Robotic Mission reference trajectory.

# Chapter 7

## Optimization of the segments

In order to find the optimal control law for the thrusters indirect methods are used. As said, indirect methods are based on the theory of optimal control [3] and solve the optimization problem by defining and solving a boundary value problem [1].

An adjoint variable is associated with each differential equation and the Hamiltonian is defined. The usual expression is:

$$H = \boldsymbol{\lambda}_r^T \mathbf{V} + \boldsymbol{\lambda}_V^T \mathbf{g} + T S_F \quad (7.1)$$

where the thrust coefficient:

$$S_F = \frac{\boldsymbol{\lambda}_V^T \mathbf{T} / T}{m} - \lambda_m \frac{q}{T} \quad (7.2)$$

is named the *switching function*.

The theory of optimal control provides differential equations for the controls and adjoint variables (Euler-Lagrange equations) and also boundary conditions for optimality [1], which depend on performance index and applied boundary conditions. Refer to section (5.2) for more details.

The optimal controls must maximize  $H$  at any given point along the trajectory, in agreement with Pontryagin's maximum principle (PMP). One deduces that the thrust must be parallel to the velocity adjoint vector  $\boldsymbol{\lambda}_V$  and the switching function becomes:

$$S_F = \frac{\lambda_V}{m} - \lambda_m \frac{q}{T} \quad (7.3)$$

If the propulsion system has constant effective exhaust velocity  $c = T/q$ , the thrust magnitude is the only remaining control, and one easily recognizes that a bang-bang control is required. The thrust assumes its maximum value when  $S_F > 0$ , whereas the engine is switched off when  $S_F < 0$ . Only in special cases, usually involving atmospheric flight, the switching function remains null along a non-zero interval and the thrust assumes an intermediate value (singular arc).

PMP requires the maximization of  $S_F$ . In the general case of non-constant  $c$  the function:

$$\bar{H} = T - \frac{m\lambda_m}{\lambda_V}q \quad (7.4)$$

must be maximized. It is interesting to note that  $\bar{H}$  is a linear combination of  $T$  and  $q$ , and it depends on a single parameter  $K = m\lambda_m/\lambda_V$  which is varying along the trajectory. At any given trajectory point,  $K$  is known and the power level that maximizes  $\bar{H}$  must be sought.

The problem is more complex when more than one engine is available and the electric power is split between the engines. Each thruster provides its own thrust and has its own propellant consumption, which both depend on its input power.  $\bar{H}$  becomes:

$$\bar{H} = \sum_{i=1}^N T_i - Kq_i \quad (7.5)$$

Three equal thrusters ( $N = 3$ ) will be considered here. By introducing the coefficients  $c_j = a_j - Kb_j, j = 0, 1, 2, 3$ , one has:

$$\bar{H} = \sum_{i=1}^3 c_0 + c_1P_i + c_2P_i^2 + c_3P_i^3 = \sum_{i=1}^3 f_i \quad (7.6)$$

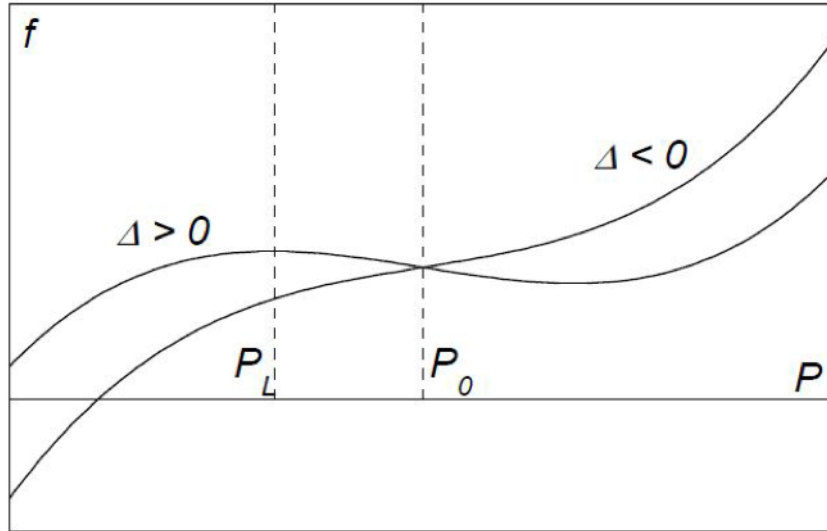


Figure 7.1: Generic behavior of function  $f$

The function  $f = c_0 + c_1P + c_2P^2 + c_3P^3$  is shown in Figure (7.1) with arbitrary scales for  $c_3 > 0$ , which is the case considered here. The curve second derivative changes its sign from negative to positive at  $P_0 = -c_2/(3c_3)$ . Two cases exist, depending on  $\Delta = c_2^2 - 3c_1c_3$ , the discriminant of the quadratic equation that nullifies the first derivative of  $f$ . When  $\Delta > 0$  a local maximum exists at  $P = P_L = -P_0 - \sqrt{\Delta}/(6c_3)$ , with a local minimum at a symmetric position with respect to  $P_0$ . The curve is stationary at  $P_0$  for  $\Delta = 0$ . The curve is monotonic and no stationary points exist for  $\Delta < 0$ .

Each engine can either be turned off ( $P_i = 0$ ) or operate between minimum and maximum limits ( $P_m \leq P_i \leq P_M$ ). In addition, the total power cannot exceed the available power, that is,  $\sum_{i=1}^3 P_i \leq P_a$ .

The determination of the optimal power partitioning at any trajectory point is turned into finding  $P_1, P_2, P_3$  that maximize  $\bar{H}$ , that is, a cubic function of the three variables, with the linear constraints  $P_i = 0$  or  $P_m \leq P_i \leq P_M$  and  $\sum_{i=1}^3 P_i \leq P_a$ . Feasible solutions satisfy all the constraints. At a feasible point, a constraint is said to be *active* when the equality sign holds; it is said to be *inactive* when a strict inequality holds. Local maxima of  $\bar{H}$  are sought for any combination of active and inactive constraints, and then compared to select the global maximum.

The function  $\bar{H}$  is locally maximum if its variation is non-positive for any variation of the control variables. The constrained maximization problem is treated with an approach based on Lagrangian multipliers  $\mu$ . Instead of  $\bar{H}$ , the augmented function:

$$\bar{H}^* = \sum_{i=1}^3 f_i + \mu_a \left( \sum_{i=1}^3 P_i - P_a \right) + \sum_{i=1}^3 \mu_{i,M} (P_i - P_M) + \sum_{i=1}^3 \mu_{i,m} (P_i - P_m) \quad (7.7)$$

is maximized. Its first variation is:

$$\delta^1 \bar{H}^* = \sum_{i=1}^3 (\partial f_i / \partial P_i + \mu_a + \mu_{i,M} + \mu_{i,m}) \delta P_i \quad (7.8)$$

and the second variation is:

$$\delta^2 \bar{H}^* = \sum_{i=1}^3 (\partial^2 f_i / \partial^2 P_i) \delta P_i^2 \quad (7.9)$$

For inactive constraints, the corresponding Lagrangian multipliers are set to zero.

When the active constraints are fulfilled,  $\bar{H}^* = \bar{H}$  for any choice of the Lagrangian multipliers that correspond to the active constraints. It is therefore possible to find values of  $\mu$ s and  $P_i$  that satisfy the constraints and simultaneously nullify  $\delta^1 \bar{H}^*$  for any variation

of the control variables. This is done by setting the coefficient of  $\delta P_i$  to zero for any  $i$ . At this point, the first variation of  $\bar{H}$  is also zero for *any admissible* variation of the control variables. That is, the solution is a stationary point for the selected constraints combination. Inspection of  $\delta^2 \bar{H}^* = \delta^2 \bar{H}$  allows analysis of the nature of the stationary point (maximum, minimum or inflection point):  $\delta^2 \bar{H} < 0$  for any admissible variation is required for a local maximum. Final checks must concern the selected constraint combination. First, constraint removal must be considered to check if  $\bar{H}$  can be improved by turning an active constraint into an active one. Second, it is necessary to check the inactive constraints and discard the solutions if any of them is violated.

## 7.1 Optimal Case

### 7.1.1 Three Thrusters On

The three-thruster case with cubic functions for  $T$  and  $q$  and  $c_3 > 0$  is treated here. First, solutions with three thrusters on are considered. Numbering is arranged to have  $P_1 \geq P_2 \geq P_3$ .

- Case 3a, "No Active Constraint". All the multipliers are zero and maximization requires:

$$\frac{\partial f_i}{\partial P_i} = 0 \quad i = 1,2,3 \quad (7.10)$$

The only solution with  $\delta^2 \bar{H} < 0$  is  $P_i = P_L$  for any  $i$  when  $\Delta > 0$ . The thrusters operate at the same power level. No optimal solution is instead found for  $\Delta < 0$ .

- Case 3b, "Available Power Constraint". Only  $\mu_a$  is non-zero and maximization implies:

$$\frac{\partial f_i}{\partial P_i} + \mu_a = 0 \quad i = 1,2,3 \quad (7.11)$$

The partial derivatives are equal either with three thrusters at the same power level  $P_i = P_a/3$  or with two engines at the same power ( $P_1 = P_2 = P_a - 2P_0$ ) and the third one at a symmetric level with respect to  $P_0$ , that is,  $P_3 = 4P_0 - P_a$ . The latter solution is an inflection point as it is always easy to select variations which fulfill  $\delta P_1 + \delta P_2 + \delta P_3 = 0$  and make  $\delta^2 \bar{H}$  either positive or negative. The uniform repartition solution corresponds to a maximum only if  $P_i < P_0$  (that is,  $\partial^2 f_i / \partial^2 P_i < 0$ ).

- Case 3c, "One Thruster at Maximum Power  $P_1 = P_M$ ". Only  $\mu_{1,M}$  is non-zero. Equation (7.10) holds for  $i = 2,3$  and gives  $P_2 = P_3 = P_L$  (only for  $\Delta > 0$ ). This solution is a local maximum only if  $\partial f_i / \partial P_i > 0$ , whereas, in the opposite case,  $\bar{H}$  grows if the constraint is removed.

- Case 3d, "Available Power Constraint, One Thruster at Maximum Power  $P_1 = P_M$ ". Only  $\mu_a$  and  $\mu_{1,M}$  are non-zero.  
One has Equation (7.11) for  $i = 2,3$ , and these thrusters must operate at the same power  $P_2 = P_3 = (P_a - P_M)/2$ . A maximum occurs only if  $P_2 = P_3 < P_0$  and  $\partial f_1/\partial P_1 > \partial f_2/\partial P_2$ . In general, excluding maximum and minimum values, two thrusters at the same power level cannot occur when  $\partial^2 f/\partial^2 P > 0$  ( $P > P_0$  for  $c_3 > 0$ ).
- Case 3e, "Two Thrusters at Maximum Power  $P_1 = P_2 = P_M$ ". Only  $\mu_{1,M}$  and  $\mu_{2,M}$  are non-zero.  
Equation (7.10) holds for  $i = 3$  and  $P_3 = P_L$  (only for  $\Delta > 0$ ). This solution is a maximum only if  $\partial f_1/\partial P_1 > 0$
- Case 3f, "Available Power Constraint, Two Thrusters at Maximum Power  $P_1 = P_2 = P_M$ ". The third engine power is defined  $P_3 = P_a - 2P_M$ . The case with three thrusters at  $P_M$  can be seen as a special solution, when  $P_a \geq 3P_M$ . For a maximum,  $\partial f_1/\partial P_1 > \partial f_3/\partial P_3 > 0$  is required. With one thruster at maximum power  $P_1 = P_M$  and one at minimum power  $P_3 = P_m$  only  $\mu_{1,M}$  and  $\mu_{3,m}$  are non-zero.  
Equation (7.10) is enforced for  $i = 2$  to obtain  $P_2 = P_L$  (only for  $\Delta > 0$ ). The solution however, improves if the constraint on  $P_3$  is removed as  $\partial f_3/\partial P_3 > \partial f_2/\partial P_2 = 0$
- Case 3g, "Available Power Constraint, One Thruster at Maximum Power  $P_1 = P_M$  And One at Minimum Power  $P_3 = P_m$ ". One has  $P_2 = P_a - P_M - P_m$ . This solution may or may not be a maximum, depending on the specific values of  $f$  derivatives at the relevant points; details are omitted. A special case is  $P_2 = P_M$  when  $P_a > 2P_M + P_m$ .  
In the case of two thrusters at minimum power  $P_2 = P_3 = P_m$ , Equation (7.10) for  $i = 1$  gives  $P_1 = P_L$  (only for  $\Delta > 0$ ). The solution however, improves if the constraints on  $P_2$  (and  $P_3$ ) are removed as  $\partial f_2/\partial P_2 > \partial f_1/\partial P_1 = 0$ .
- Case 3h, "One Thruster at Minimum Power  $P_3 = P_m$ ". Others thrusters have  $P_1 = P_2 = (P_a - P_m)/2$ . The cases with one thruster at minimum power  $P_3 = P_m$ , with and without the available power constraint are analogous to the cases with one thruster at maximum power (3c and d). However, the  $P_a$ -unconstrained case improves if the constraint on  $P_3$  is removed, as  $\partial f_3/\partial P_3 > 0$  and  $P_m$  must be lower than  $P_0$  for a feasible solution of Equation (7.10). The  $P_a$ -unconstrained solution is a minimum for  $P_1 > P_0$  but improves if the constraint on  $P_3$  is removed, as  $\partial f_3/\partial P_3 > \partial f_1/\partial P_1$  for  $P_3 < P_1 < P_0$ .
- Case 3j, "Available Power Constraint, Two Thrusters at Minimum Power  $P_2 = P_3 = P_m$ ". One has  $P_1 = P_a - 2P_m$ . Again, this solution may or may not be a

maximum, depending on the specific values of  $f$  derivatives at the relevant points. A special case is  $P_1 = P_M$  when  $P_a > P_M + 2P_m$ .

- Case 3k, "Three Thrusters at Minimum Power  $P_i = P_m$ ".  
Maximum if  $\partial f_i / \partial P_i < 0$ .

### 7.1.2 Two Thrusters On

Solution with two thrusters on ( $P_3 = 0$ ) are treated here.

- Case 2a, "No Active Constraint".  
Equation (7.10) for  $i = 1,2$  gives a local maximum for  $P_1 = P_2 = P_L$  (only for  $\Delta > 0$ ).
- Case 2b, "Available Power Constraint".  
Equation (7.11) for  $i = 1,2$  gives  $P_1 = P_2 = P_a/2$ , which is a maximum only for  $P_1 < P_0$ .
- Case 2c, "One Thruster at  $P_M$ " requires Equation (7.10) for  $i = 2$ , that is  $P_2 = P_L$  ( $\Delta > 0$ ). Maximum only for  $\partial f_1 / \partial P_1 > 0$ .
- Case 2d, "Available Power Constraint, One Thruster at  $P_M$ ", has  $P_2 = P_a - P_M$  (and the special case  $P_2 = P_M$  for  $P_a > 2P_M$ ). The derivatives of  $f$  at the relevant points determine if this solution is a maximum or not. One thruster at  $P_m$  cannot be a maximum, based on the same reason of the three.thrusters case.
- Case 2e, " Available Power Constraint, One Thruster at  $P_m$ ", has  $P_1 = P_a - P_m$  (and the special case  $P_1 = P_M$  for  $P_a > P_M + P_m$ ). The derivatives of  $f$  at the relevant points determine if this solution is a maximum.
- Case 2f, "Two Thrusters at Minimum Power  $P_i = P_m$ ".  
Maximum if  $\partial f_i / \partial P_i < 0$ .

### 7.1.3 One Thruster On

The one thruster case ( $P_2 = P_3 = 0$ ) has only three options:

- Case 1a, "No Active Constraint".  
Equation (7.10) for  $i = 1$  gives a local maximum for  $P_1 = P_L$  (only for  $\Delta > 0$ ).
- Case 1b, "Available Power Constraint".  
Equation (7.11) for  $i = 1$  gives  $P_1 = P_a$  (with the special case  $P_1 = P_M$  for  $P_a > P_M$ , the derivatives of  $f$  must be positive at  $P_M$ ).
- Case 1c, "One Thrusters at Minimum Power  $P_1 = P_m$ ". The derivatives of  $f$  must be negative at  $P_m$ .

### 7.1.4 Operating Modes

All the locally optimal solutions are considered and the corresponding values of  $\bar{H}$  are compared to select the global maximum. There are 26 possible optimal operating modes comprising the special cases: all thrusters off, 4 modes with one thruster on, 8 with two thrusters on and 13 modes with three thrusters on. They are summarized in Tables (7.1) and (7.2). It is worth noting that the analysis has greatly reduced the number of modes that can be optimal with respect to the total number of operating modes, as each engine could theoretically operate in any of five modes:  $P = 0, P_M, P_m, P_L$  and at the available power, somehow distributed among the engines. The value of  $\bar{H}$  is evaluated for the potentially optimal modes and compared at any point during integration, selecting the mode that corresponds to the maximum value. The evaluation is purely algebraic and the speed of integration is not remarkably affected with respect to a simple constant- $c$  model.

$i$		1b	1b(sc)	1a	1c	2b	2b(sc)	2d	2e	2e(sc)	2a	2c	2f
1	0	$P_a$	$P_M$	$P_L$	$P_m$	$P_a/2$	$P_M$	$P_M$	$P_a - P_m$	$P_M$	$P_L$	$P_M$	$P_m$
2	0	0	0	0	0	$P_a/2$	$P_M$	$P_a - P_M$	$P_m$	$P_m$	$P_L$	$P_L$	$P_m$

Table 7.1: Operating Modes (0, 1 and 2 thrusters on)

$i$	3b	3b(sc)	3d	3f	3g	3g(sc)	3j	3j(sc)	3h	3a	3c	3e	3k
1	$P_a/3$	$P_M$	$P_M$	$P_M$	$P_M$	$P_M$	$P_a - 2P_m$	$P_M$	$(P_a - P_m)/2$	$P_L$	$P_M$	$P_M$	$P_m$
2	$P_a/3$	$P_M$	$(P_a - P_M)/2$	$P_M$	$P_a - P_M - P_m$	$P_M$	$P_m$	$P_m$	$(P_a - P_m)/2$	$P_L$	$P_L$	$P_M$	$P_m$
3	$P_a/3$	$P_M$	$(P_a - P_M)/2$	$P_a - 2P_M$	$P_m$	$P_m$	$P_m$	$P_m$	$P_m$	$P_L$	$P_L$	$P_L$	$P_m$

Table 7.2: Operating Modes (3 thrusters on)

## 7.2 Thrustmax Case

In addition to the optimal partitioning of power, a further case was evaluated, which we will call "*thrustmax*", in which the partitioning of power is made in such a way as to have always a thruster at maximum power. Numbering is arranged to have  $P_1 \geq P_2 \geq P_3$ . Solutions with three thrusters on are treated here:

- Case 3a, "Available Power Constraint, Three Thrusters at Maximum Power  $P_1 = P_2 = P_3 = P_M$ ", when  $P_a \geq 3P_M$ .
- Case 3b, "Available Power Constraint, Two Thrusters at Maximum Power  $P_1 = P_2 = P_M$ ". The third engine power is defined  $P_3 = P_a - 2P_M$ . This when  $2P_M + P_m \leq P_a < 3P_M$ .

Solutions with two thrusters on ( $P_3 = 0$ ) are treated here:

- Case 2a, "Available Power Constraint, Two Thrusters at Maximum Power  $P_1 = P_2 = P_M$ ", when  $2P_M \leq P_a < 2P_M + P_m$ .
- Case 2b, "Available Power Constraint, One Thruster at Maximum Power  $P_1 = P_M$ ". The second engine power is defined  $P_2 = P_a - P_M$ . This when  $P_M + P_m \leq P_a < 2P_M$ .

The one thruster case ( $P_2 = P_3 = 0$ ) has only one option:

- Case 1a, "Available Power Constraint, One Thruster at Maximum Power  $P_1 = P_M$ ", when  $P_M \leq P_a < P_M + P_m$ .

$i$	$1a$	$2b$	$2a$	$3b$	$3a$
1	$P_M$	$P_M$	$P_M$	$P_M$	$P_M$
2	0	$P_a - P_M$	$P_M$	$P_M$	$P_M$
3	0	0	0	$P_a - 2P_M$	$P_M$

Table 7.3: Operating Modes for *Thrustmax* Case (1, 2 and 3 thrusters on)

## 7.3 Thrustuni Case

In addition to the optimal partitioning of power and the "thrustmax" case, the uniform power partitioning was evaluated, which we will indicate with "thrustuni" case, either with maximum number of thrusters used, e.g., 3 when  $P_a > 3P_m$ , or minimum number of thrusters used, e.g., 2 when  $P_a < 2P_M$ . This case requires that power is partitioned for the three engines uniformly.

### 7.3.1 Maximum number of thrusters

Solutions for "thrustuni" case with maximum number of thrusters are treated here:

- Case a: Three engines at the same power  $P_1 = P_2 = P_3 = P_a/3$ , for  $P_a \geq 3P_m$ .
- Case b: Two engines at the same power  $P_1 = P_2 = P_a/2$  and  $P_3 = 0$ , for  $2P_m \leq P_a < 3P_m$ .
- Case c: One engine on,  $P_1 = P_a$  and  $P_2 = P_3 = 0$ , for  $P_m \leq P_a < 2P_m$ .

$i$	$c$	$b$	$a$
1	$P_a$	$P_a/2$	$P_a/3$
2	0	$P_a/2$	$P_a/3$
3	0	0	$P_a/3$

Table 7.4: Operating Modes for *Thrustuni* Case with maximum number of thrusters (1, 2 and 3 thrusters on)

### 7.3.2 Minimum number of thrusters

Solutions for "thrustuni" case with minimum number of thrusters are treated here:

- Case a: Three engines at the same power  $P_1 = P_2 = P_3 = P_a/3$ , for  $P_a \geq 2P_M$ .
- Case b: Two engines at the same power  $P_1 = P_2 = P_a/2$  and  $P_3 = 0$ , for  $2P_m \leq P_a < 2P_M$ .
- Case c: One engine on,  $P_1 = P_a$  and  $P_2 = P_3 = 0$ , for  $P_m \leq P_a < 2P_m$ .

$i$	$c$	$b$	$a$
1	$P_a$	$P_a/2$	$P_a/3$
2	0	$P_a/2$	$P_a/3$
3	0	0	$P_a/3$

Table 7.5: Operating Modes for *Thrustuni* Case with minimum number of thrusters (1, 2 and 3 thrusters on)

# Chapter 8

## 433 Eros Asteroid

Eros (minor body designation: 433 Eros), is a stony and elongated asteroid of the *Amor group* and the first discovered and second-largest near-Earth object with a mean-diameter of approximately 16.8 kilometers. Visited by the *NEAR Shoemaker* space probe in 1998, it became the first asteroid ever studied from orbit.

The eccentric asteroid was discovered by German astronomer *Carl Gustav Witt* at the *Berlin Urania Observatory* on 13 August 1898, and later named after Eros, a god from Greek mythology; the son of Aphrodite who is identified with the planet Venus. [12]

Aphelion	1.7829 AU
Perihelion	1.1333 AU
Semi-major axis	1.4581 AU
Eccentricity	0.2227
Orbital period	1.76 years
Mean anomaly	47.239°
Inclination	10.829°
Longitude of ascending node	304.31°
Argument of perihelion	178.82°

Table 8.1: Orbital elements of 433 Eros at the epoch 27 April 2019 (JD 2458600.5) [2]

### 8.1 Eros Results

Orbits of Eros and Earth are non-coplanar, with an angle of  $10.83^\circ$  between the two planes [2]. Because of the geometric aspects of the problem, there are many different departure periods of the outbound journey. In fact, in a same year, the mission may start either in the period of December (node close to the aphelion of Eros), or in the period of June (node close to the perihelion of Eros). Nevertheless, a same departure from a specific node, but in different years, may have different performances in terms of optimal

consumption, due to the synodic period<sup>1</sup> between Earth and Eros, which is about 2.31 years [2]. In the same way, there are different periods of fly-by for the inbound journey. A trajectory based on the *Asteroid Redirect Mission scenario* is considered. Some simplifications are introduced with respect to the actual ARRM study. No forced coast arcs are introduced and additional propellant consumption (engine calibration, attitude control) is neglected. Relevant dates are fixed: Earth escape is on January 16, 2022; arrival at Eros July 5, 2024; departure from Eros is on December 26, 2024, arrival at Earth is on March 20, 2027. C3 is  $2\text{km}^2/\text{s}^2$  both at Earth escape and arrival.

The indirect method is used to compare optimal power partitioning, "thrustmax" case and uniform power partitioning, either with maximum number of thrusters used or minimum number of thrusters used.

Optimization results are presented separately for the outbound and inbound trajectory.

### 8.1.1 Outbound Flight

Preliminary solutions of the outbound flight are found by removing the constraint of the asteroid rendezvous, imposing instead only the arrival in a generic point of Eros' orbit, not caring about the real presence of the asteroid. In this way, it is possible to find an hypothetical trajectory with the best performance in terms of propellant consumption.

In Figure (8.1) is shown how the number of active thrusters varies during the mission for the four cases.

---

<sup>1</sup>Synodic period is defined as the time required for any phase angle to repeat itself.

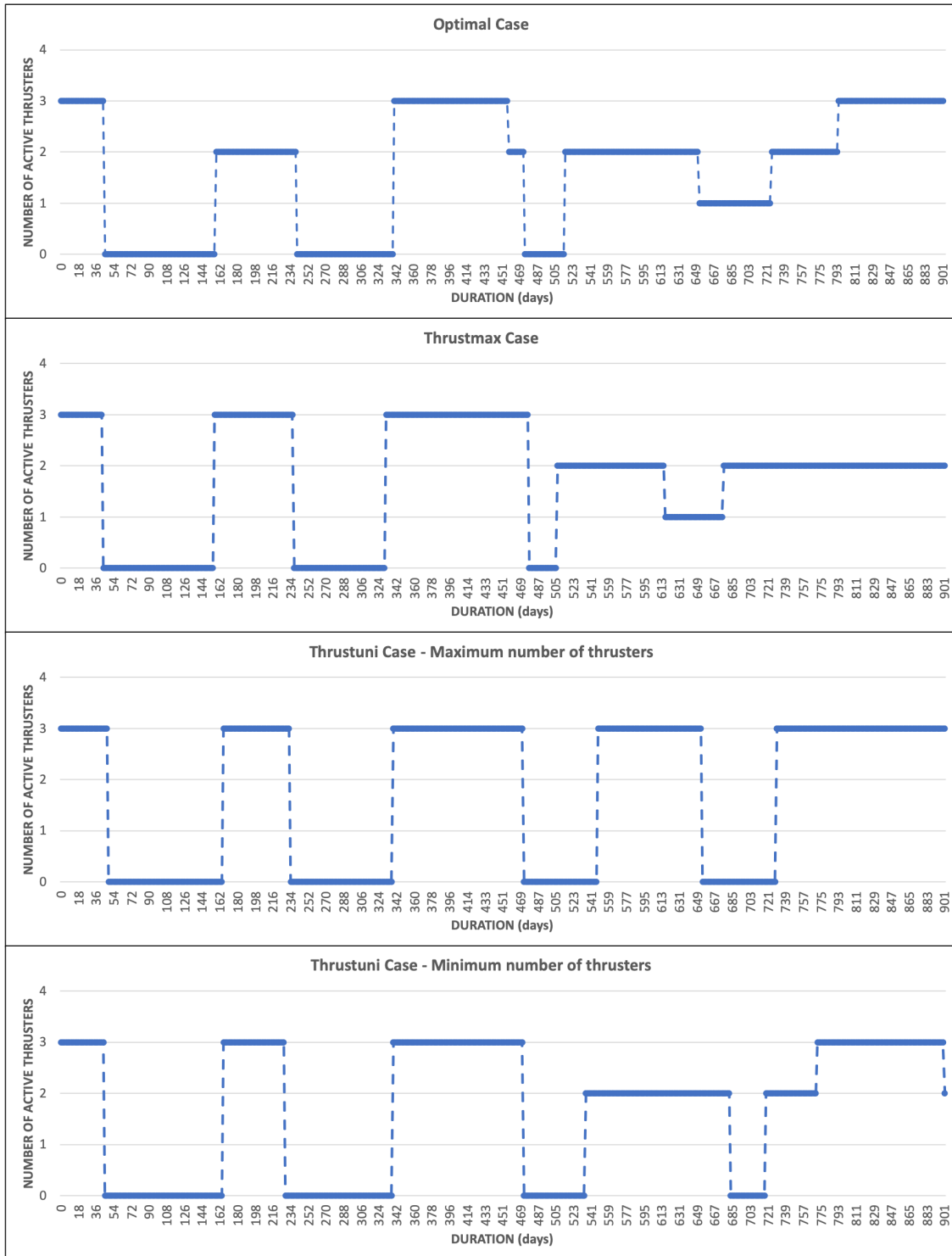


Figure 8.1: Number of active thrusters during the mission

In the 4 cases the mission starts with all the thrusters on, turning off respectively on days 45, 43, 49 and 45. The thrusters turn off, that is they do not produce thrust, when the thrust coefficient (*switching function*) is negative,  $S_f < 0$ . From day 159 to day 240 it is noted that in the optimal case only 2 thrusters are used compared to the 3 used in the other cases, indicating that less thrust is needed. This is mainly due to the higher specific impulse (and therefore to the higher effective exhaust velocity) that the optimal case presents, in the same period, compared to the other three cases. The main differences are from around 475<sup>th</sup> day: in the optimal case there is an alternation of periods in which there are 1, 2 or 3 thrusters on, then ending the mission with 3 thrusters on, while in the "thrustmax" case there is an alternation of periods in which there are 1 or 2 thrusters on, then ending the mission with 2 thrusters on. Instead, in the remaining cases in which the power is distributed uniformly, it is possible to have either all thrusters on (and at the same power) or all thrusters off for the "Maximum number of thrusters" case, while in the "Minimum number of thrusters" case there are intervals in which all 3 thrusters are needed and other intervals in which there are conditions for turning off a thruster.

The available power along a trajectory influences the performance in terms of propellant consumption. This aspect may be clearly visible in Figure (8.2), that shows how the available power is distributed for the three thrusters.



Figure 8.2: Power partitioning between thrusters

The light blue curve is the power  $P_a$  which is available for thrusting, and depends on the spacecraft's position relative to the Sun. The blue, orange and grey curves are the electric power  $P_i$  used by each thruster, while the yellow curve is the cumulative power  $P_T$  used by all the three thrusters. The available power follows an oscillatory trend between a maximum of about  $46kW$  and a minimum of about  $21kW$ . As for the power of a single engine, it is between a maximum value of  $13.95kW$  and a minimum value of  $7kW$ . Eros was chosen because, being quite eccentric, the available power varies widely.

The most remarkable features, however, are the arcs that do not use all the available power. In the optimal case, in particular, in the period between  $159^{th}$  and  $240^{th}$  days, even though there would be enough power for the third engine to operate ( $P_a \geq 2P_M + P_m$ ), there are only two thrusters on. On the contrary, in "thrustmax" case and in both "thrustuni" cases, the third thruster is also active and all the available power is used. This result suggests that in the proximity of the zone where thrusting is less convenient an intermediate thrust level at higher effective exhaust velocity (with two or one thruster at maximum power) becomes beneficial.

Compared to the "thrustuni" case in which the power is uniformly distributed among the 3 thrusters, between the optimal case and the "thrustmax" case it is known that T1 and T2 always have the same power except in the period between  $530^{th}$  and  $770^{th}$  days about. Another difference that distinguishes the cases of optimum and "thrustmax" is the trend of the power of T1: while in the "thrustmax" case it always assumes a maximum value of  $13.95kW$ , in the optimal case it can vary. In fact, it decreased in the period between  $575^{th}$  and  $647^{th}$  days and assumed a parabolic trend in the last mission segment, reaching a minimum of  $9.26kW$ . As for T3, in the "thrustmax" case and in the period between  $155^{th}$  and  $235^{th}$  days approximately, it has an average power of about  $9.22kW$  compared to the null power assumed instead in the case of optimum. Furthermore, in the "thrustmax" case, after reaching a minimum power of  $7.23kW$  on the  $475^{th}$  day, it is turned off until the end of the mission.

The arc at low power at the end of the outbound leg of optimal case, is also related to the convenience of having a single thruster at full-power when the available power is limited even though no coast arc is required in its vicinities.

In the two cases in which the power is distributed evenly for the three thrusters, we note how the difference between the two cases occurs in the period of time between 05/07/2023 and 24/02/2024. If in fact in the "Maximum number of thrusters" case you can have either all 3 thrusters on or all off, in the "Minimum number of thrusters" case, in this time interval, you have the conditions to turn off the T3 and use only two. In this way, as you will see from the mass value of the spacecraft on arrival on the asteroid, you can save about 100 kg of fuel.

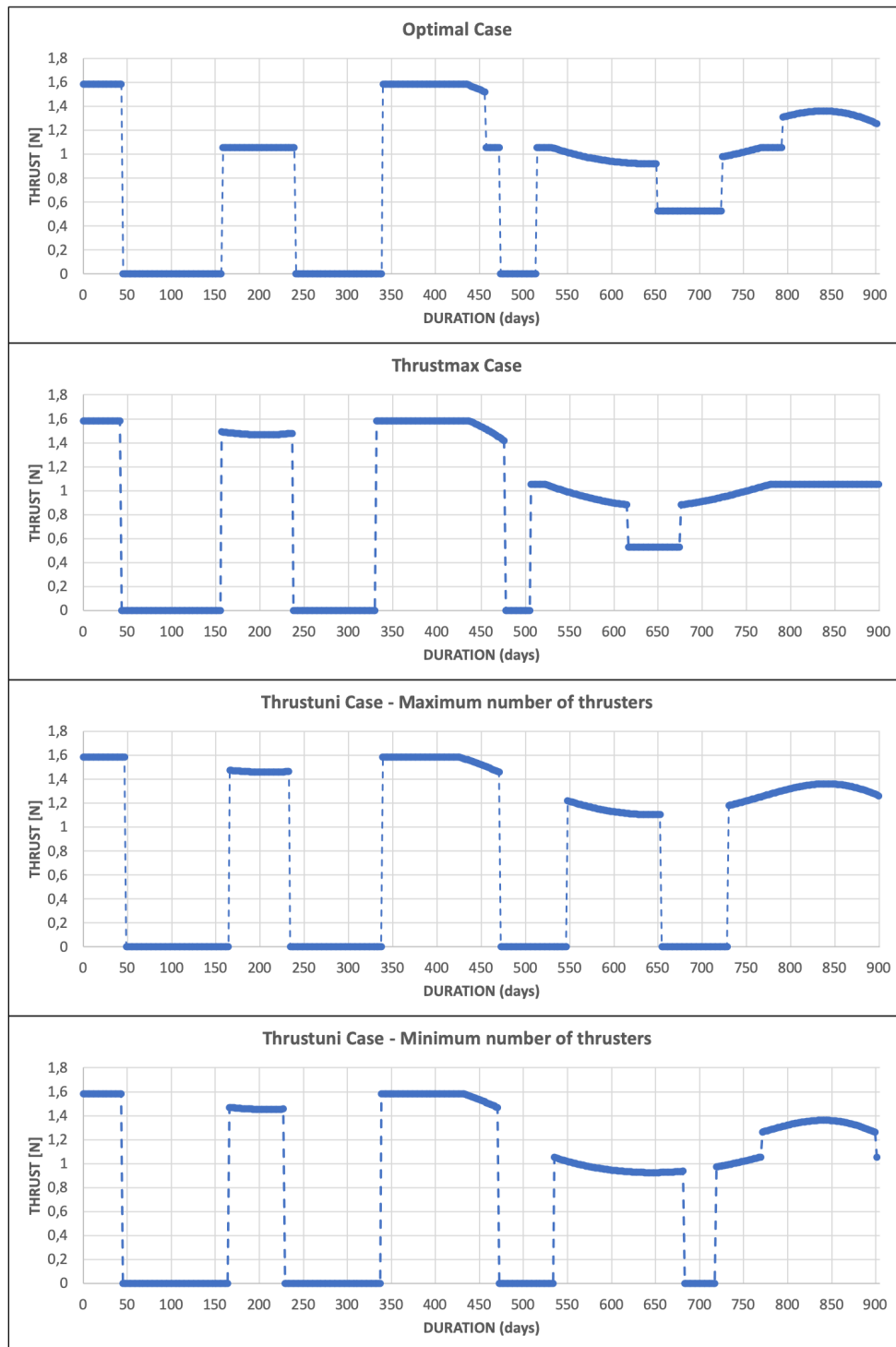


Figure 8.3: Behavior of the thrust during the mission

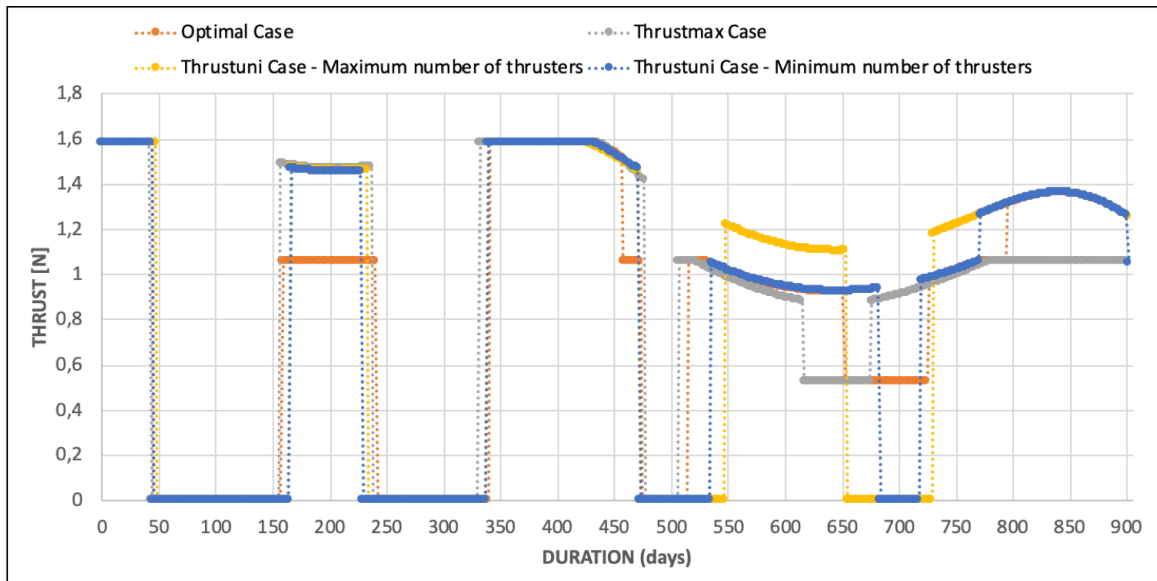


Figure 8.4: Comparison of the thrust for the different cases

Comparing the trend of the thrust for the cases of optimal and "thrustmax", it is noted that the two trends tend to be quite similar to each other, except in the periods between 160<sup>th</sup> and 240<sup>th</sup> days approximately, in which the thrust generated by the "thrustmax" case is higher compared to that generated by the optimum case, and between 795<sup>th</sup> and 901<sup>th</sup> days in which the thrust generated by the optimum case is higher than that generated by the "thrustmax" case. These differences are due to the fact that, in these time intervals, the number of thrusters turned on is different for the two cases.

As regards the thrust generated by the "thrustuni" case, it faithfully follows the trend of the thrust generated by the other two cases, with the difference that it is zero in four time intervals. On the other hand, when it is not equal to zero, it is always equal to or greater than the thrust generated by the other two cases.

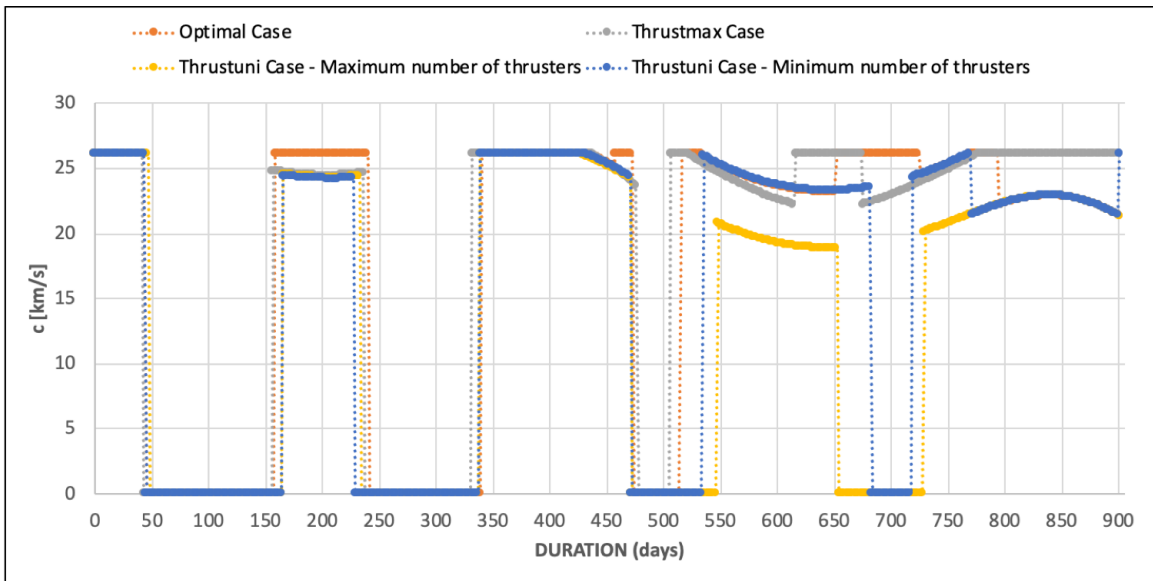


Figure 8.5: Comparison of the effective exhaust velocity for the different cases

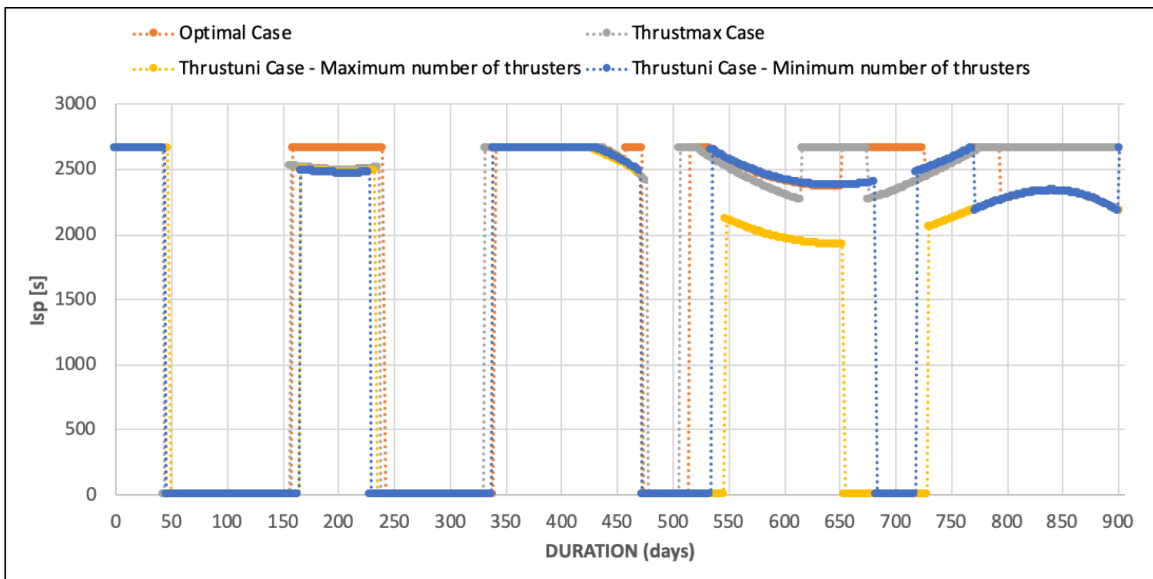


Figure 8.6: Comparison of the specific impulse for the different cases

If, however, you go to see the trend of the specific impulse, you notice how the optimal case presents a higher specific impulse for most of the mission. This difference is very evident between the optimal case and the "Maximum number of thrusters" case, while compared to the "thrustmax" and "Minimum number of thrusters" cases, the optimal case has advantages but not so relevant (except in the vicinity of 700<sup>th</sup> days in which the difference is more marked).

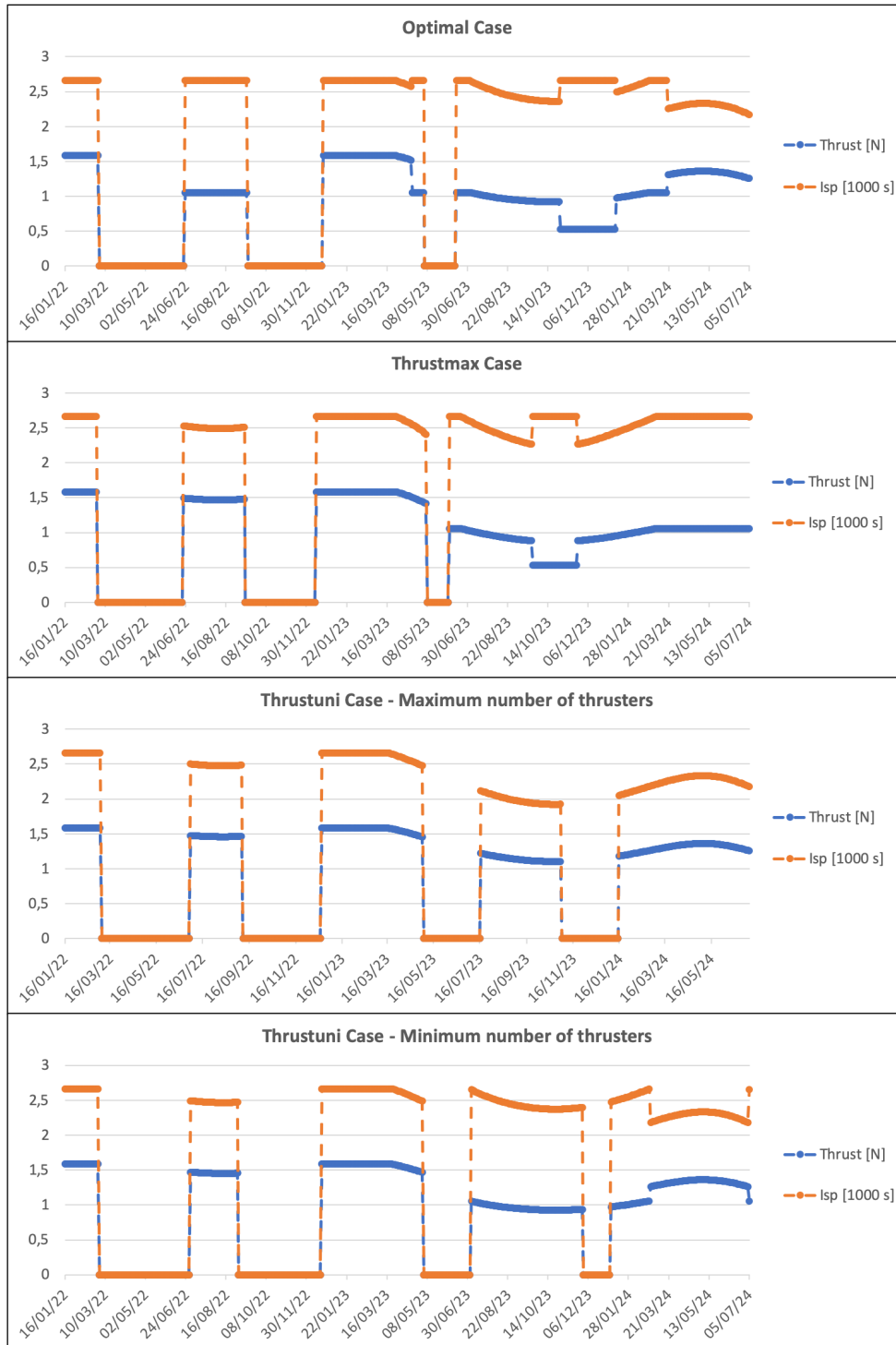


Figure 8.7: Comparison between the thrust and the specific impulse during the mission for the different cases

The optimal control law is compared to the values that would be assumed for the "thrustmax" case for a uniform power repartition on the same trajectory.

It confirms that arcs with lower thrust level are used in convenient places to better use the propellant with a larger specific impulse.

The table:

Strategy	$m_1[kg]$
optimal	7409
thrustmax	7329
Maximum thrusters	7274
Minimum thrusters	7382

shows the values of the final mass of the spacecraft upon arrival on the asteroid, for the 4 cases.

It is easy to understand how the case concerning the optimal power partitioning has the largest final mass, indicating that there has been less propellant consumption. Again from the consumption point of view, the worst case is therefore the "Maximum number of thrusters" case, in which the power is distributed uniformly for the 3 thrusters, either all on or all off.

These results reflect the trend of the effective exhaust velocity and the specific impulse.

In Figure (8.8) is shown the outbound trajectory (projected in the ecliptic plane), where departure and arrival points are marked with an asterisk on the respective orbit.

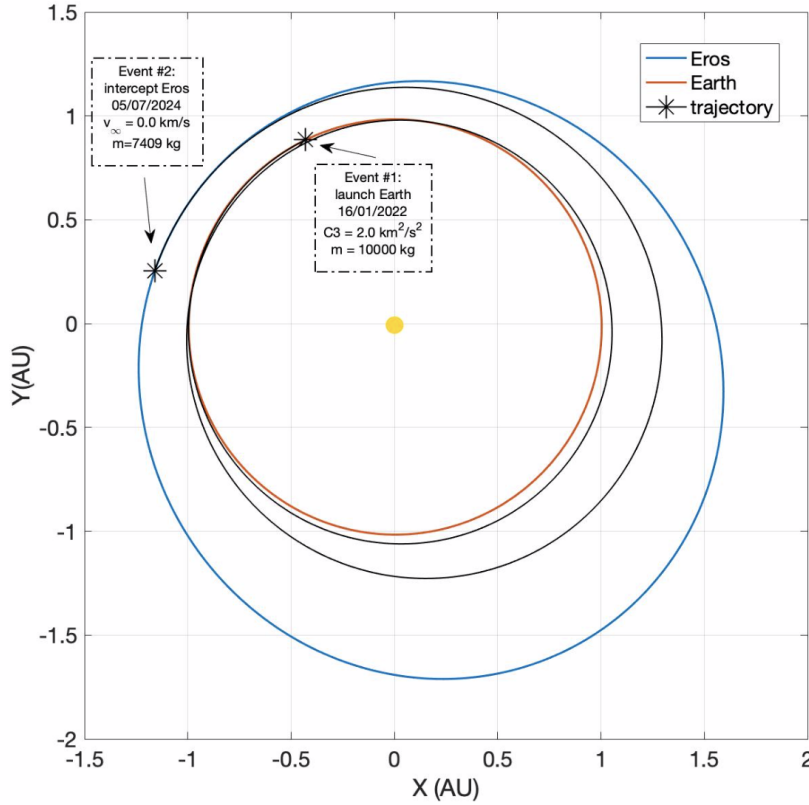


Figure 8.8: 2D Trajectory

From the figures (8.8) and (8.10) and from the trend of the available power, it can be seen that there are two passages near the perihelion (including departure) and one passage near the aphelion. This is because we prefer to push much with small radii (perihelion) and less with large radii (aphelion), in order to have a lower consumption and therefore energy expenditure. In fact, according to the formula of energy variation:

$$\Delta\xi = V\Delta V \tag{8.1}$$

there is an energy gain  $\Delta\xi$  at the expense of a cost  $\Delta V$ . In order for this cost to be minimal, with the same variation of energy, we want a high speed  $V$  and, considering a circular speed (as if the orbit for the moment was circular and not elliptical), we would have that:

$$V = \sqrt{\frac{\mu}{r}} \tag{8.2}$$

Therefore, with small radii (perihelion in an elliptical orbit), you will have a greater speed.

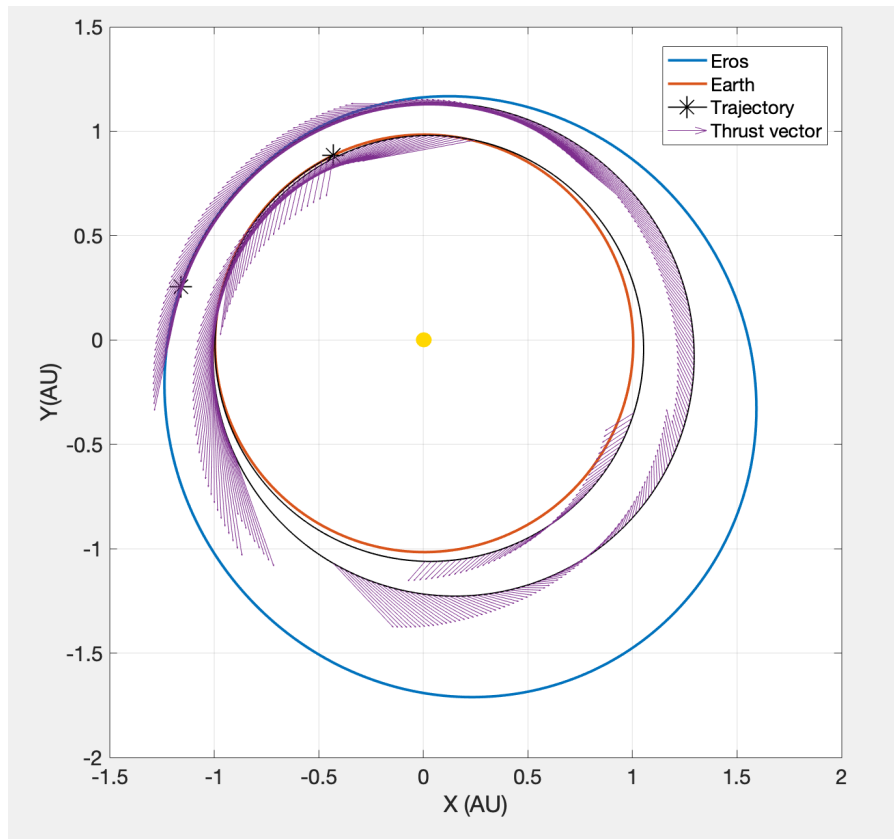


Figure 8.9: Thrust vectors along trajectory

In Figure (8.9) the thrust vectors along the departure 2D trajectory are shown. From this visualization is clear once again that the number of switched on engines depends on the spacecraft's position relative to the Sun. For this reason, the thrust segment with the greatest intensity of thrust vectors (about 1.6 N) are placed in the most efficient positions in terms of available power, namely in proximity of the perihelion of the outbound trajectory. It is also possible to notice how thrust vectors in this case (and in almost every outbound trajectory) are substantially tangential to the trajectory.

By analysing Figures (8.10) and (8.11) it is possible to understand how the inclination of the trajectory varies along the journey. The angle  $\phi$  is the angle between the position vector of the spacecraft and the ecliptic plane, where a reference frame centered in the Sun is used. As one can see, inclination varies only when trajectory passes for one of the nodes, and it remains unchanged between the passages. This is clearly visible also in the 3D vision of the trajectory, where the Z scale is enlarged to highlight the inclination of Eros' orbit.

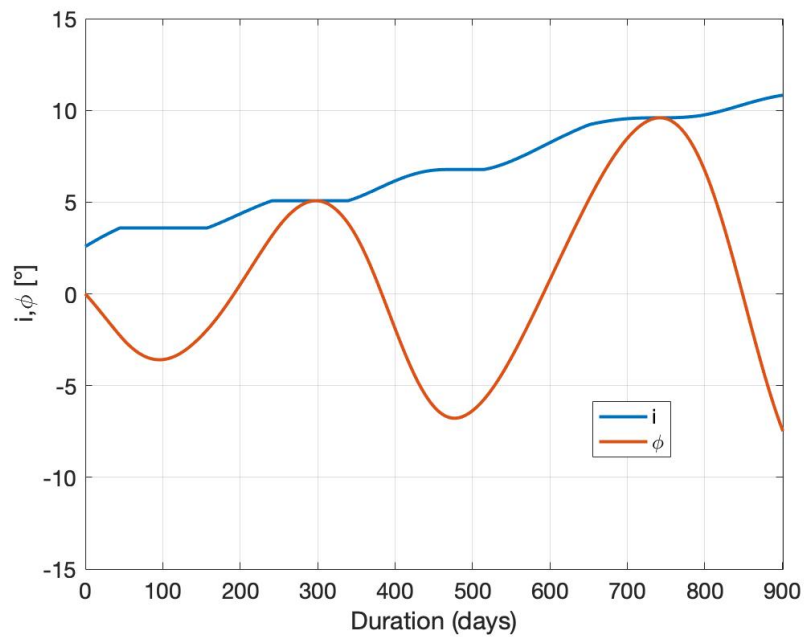


Figure 8.10: How inclination of the trajectory and angle  $\phi$  vary during the mission for *optimal case*

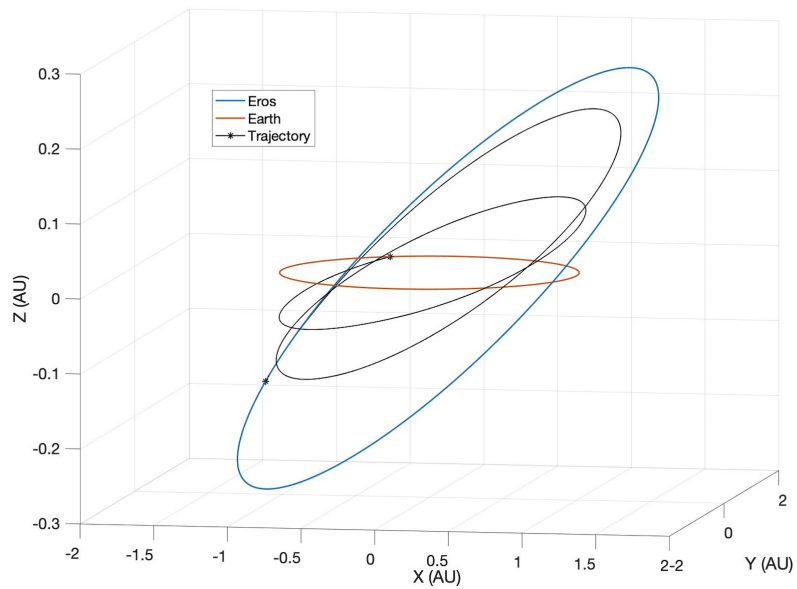


Figure 8.11: 3D Trajectory

### 8.1.2 Inbound Flight

A similar analysis can be made for the inbound flight. In this case the optimization index to be maximized is the initial mass  $m_2$  departing from Eros.

As said, the inbound journey is characterized by the period of fly-by. Choosing a proper period of time, in base of the arrival date of the outbound trajectory, the inbound journey has a fly-by in February 2026 and a value of the initial mass  $m_2$  about 12000 kg. The above mentioned geometric aspects, together with the available electric power, are again critical for a positive or negative performance in terms of optimized mass. More in detail, since the amount of propellant for the inbound journey is the same for every trajectory, the key for a better result is how efficiently it is possible to manage this amount of propellant in the Eros-Earth segment, in order to have a greater mass of propellant left to assist the fly-by in breaking the spacecraft and changing the plane towards the ecliptic plane.

In Figure (8.12) is shown how the number of active thrusters varies during the mission for the four cases.

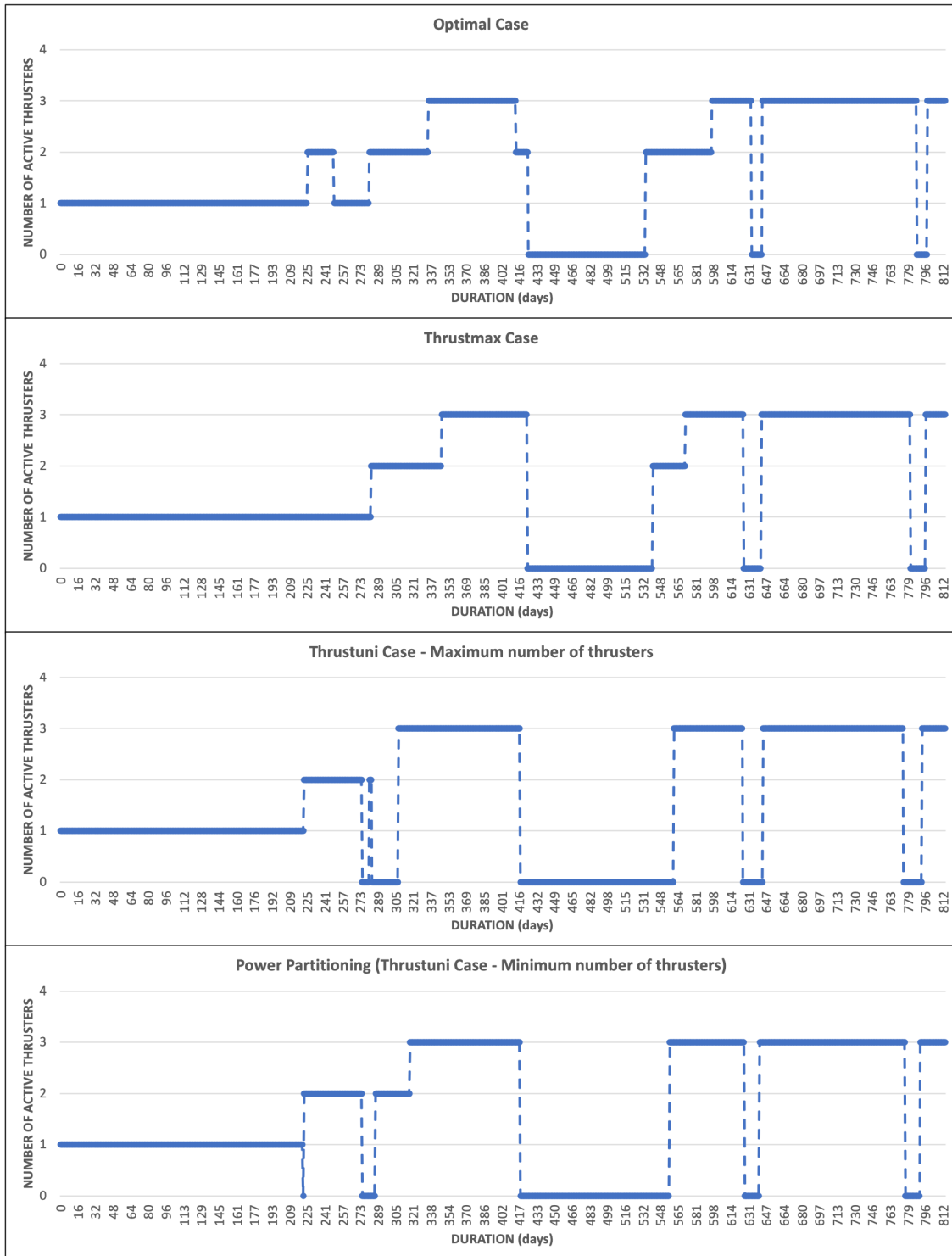


Figure 8.12: Number of active thrusters during the mission

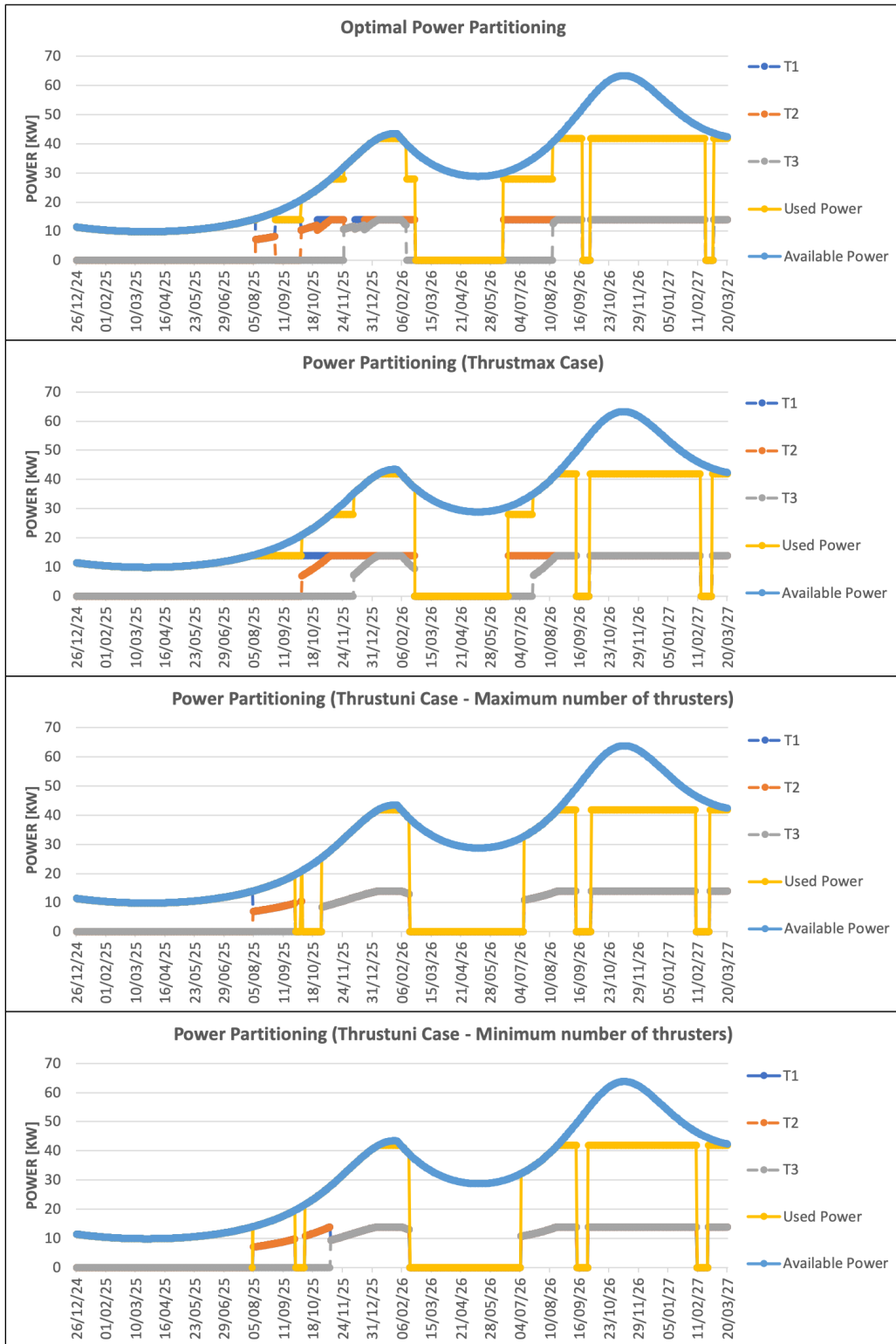


Figure 8.13: Power partitioning between thrusters

From the figure (8.13) it is possible to notice the trend of the available power. It is evident that in the first mission segment there is a very low available power so that only one thruster can be turned on. This is due to the fact that in this section you are close to the aphelion. As you approach the perihelion, or in any case the Earth's orbit, the distance between the Sun and the spacecraft  $r$  decreases allowing to obtain higher available powers. In particular, there are two peaks of the  $P_a$ : the first peak of about 43 kW occurs near the flyby, the second peak of about 63 kW occurs in the last mission segment as it is in the point of the trajectory closest to the Sun.

As for the power partitioning between the thrusters, in the first mission segment in which the available power is very low, it is exploited completely first by T1 and then by T2. It is noted that the conditions for turning on the T3 arrive very late, just before the flyby. Immediately after the flyby it can be seen that all thrusters are turned off for a fairly long period.

The only big difference between the cases occurs when the thrusters are turned on again after the period in which they were turned off. Note how, even if there are available powers that allow the ignition of all three thrusters ( $P_a > 3P_m$ ), in the optimal and "thrustmax" cases it is preferred to have T1 and T2 at maximum power and T3 off, while in the two "thrustuni" cases the available power is correctly distributed uniformly between the three thrusters. Only when  $P_a > 2P_M + P_m$  the T3 is switched on, first in the "thrustmax" case and a little later in the optimal case. This is explained by looking at the figure (8.18): the optimal case presents a higher  $Isp$  for a longer mission range, and this entails the possibility of re-starting the T3 later, as the maximum  $Isp$  is used for reduce the thrust produced and therefore the consumption.

In the last mission segment, having a very high available power, all thrusters are exploited at maximum power until the end of the mission.

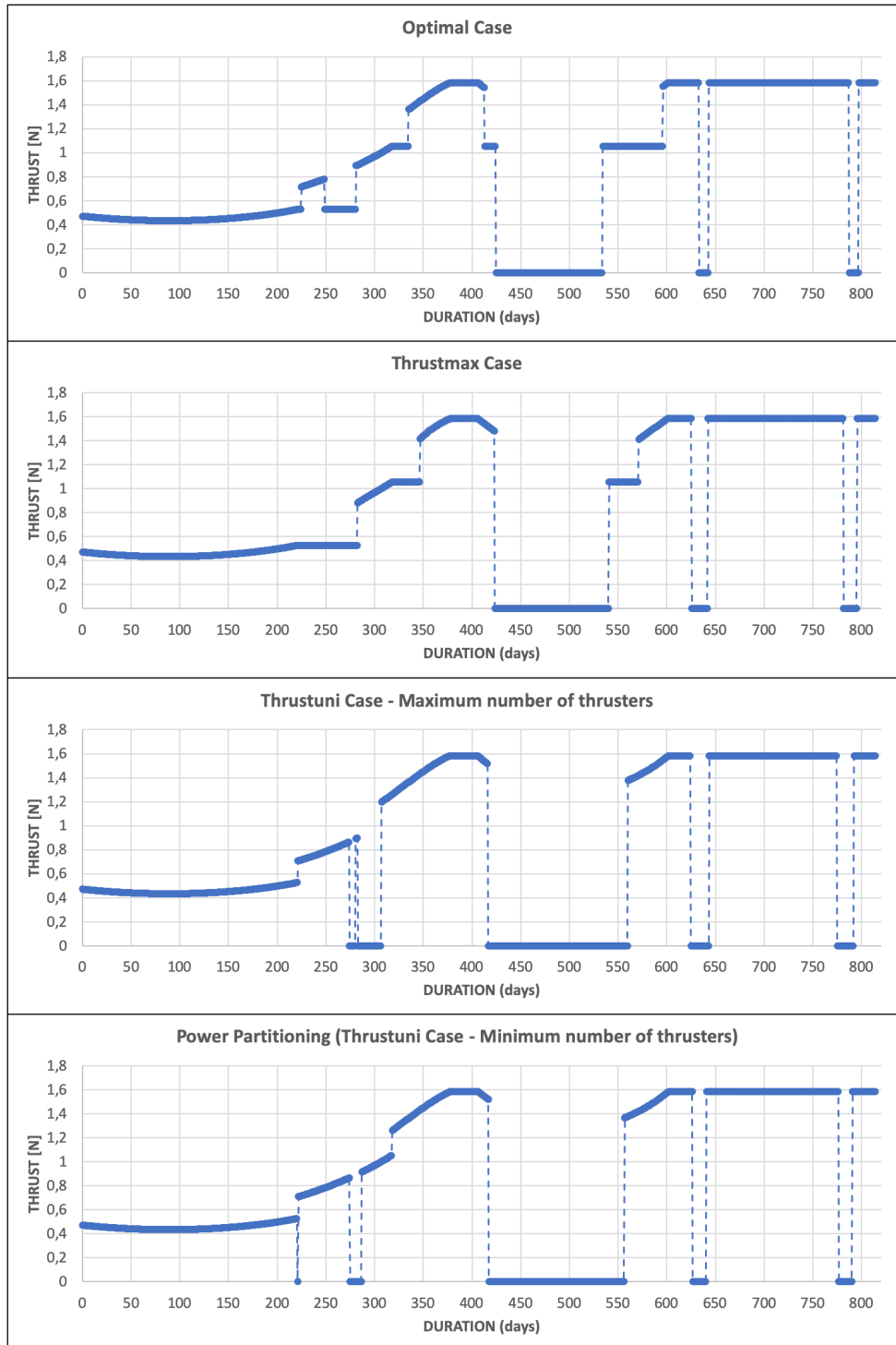


Figure 8.14: Behavior of the thrust during the mission

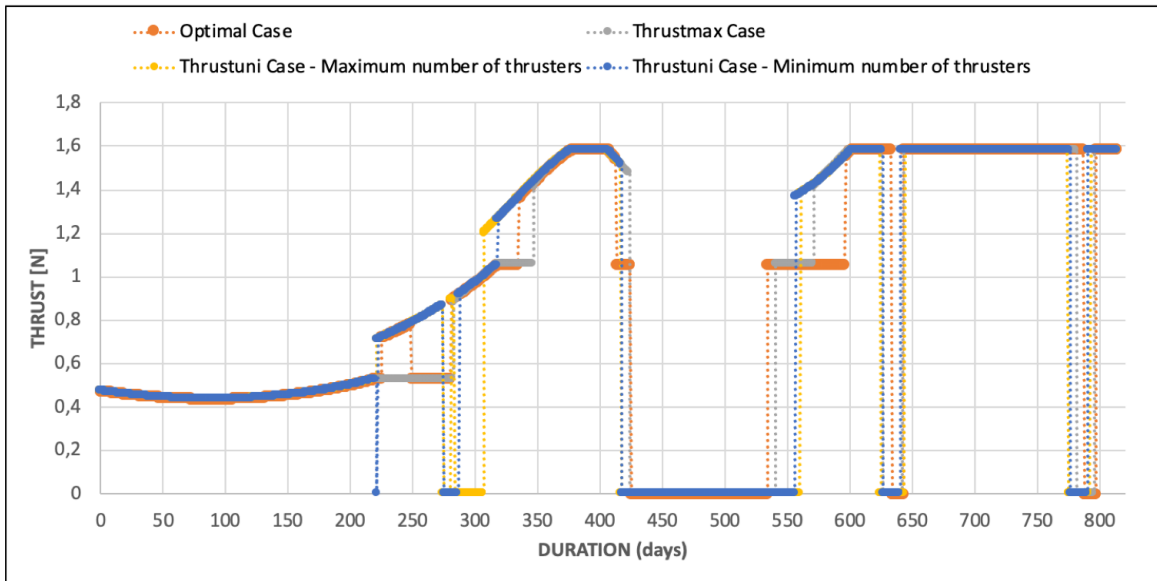


Figure 8.15: Comparison of the thrust for the different cases

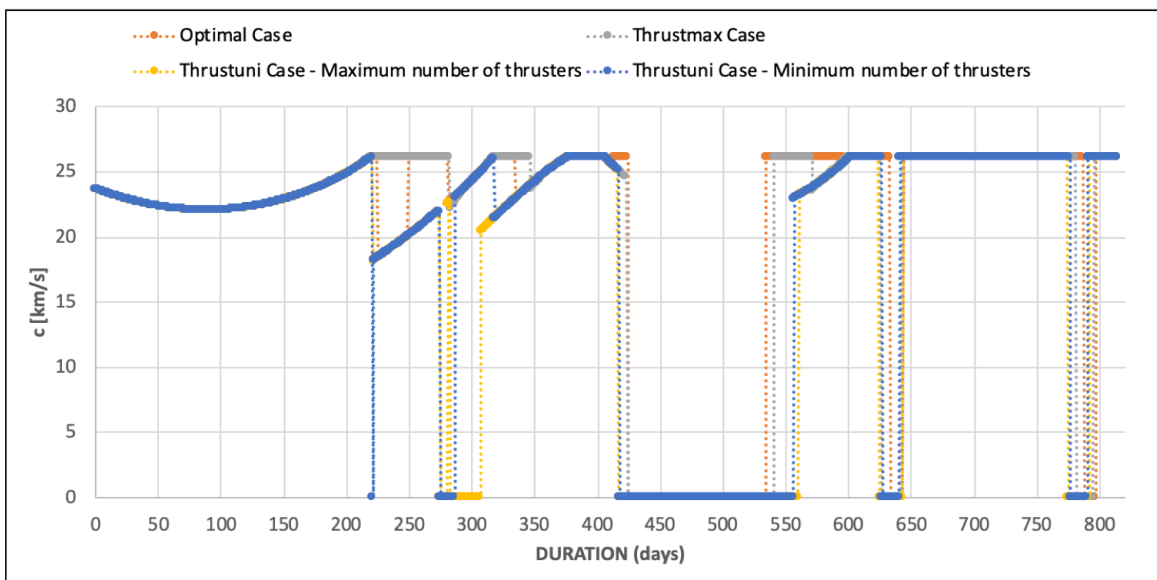


Figure 8.16: Comparison of the effective exhaust velocity for the different cases

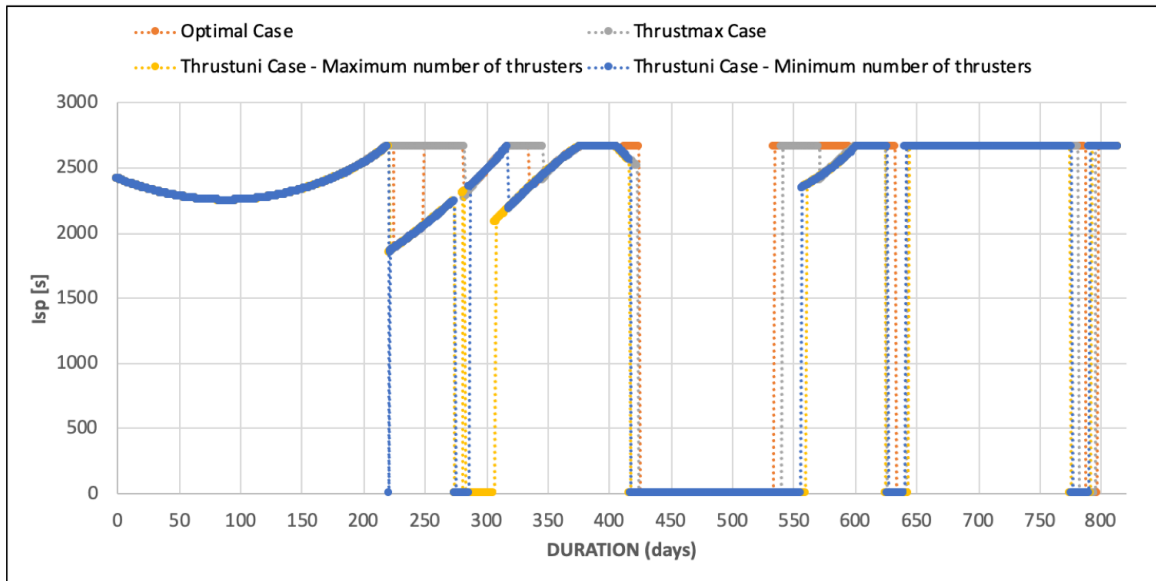


Figure 8.17: Comparison of the specific impulse for the different cases

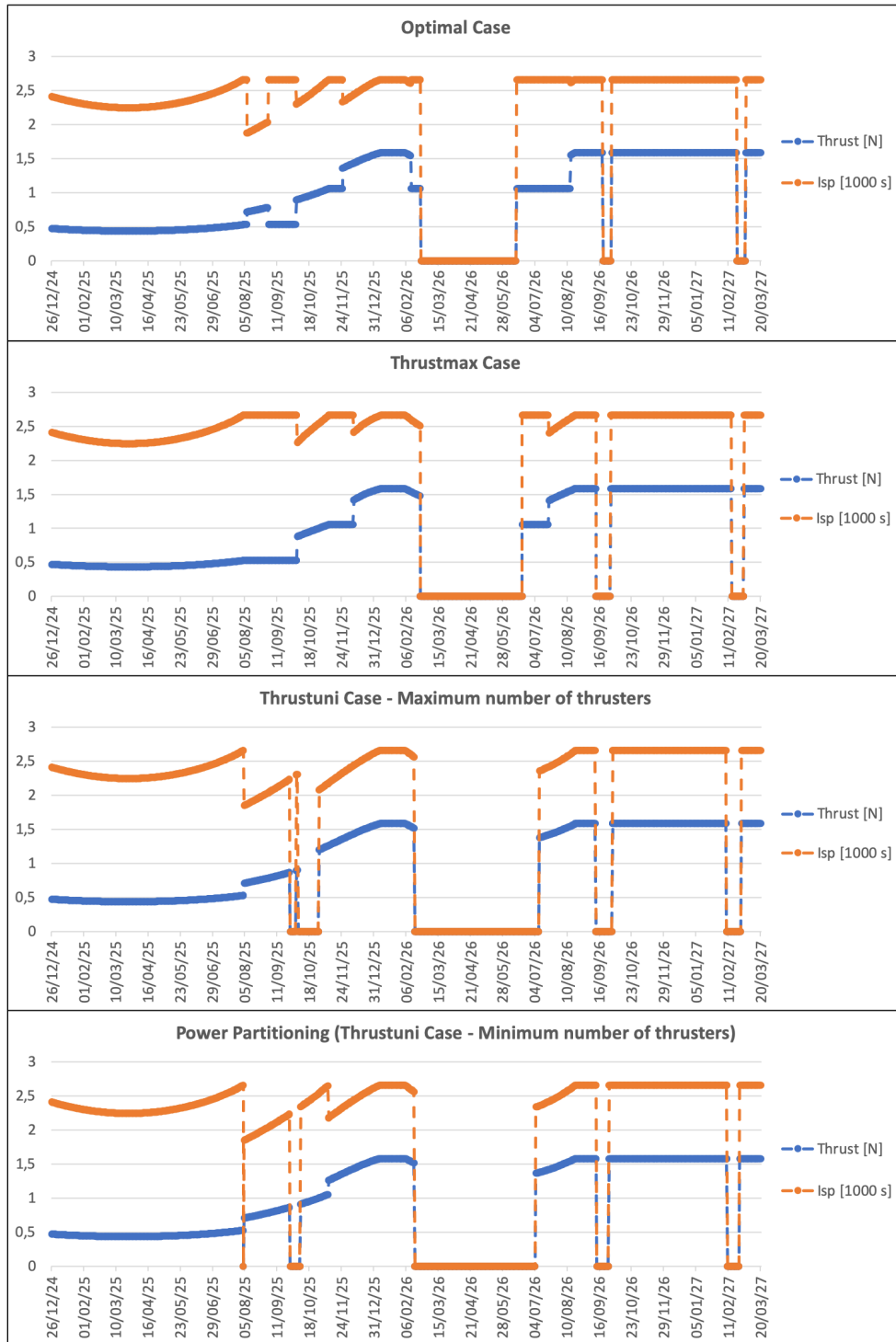


Figure 8.18: Comparison between the thrust and the specific impulse during the mission for the different cases

As mentioned previously, the objective of the mission is to maximize the mass of the boulder taken from the asteroid, or to maximize the mass of departure from the asteroid  $m_2$ . The mass of the boulder is equal to  $m_2 - m_1$ , that is the difference between the mass of departure from the asteroid  $m_2$  minus the mass of arrival on the asteroid  $m_1$ . In this case, however, not knowing the mass  $m_2$ , we obtain the  $m_{boulder}$  in another way: given the arrival mass on the asteroid  $m_1$ , we calculate the mass of propellant remaining from the formula  $m_1 - 5000kg$  (about 2400 kg) and, through the iterative calculation, we proceed to the calculation of the mass of the spacecraft upon arrival on Earth  $m_f$ , assuming that it has been consumed all fuel on board. From this mass, subtracted the 5000 kg of dry mass, the maximized boulder mass is obtained which, added to the mass of the spacecraft upon arrival on the asteroid, provides the optimal mass of the spacecraft departing from the asteroid for the inbound flight .

Strategy	$m_1[kg]$	$m_2[kg]$	$m_f[kg]$	$m_{boulder}[kg]$
optimal	7409	12181	9772	4772
thrustmax	7329	11915	9586	4586
Maximum thrusters	7274	11630	9356	4356
Minimum thrusters	7382	12007	9625	4625

Table 8.2: Results of indirect optimization

Also for the inbound flight, from table (8.2) it can be seen how with the optimal distribution of power it is possible to take from the asteroid a boulder heavier than 4% compared to the "thrustmax" case and 9% compared to the "maximum number of thrusters" case, which is therefore the worst.

The inbound trajectory is shown in Figure (8.19):

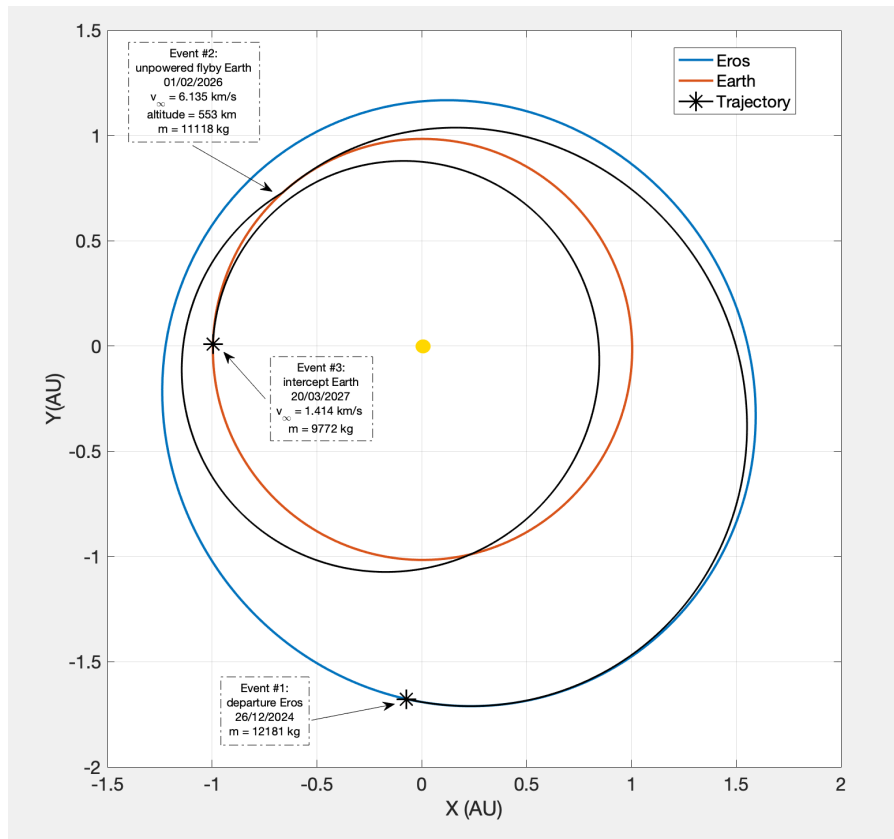


Figure 8.19: 2D Trajectory

The spacecraft leaves Eros in December 2024 with an initial mass about 12000 kg and intercept Earth in March 2027 with a final mass about 9700 kg. Even in this case, departure and arrival epochs are marked with an asterisk on the respective orbit.

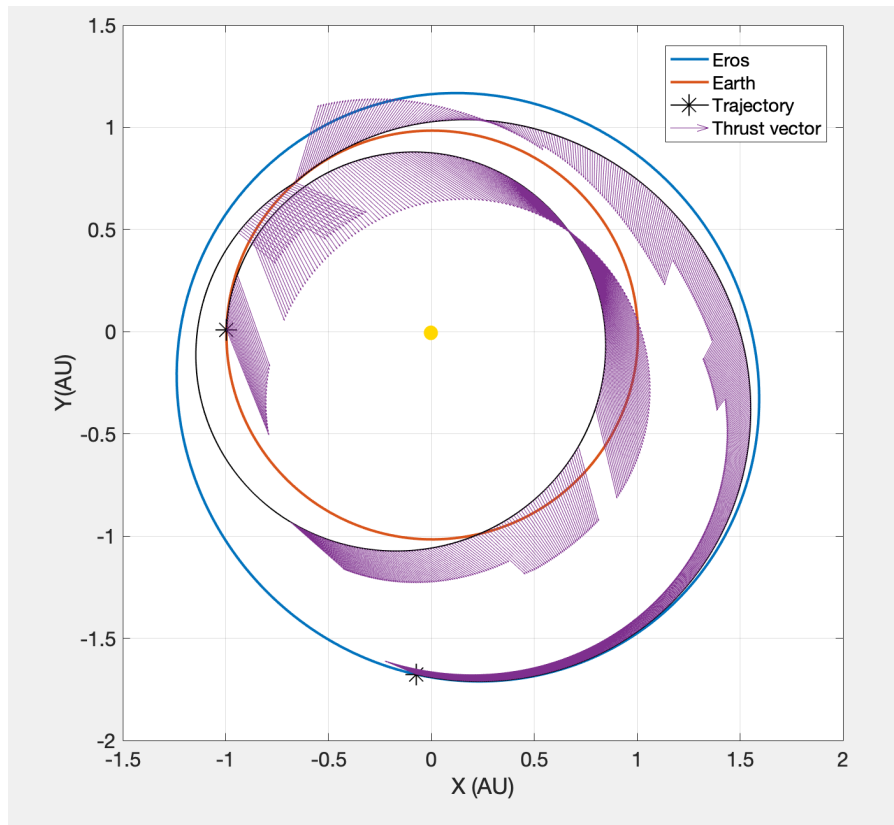


Figure 8.20: Thrust vectors along trajectory

In Figure (8.20) the thrust vectors along the fly-by 2D trajectory are shown. This visualization confirms, as shown in Figure (8.13), that in this case almost all of the propellant is used to break the spacecraft after the Earth fly-by. Unlike the trajectory in Figure (8.9), in this case (and in almost every inbound trajectory) thrust vectors have a significant radial component and are mostly not tangential to the trajectory.

In the graph of  $\phi$  and inclination of the trajectory is possible to see how almost all the inclination variation is due to the Earth fly-by. This is also clearly visible in the 3D vision of the trajectory, where again the Z scale is enlarged. These graphs are shown in Figure (8.21) and (8.22).

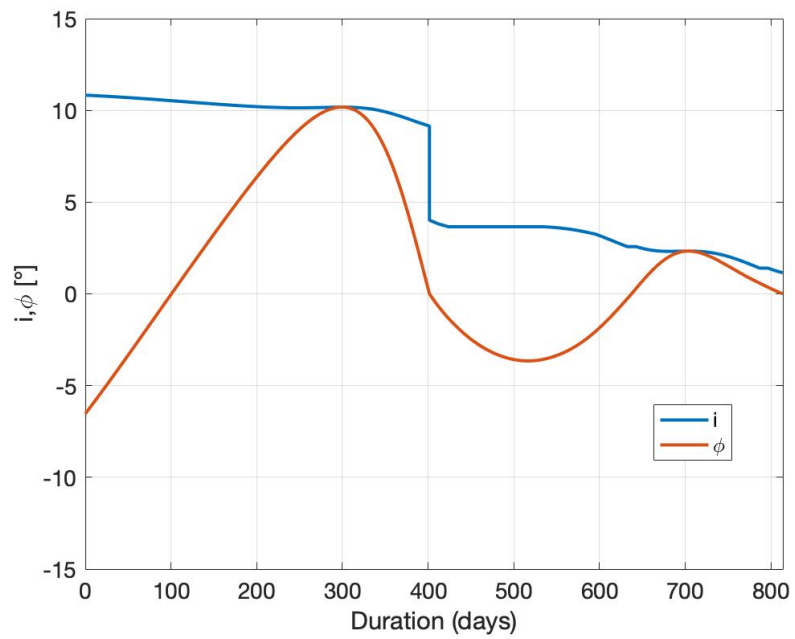


Figure 8.21: How inclination of the trajectory and angle  $\phi$  vary during the mission for *optimal case*

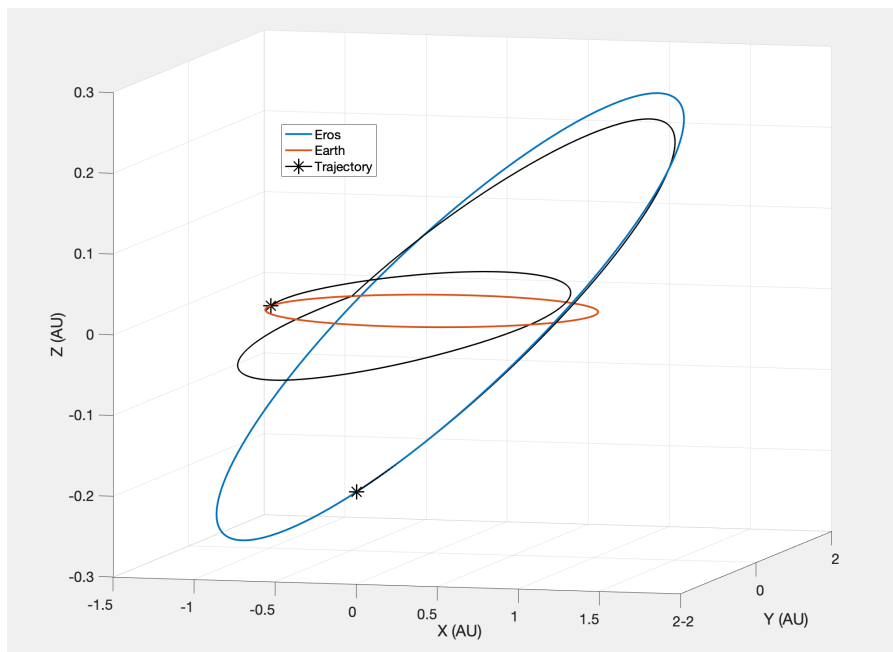


Figure 8.22: 3D Trajectory

# Chapter 9

## 2008EV5 Asteroid

(341843) 2008 EV5, is a sub-kilometer asteroid, classified as a near-Earth object and potentially hazardous asteroid of the *Aten group*, approximately 400 metres (1,300 feet) in diameter. It was discovered on 4 March 2008, by astronomers of the *Mount Lemmon Survey* at *Mount Lemmon Observatory* near Tucson, Arizona, United States.

2008 EV5 was the preliminary baseline target of NASA's proposed *sample-return Asteroid Redirect Mission*. [13]

Aphelion	1.0381 AU
Perihelion	0.8783 AU
Semi-major axis	0.9582 AU
Eccentricity	0.0834
Orbital period	0.94 years
Mean anomaly	123.95°
Inclination	7.4374°
Longitude of ascending node	93.382°
Argument of perihelion	234.85°

Table 9.1: Orbital elements of 2008 EV5 at the epoch 27 April 2019 (JD 2458600.5) [2]

### 9.1 2008EV5 Results

#### 9.1.1 Outbound Flight

In Figure (9.1) is shown how the number of active thrusters varies during the mission for the three cases.

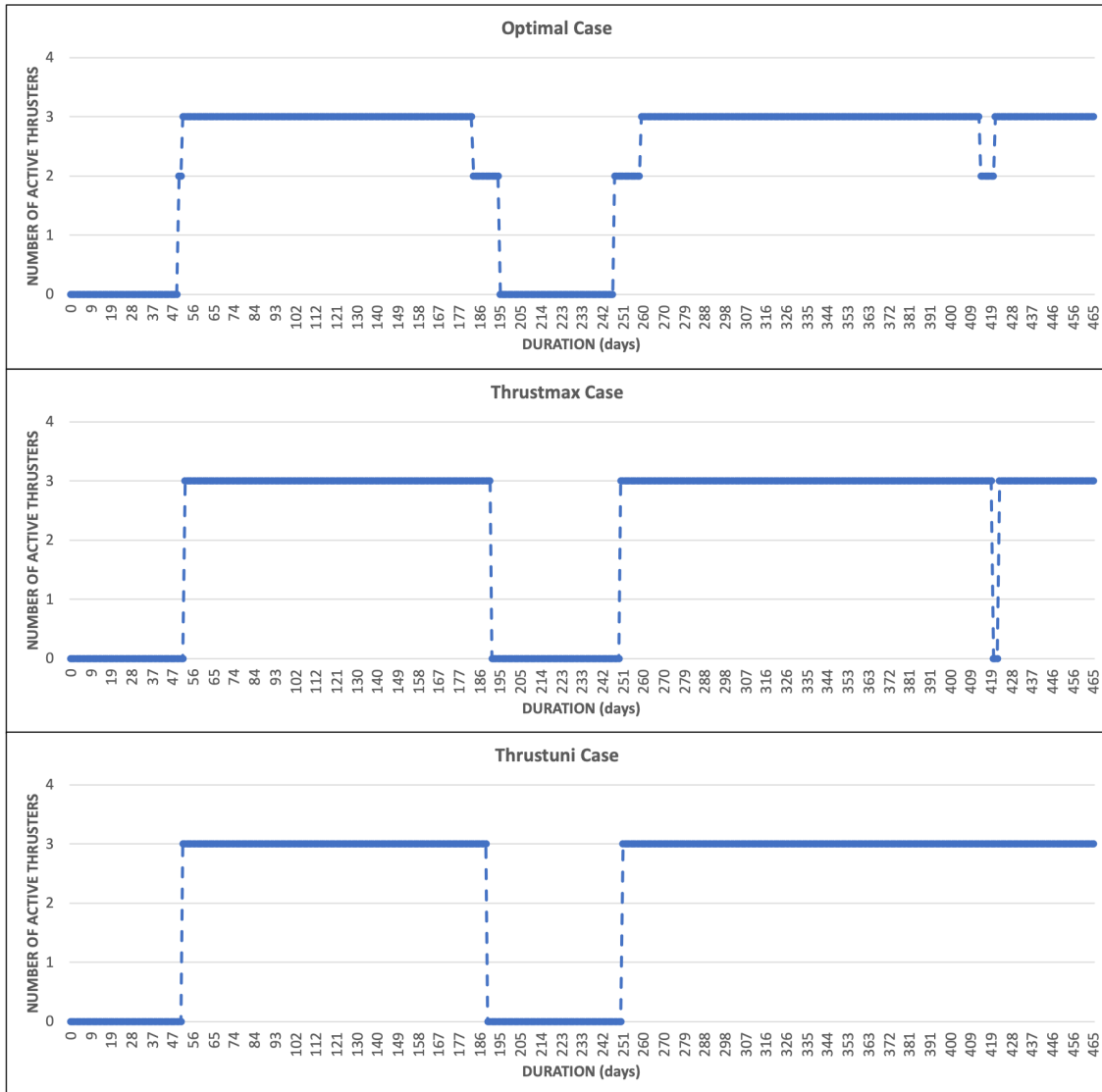


Figure 9.1: Number of active thrusters during the mission

In the first place it must be underlined how the asteroid 2008EV5 being much closer to the Earth, allows to be reached in a much shorter period. The outbound flight has in fact a duration of about 465 days, compared to the 900 days needed to arrive on the asteroid Eros.

From figure (9.1) it can be seen that for the majority of the mission all three thrusters are turned on, and this applies to all the cases examined.

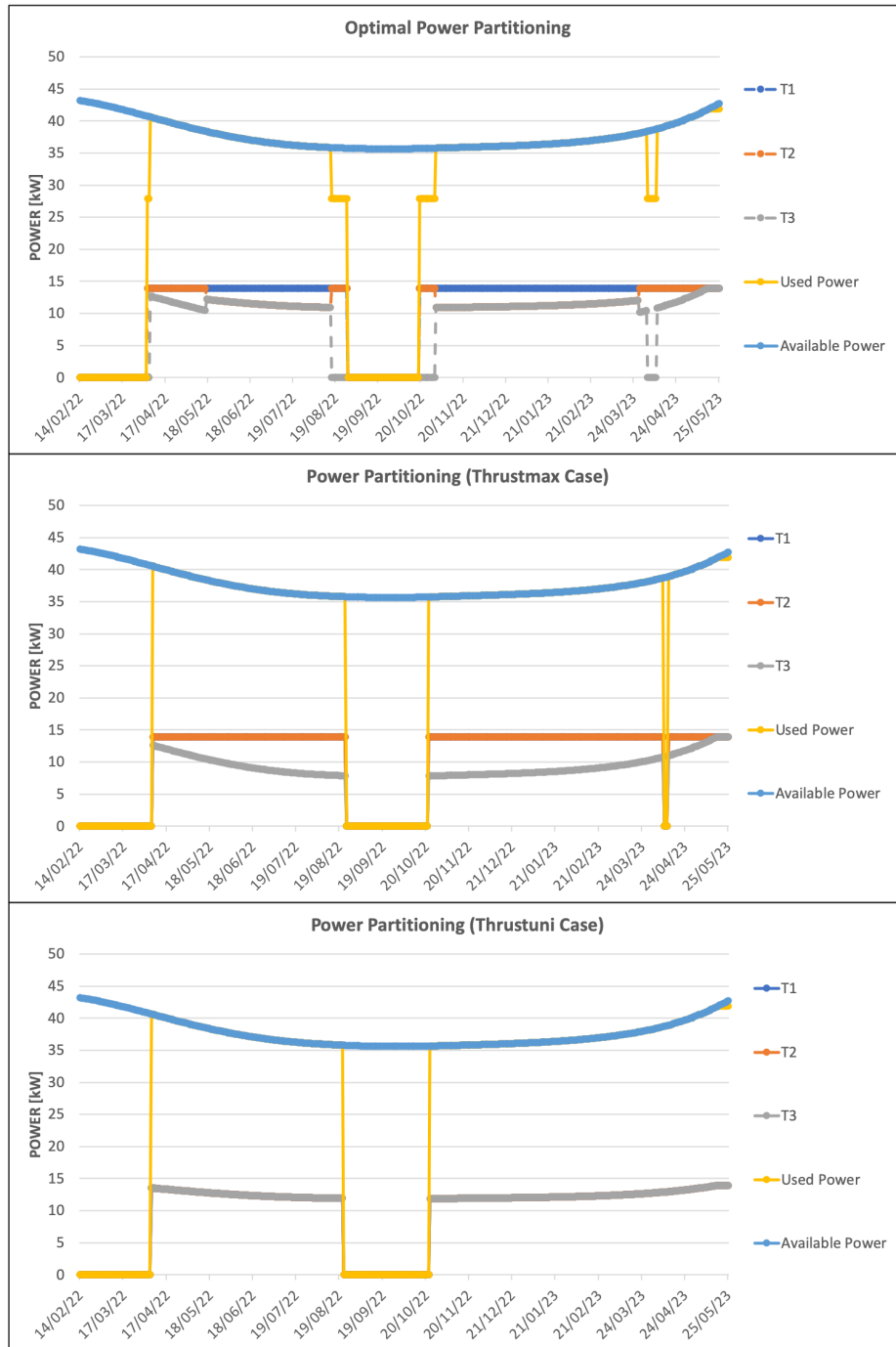


Figure 9.2: Power partitioning between thrusters

The asteroid 2008EV5 was chosen precisely because, being much less eccentric than Eros, it presents a much less variable variation in the available power. In fact, it has a parabolic trend and is between a maximum of 43 kW and a minimum of 35 kW. Therefore,

having high available powers for the whole mission, and being  $P_a > 2P_M + P_m$ , there are the conditions to have all three thrusters on for the whole mission. Only the optimal case has three arcs in which the T3 is turned off, despite the conditions for turning it on. This is because, from figure (9.5), it can be seen that in those arches there is a greater specific impulse, so we prefer to have less thrust but a higher  $I_{sp}$  to consume less.

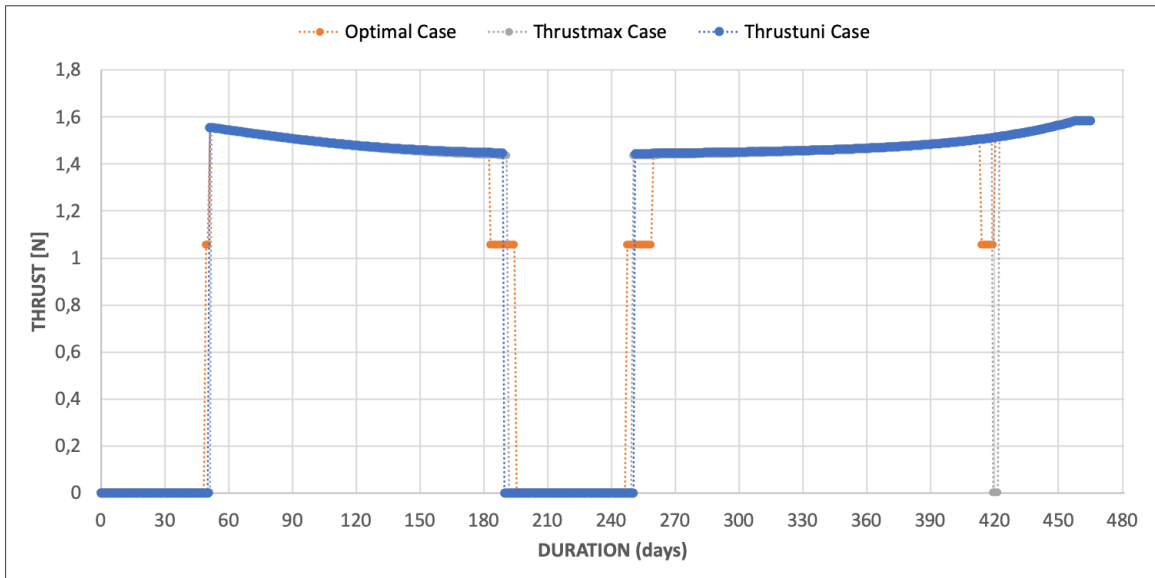


Figure 9.3: Comparison of the thrust for the different cases

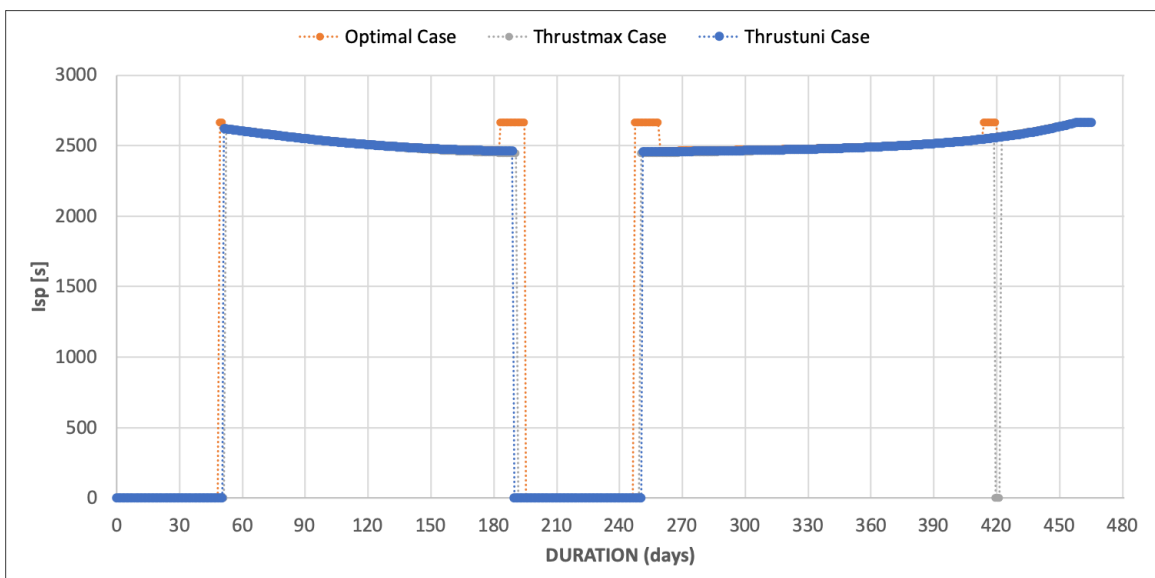


Figure 9.4: Comparison of the specific impulse for the different cases

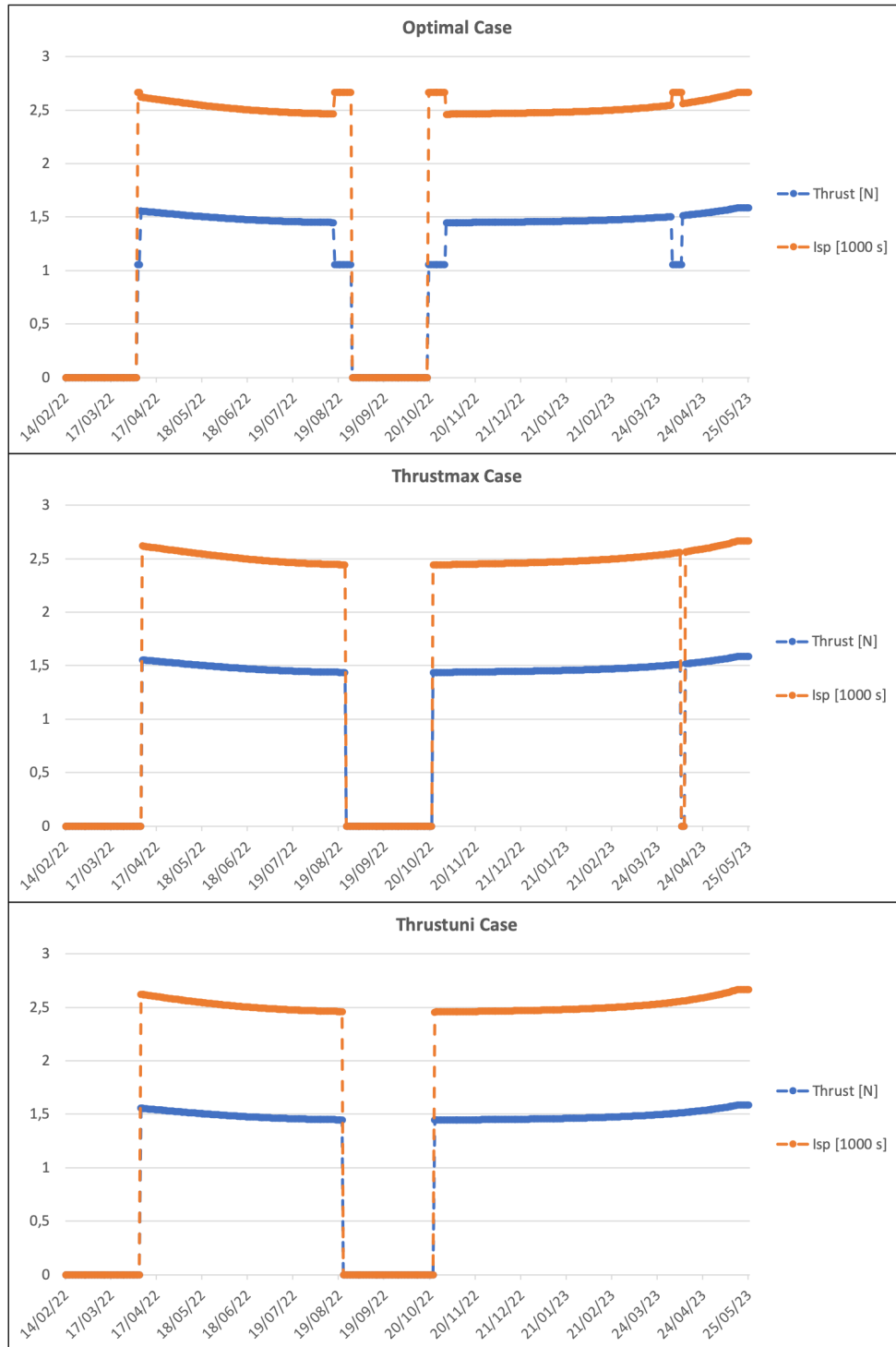


Figure 9.5: Comparison between the thrust and the specific impulse during the mission for the different cases

The table:

Strategy	$m_1[kg]$
optimal	8166
thrustmax	8153
thrustuni	8161

shows the values of the final mass of the spacecraft upon arrival on the asteroid, for the 3 cases.

It is clearly visible how the variations of  $m_1$  for the different cases are smaller than asteroid Eros. Due to the less eccentricity, asteroid 2008EV5 allows to have a smaller variation of available power. This is why the results are similar.

In Figure (9.6) is shown the outbound trajectory (projected in the ecliptic plane), where departure and arrival points are marked with an asterisk on the respective orbit.

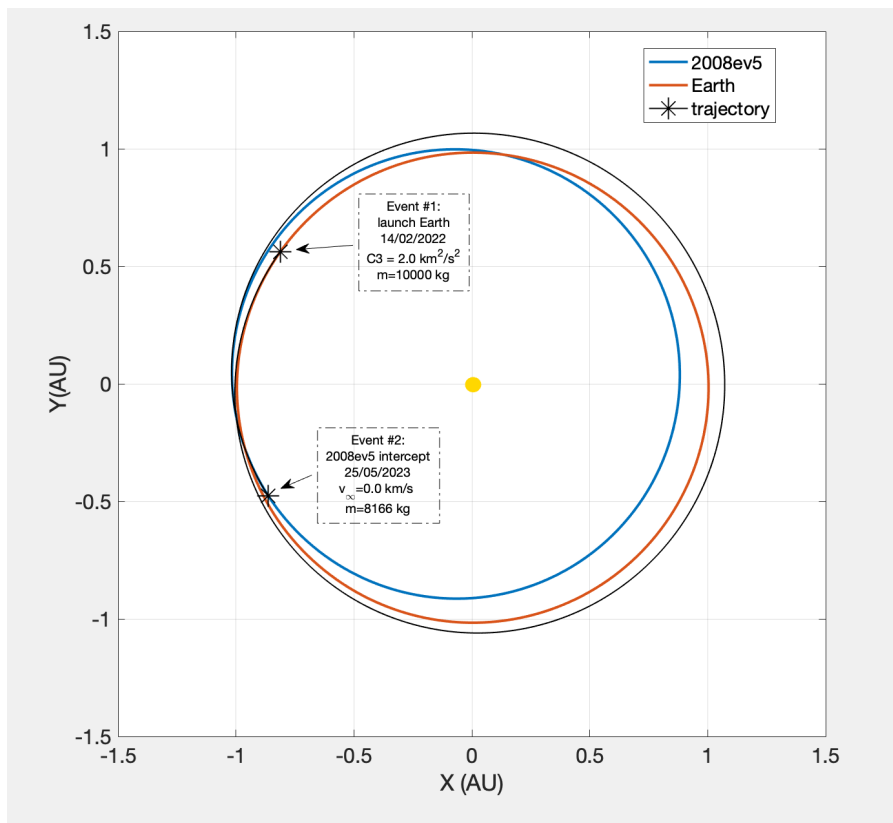


Figure 9.6: 2D Trajectory

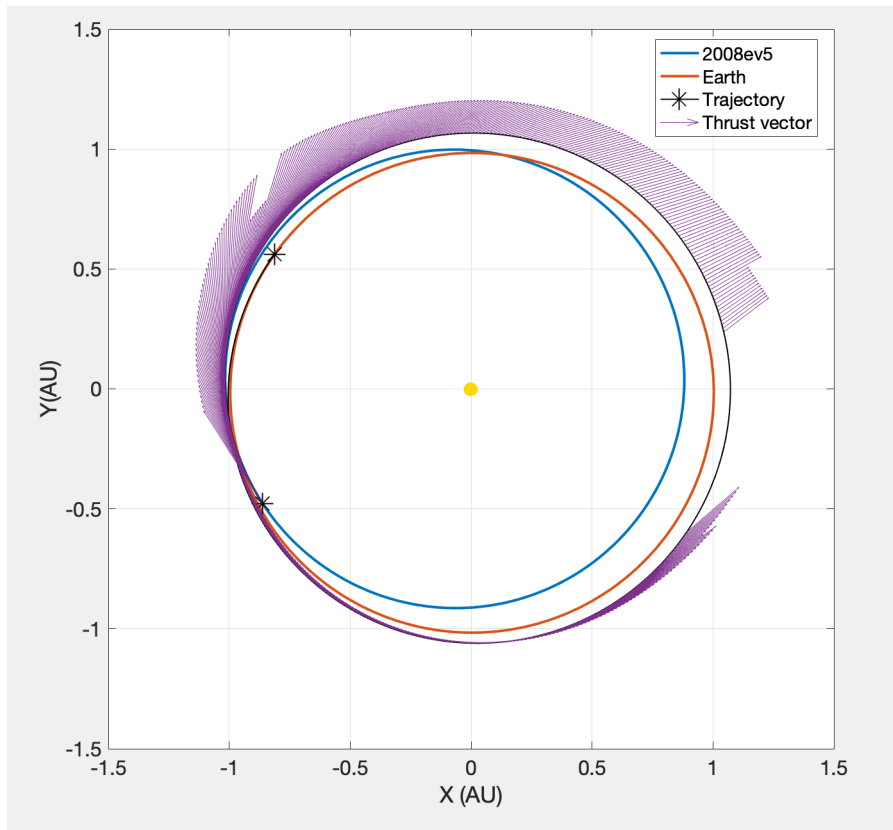


Figure 9.7: Thrust vectors along trajectory

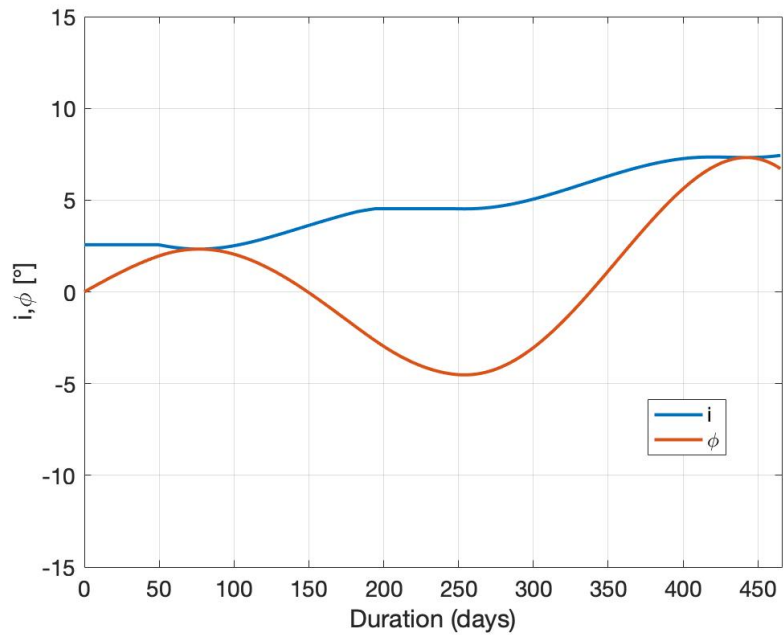


Figure 9.8: How inclination of the trajectory and angle  $\phi$  vary during the mission for *optimal case*

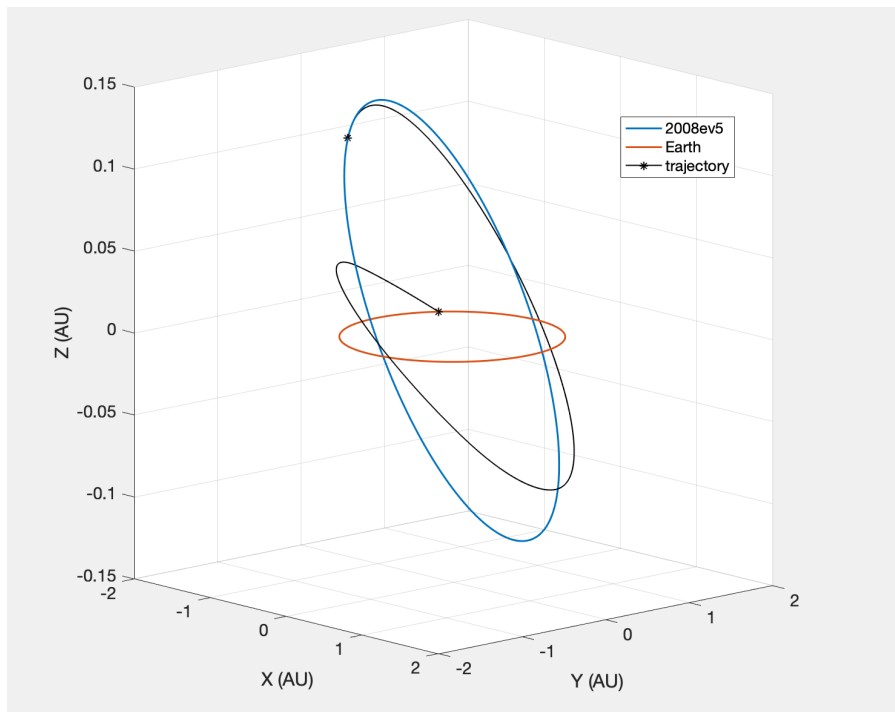


Figure 9.9: 3D Trajectory

### 9.1.2 Inbound Flight

In Figure (9.10) is shown how the number of active thrusters varies during the mission for the four cases.

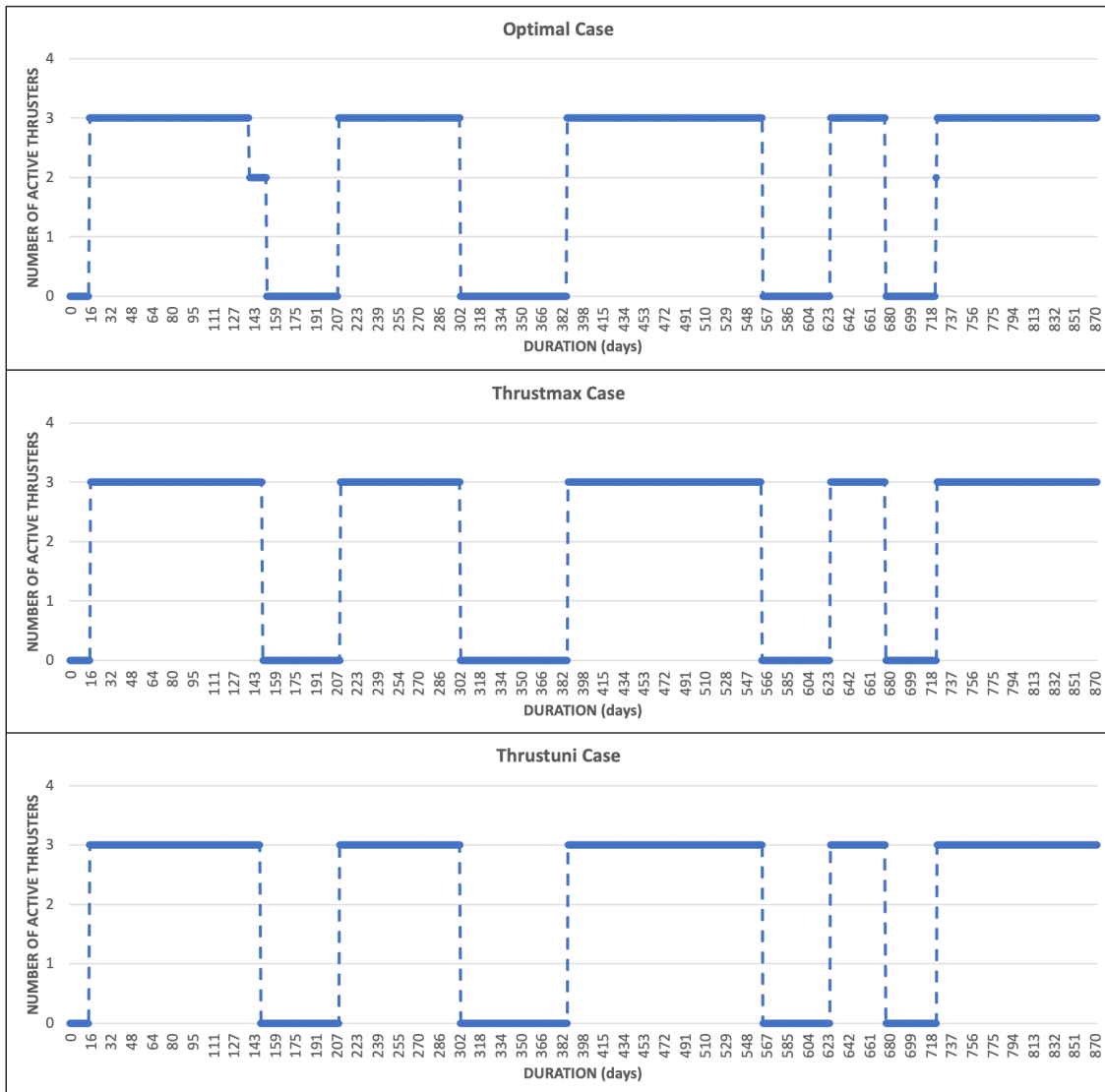


Figure 9.10: Number of active thrusters during the mission

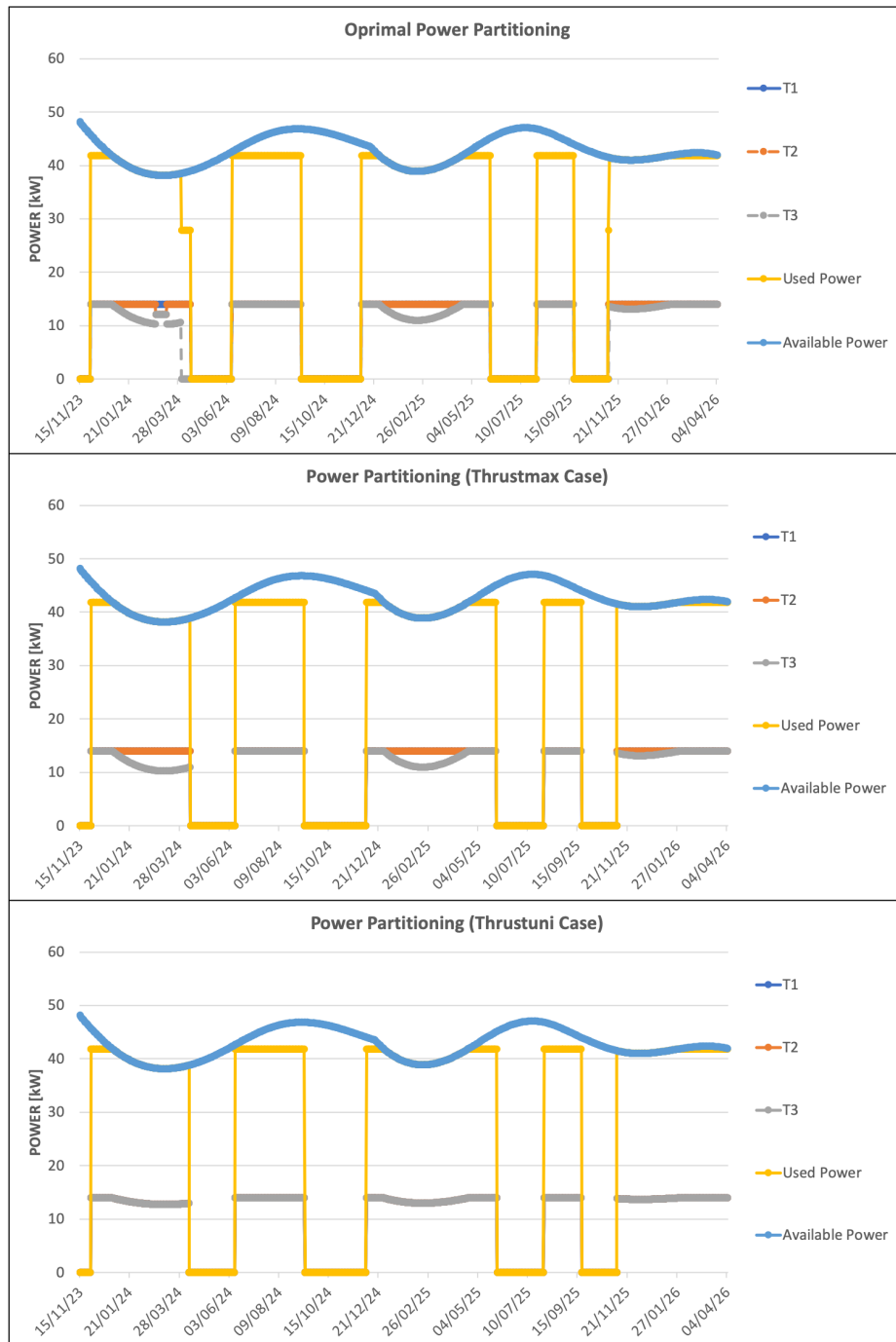


Figure 9.11: Power partitioning between thrusters

The duration is longer for the inbound flight as an arrival speed of  $v_{\infty} = 0.7km/s$  has been chosen.

As can be seen from the trend of the available power, it varies between a maximum of 47

kW and a minimum of 38 kW. This trend has two maximums and two minimums, which means that spacecraft moves twice near the perihelion and twice near the aphelion. So, as for the outbound flight, there are always the conditions to have all three thrusters on. As can be seen from figure (9.11), only in an arc of the optimal case, in the initial mission segment, is not all the available power used. In fact, from figure (9.14) it is evident that in that arc it is not convenient to have high thrust values as there is a higher specific impulse. So it is preferable to have a medium thrust level, turning off the T3, to consume less.

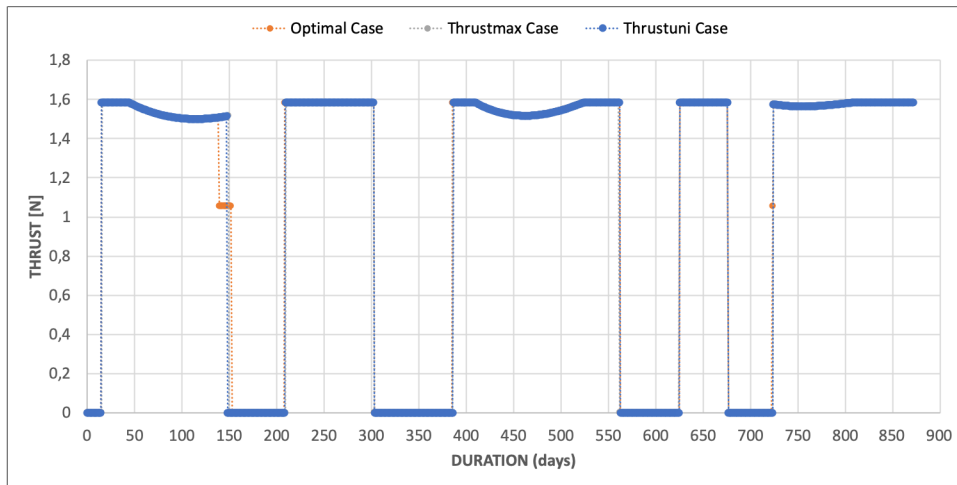


Figure 9.12: Comparison of the thrust for the different cases

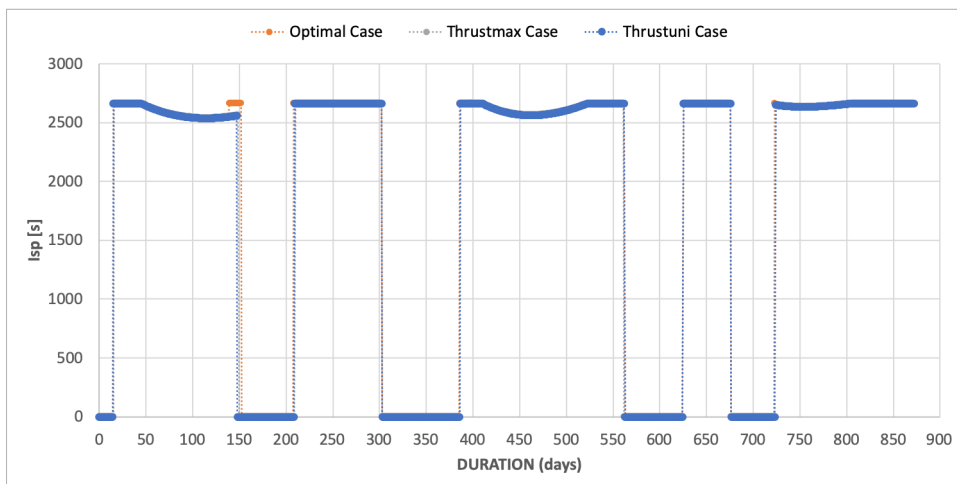


Figure 9.13: Comparison of the specific impulse for the different cases

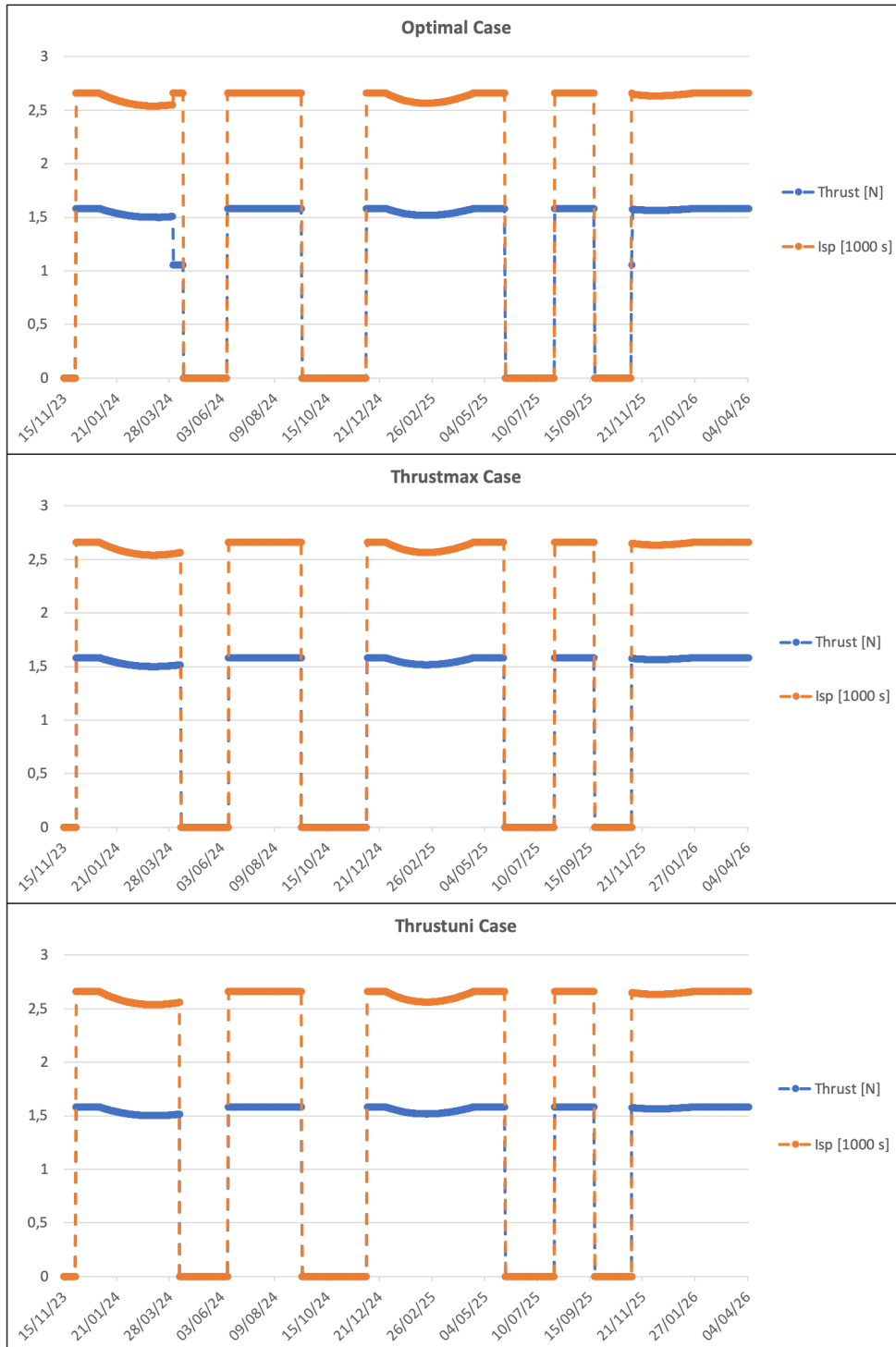


Figure 9.14: Comparison between the thrust and the specific impulse during the mission for the different cases

Below are the results for the three cases, as regards the masses:

Strategy	$m_1[kg]$	$m_2[kg]$	$m_f[kg]$	$m_{boulder}[kg]$
optimal	8166	19730	16564	11564
thrustmax	8153	19668	16515	11515
thrustuni	8161	19703	16542	11542

Table 9.2: Results of indirect optimization

With the optimal distribution of power it is possible to transfer the heaviest boulder. Unlike the asteroid Eros, the masses are much higher as the asteroid is much closer, always considering the hypothesis that upon arrival all 5000 kg of propellant were consumed. With the power partitioning according to the "thrustmax" case, it is possible to transport a boulder that is 0.4% lighter, while with the "thrustuni" case, it is possible to transport a boulder that is 0.2% lighter. Since the asteroid 2008EV5 is much closer, it is easy to understand how the type of power partitioning has little influence on the optimization of the final mass.

The inbound trajectory is shown in Figure (9.15):

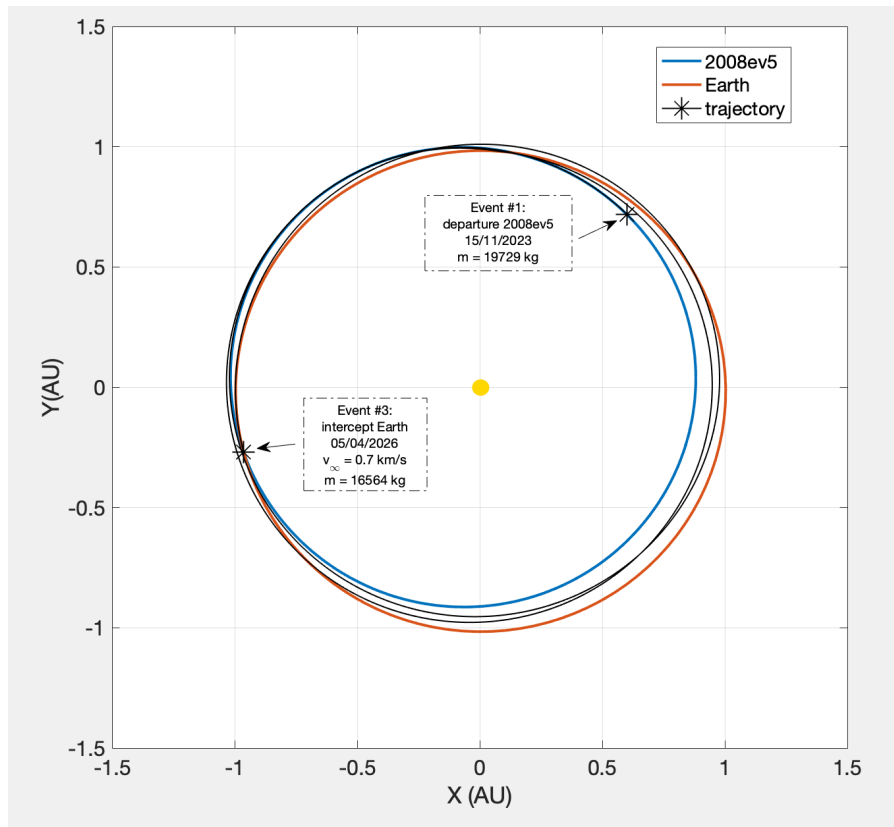


Figure 9.15: 2D Trajectory

The spacecraft leaves asteroid in November 2023 with an initial mass about 19700 kg and intercept Earth in April 2026 with a final mass about 16500 kg. Even in this case, departure and arrival epochs are marked with an asterisk on the respective orbit.

In the graph of  $\phi$  and inclination of the trajectory is possible to see how almost all the inclination variation is due to the Earth fly-by. This is also clearly visible in the 3D vision of the trajectory, where again the Z scale is enlarged. These graphs are shown in Figure (9.16) and (9.17).

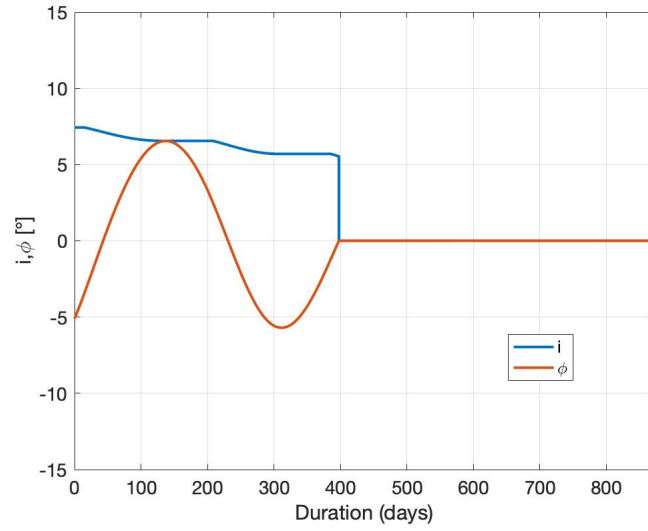


Figure 9.16: How inclination of the trajectory and angle  $\phi$  vary during the mission for *optimal case*

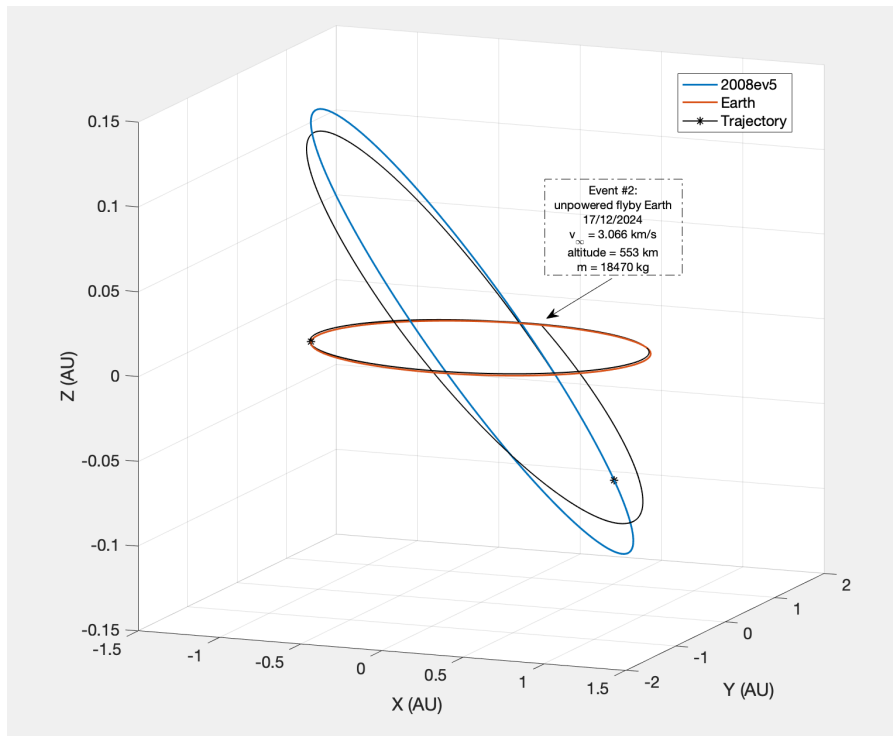


Figure 9.17: 3D Trajectory

# Chapter 10

## Conclusions

The cancelled NASA's Asteroid Redirect Mission has been selected for a validation analysis of the opportune trajectories for a sample-return mission. Main purpose of the mission was to transfer a boulder from the surface of a NEA to a stable lunar orbit, where it could be further analyzed by other missions. For this analysis the NEA (433) Eros has been selected. In order to quantify the mass of the transportable boulder inside the Earth's influence sphere an optimization process of the trajectory has been carried out studying separately the outbound and inbound flight, considering an Earth gravity assist in the inbound leg. Commonly adopted approximations have been used.

Methods to split the available power among electric thrusters have been presented. An indirect method is used to the optimization of the trajectory and for point-by-point selection of the optimal partitioning, providing the maximum benefit. From the comparison between the asteroid Eros and the asteroid 2008EV5, it has been seen how, increasing the eccentricity and the distance from the Sun, greater is the need of an optimal power partitioning between the thrusters. Results shows that an optimal power partitioning strategy, respect to other power partitioning strategies simpler, provides relevant savings in terms of propellant consumption.

Given the great influence that the consumption of propellant has on the costs of an orbital transfer, this method allows to carry out the orbital transfer by maximizing the mass at the end of the maneuver, or minimum the consumption of propellant.

For long-term missions, electric propulsion, used in the post-launch phase, is preferred. This, even if it provides a small thrust for long times, favors a large specific impulse and a reduction in costs.

The amounts of propellant for orbit control around the asteroid and for ascending and descending manoeuvres are not considered as well. All these propellant contributions may vary critically the mass of boulder that the spacecraft can transport towards Earth, so, for this reason, a new and more accurate analysis of the mission could be necessary.

# Appendix A

## Spherical Coordinate System

The vector form of the equations of motion must be explicit, projecting the equations into a suitable reference. An inertial reference is chosen as it is more convenient due to the absence of drag and Coriolis accelerations (which would complicate the Jacobian evaluation of the system required for the BVP solution) and above all for the correspondence between the variables added to the speed components in the inertial system and the component of the primer vector. We therefore adopt spherical coordinates in a inertial reference system based on the equatorial plane: the position of the vehicle is described by the radius  $r$ , by the longitude  $\theta$  and by the latitude  $\phi$ , while the speed by the radial components (i.e. toward the Zenith)  $u$ , in the East  $v$  and North  $w$  direction, in a local reference.

As for speed, it was preferred to project the differential equation in this reference, and not in one with an axis parallel to the speed itself, to have a simpler relationship between relative and absolute speed.

By projecting the equations of state into chosen reference we have:

$$\frac{dr}{dt} = u \quad (\text{A.1})$$

$$\frac{d\theta}{dt} = \frac{v}{r \cos \phi} \quad (\text{A.2})$$

$$\frac{d\phi}{dt} = \frac{w}{r} \quad (\text{A.3})$$

$$\frac{du}{dt} = -\frac{1}{r^2} + \frac{v^2}{r} + \frac{w^2}{r} + \frac{T}{m} \sin \gamma_T + \frac{qS}{m} \left[ -C_D \sin \gamma + C_L \cos \sigma \cos \gamma \right] \quad (\text{A.4})$$

$$\begin{aligned} \frac{dv}{dt} = & -\frac{uv}{r} + \frac{vw}{r} \tan \phi + \frac{T}{m} \cos \gamma_T \cos \psi_T + \frac{qS}{m} \left[ -C_D \cos \gamma \cos \psi + \right. \\ & \left. + C_L \left( -\cos \sigma \sin \gamma \cos \psi + \sin \sigma \sin \psi \right) \right] \end{aligned} \quad (\text{A.5})$$

$$\begin{aligned} \frac{dw}{dt} = & -\frac{uw}{r} - \frac{v^2}{r} \tan \phi + \frac{T}{m} \cos \gamma_T \sin \psi_T + \frac{qS}{m} \left[ -C_D \cos \gamma \sin \psi + \right. \\ & \left. + C_L \left( -\cos \sigma \sin \gamma \sin \psi - \sin \sigma \cos \psi \right) \right] \end{aligned} \quad (\text{A.6})$$

$$\frac{dm}{dt} = -\frac{T}{c} \quad (\text{A.7})$$

where  $\gamma$  e  $\psi$  are the elevation angle (*flight path angle*) and heading angle (measured respectively from the horizontal plane, with positive angles upwards, and counterclockwise from the parallel, with positive angles to the north) of the relative speed  $\mathbf{V}_r$ , while  $\gamma_T$  and  $\psi_T$  are the same angles fo the thrust  $\mathbf{T}$ ;  $\sigma$  is the roll angle, or *bank angle*, i.e. the angle which the aerodynamic lift is rotated with respect to the plane of the trajectory (i.e. the plane determined by the vectors  $\mathbf{r}$  and  $\mathbf{V}_r$ ), measured clockwise around the relative speed, starting from the radial direction.

The angle  $\sigma$  breaks down the lift into a component in the plane of the trajectory ( $L \cos \sigma$ ), which controls the flight altitude, and a normal component to the plane ( $L \sin \sigma$ ) which rotates the speed vector and therefore varies the inclination of the orbit. For direct orbits ( $\cos \psi > 0$ ), positive values of  $\sin \sigma$  give a negative contribution to the derivate of  $w$  and therefore lead to an increase in inclination if the flight proceeds from North to South.

$\gamma$  and  $\psi$  angles depend only on state variables:

$$\sin \gamma = \frac{u}{V_r} \quad (\text{A.8})$$

$$\cos \gamma \cos \psi = \frac{v - \omega r \cos \phi}{V_r} \quad (\text{A.9})$$

$$\cos \gamma \sin \psi = \frac{w}{V_r} \quad (\text{A.10})$$

where the relative speed module is equal to:

$$V_r = \sqrt{u^2 + (v - \omega r \cos \phi)^2 + w^2} \quad (\text{A.11})$$

The angles  $\gamma_T$  and  $\psi_T$  are the controls that determine the direction of the thrust, while the angle  $\sigma$  determines that of the lift. By expressing the expression of the Hamiltonian and canceling the partial derivatives with respect to the angles  $\gamma_T$  and  $\psi_T$ , the optimal values for the thrust angles are obtained:

$$\sin \gamma_T = \frac{\lambda_u}{\lambda_V} \quad (\text{A.12})$$

$$\cos \gamma_T \cos \psi_T = \frac{\lambda_v}{\lambda_V} \quad (\text{A.13})$$

$$\cos \gamma_T \sin \psi_T = \frac{\lambda_w}{\lambda_V} \quad (\text{A.14})$$

where:

$$\lambda_V = \sqrt{\lambda_u^2 + \lambda_v^2 + \lambda_w^2} \quad (\text{A.15})$$

is the modulus of the primer vector which is, as anticipated, parallel to the optimal thrust direction.

Similarly, by deriving the Hamiltonian from the angle  $\sigma$ , the optimal value for the roll angle is obtained:

$$\cos \sigma = \frac{\lambda_u \cos \gamma - \lambda_v \sin \gamma \cos \psi - \lambda_w \sin \gamma \sin \psi}{\lambda_V \sin \delta} \quad (\text{A.16})$$

$$\sin \sigma = \frac{\lambda_v \sin \psi - \lambda_w \cos \psi}{\lambda_V \sin \delta} \quad (\text{A.17})$$

which determines the direction of lift.

The differential equations for the added variables are provided by the Euler-Lagrange equations:

$$\frac{d\boldsymbol{\lambda}}{dt} = - \left( \frac{\partial H}{\partial \boldsymbol{x}} \right)^T \quad (\text{A.18})$$

We obtain:

$$\begin{aligned} \dot{\lambda}_r = & \frac{1}{r^2} \left[ \lambda_\theta \frac{v}{\cos \phi} + \lambda_\phi w + \lambda_u \left( -\frac{2}{r} + v^2 + w^2 \right) + \right. \\ & \left. + \lambda_v (-uv + vw \tan \phi) + \lambda_w (-uw - v^2 \tan \phi) \right] + \frac{2qS}{mV_r} \lambda_V \omega \cos \phi \\ & \left[ V_E (-C_D \cos \delta + C_L \sin \delta) + L_E (-C_D \sin \delta - C_L \cos \delta) \right] + \\ & - \frac{qS}{m} \lambda_V \frac{\partial \rho}{\partial r} \frac{1}{\rho} (-C_D \cos \delta + C_L \sin \delta) \end{aligned} \quad (\text{A.19})$$

$$\dot{\lambda}_\theta = 0 \quad (\text{A.20})$$

$$\begin{aligned} \dot{\lambda}_\phi = & \frac{1}{r \cos^2 \phi} (-\lambda_\theta v \sin \phi - \lambda_v v w + \lambda_w v^2) + \frac{2qS}{mV_r} \lambda_V \omega r \sin \phi \\ & \left[ V_E (-C_D \cos \delta + C_L \sin \delta) + L_E (-C_D \sin \delta - C_L \cos \delta) \right] \end{aligned} \quad (\text{A.21})$$

$$\begin{aligned} \dot{\lambda}_u = & \frac{1}{r} (-\lambda_r r + \lambda_v v + \lambda_w w) - \frac{2qS}{mV_r} \lambda_V \\ & \left[ V_Z (-C_D \cos \delta + C_L \sin \delta) + L_Z (-C_D \sin \delta - C_L \cos \delta) \right] \end{aligned} \quad (\text{A.22})$$

$$\begin{aligned} \dot{\lambda}_v = & \frac{1}{r} \left[ -\lambda_\theta \frac{1}{\cos \phi} - 2\lambda_u v + \lambda_v (u - w \tan \phi) + 2\lambda_w v \tan \phi \right] - \frac{2qS}{mV_r} \lambda_V \\ & \left[ V_E (-C_D \cos \delta + C_L \sin \delta) + L_E (-C_D \sin \delta - C_L \cos \delta) \right] \end{aligned} \quad (\text{A.23})$$

$$\begin{aligned} \dot{\lambda}_w = & \frac{1}{r} (-\lambda_\phi - 2\lambda_u w - \lambda_v v \tan \phi + \lambda_w u) - \frac{2qS}{mV_r} \lambda_V \\ & \left[ V_N (-C_D \cos \delta + C_L \sin \delta) + L_N (-C_D \sin \delta - C_L \cos \delta) \right] \end{aligned} \quad (\text{A.24})$$

$$\dot{\lambda}_m = \frac{T}{m^2} \lambda_V + \frac{qS}{m^2} \lambda_V (-C_D \cos \delta + C_L \sin \delta) \quad (\text{A.25})$$

where  $\delta$  is the angle between the primer and the relative speed, and have been introduced, in a local reference Zenith East North, the components of the versors parallel to the relative speed:

$$V_Z = u/V_r = \sin \gamma \quad (\text{A.26})$$

$$V_E = (v - \omega r \cos \phi)/V_r = \cos \gamma \cos \psi \quad (\text{A.27})$$

$$V_N = w/V_r = \cos \gamma \sin \psi \quad (\text{A.28})$$

and parallel to the lift:

$$L_Z = \frac{\lambda_u(1 - \sin^2 \gamma) - \lambda_v \sin \gamma \cos \gamma \cos \psi - \lambda_w \sin \gamma \cos \gamma \sin \psi}{\lambda_V \sin \delta} \quad (\text{A.29})$$

$$L_E = \frac{-\lambda_u \sin \gamma \cos \gamma \cos \psi + \lambda_v(1 - \cos^2 \gamma \cos^2 \psi) - \lambda_w \cos^2 \gamma \sin \psi \cos \psi}{\lambda_V \sin \delta} \quad (\text{A.30})$$

$$L_N = \frac{-\lambda_u \sin \gamma \cos \gamma \sin \psi - \lambda_v \cos^2 \gamma \sin \psi \cos \psi + \lambda_w(1 - \cos^2 \gamma \sin^2 \psi)}{\lambda_V \sin \delta} \quad (\text{A.31})$$

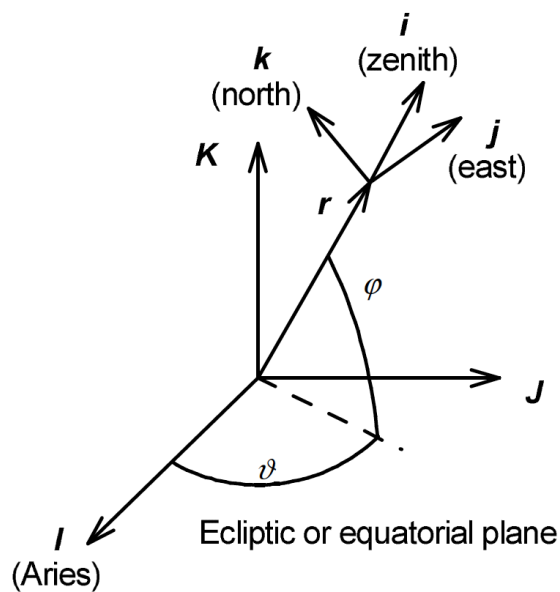


Figure A.1: Spherical coordinates

## Appendix B

# The Patched-Conic Approximation

An interplanetary spacecraft spends most of its flight time moving under the gravitational influence of the Sun. Only for brief periods, compared with the total mission duration, is its path shaped by the gravitational field of the departure or arrival planet. The perturbations caused by the other planets while the spacecraft is pursuing its heliocentric course are negligible.

Just as in lunar trajectories, the computation of a precision orbit is a trial-and-error procedure involving numerical integration of the complete equations of motion where all perturbation effects are considered. For preliminary mission analysis and feasibility studies it is sufficient to have an approximate analytical method for determining the total  $\Delta V$  required to accomplish an interplanetary mission. The best method available for such an analysis is called the *patched-conic approximation*.

The patched-conic method permits us to ignore the gravitational influence of the Sun until the spacecraft is a great distance from the Earth (perhaps a million kilometers).

# Appendix C

## Vector and Matrix Calculation

The notation chosen indicates a column vector with a bold font:

$$\mathbf{a} = \begin{pmatrix} a_1 \\ a_2 \\ \vdots \\ a_n \end{pmatrix} \quad (\text{C.1})$$

A row vector is therefore indicated as  $\mathbf{a}^T$ , where the symbol  $^T$  indicates the transposed matrix. In this way, referring to the matrix calculation, the scalar product between two vectors  $\mathbf{a} \cdot \mathbf{b}$  is written indifferently as:

$$\mathbf{a} \cdot \mathbf{b} = \mathbf{a}^T \mathbf{b} = \mathbf{b}^T \mathbf{a} \quad (\text{C.2})$$

The derivation of a column vector with respect to a scalar quantity (for example the time  $t$ ) originates a new column vector whose components are the derivatives of the single components of the original vector:

$$\frac{d\mathbf{a}}{dt} = \begin{pmatrix} da_1/dt \\ da_2/dt \\ \vdots \\ da_n/dt \end{pmatrix} \quad (\text{C.3})$$

On the contrary, the derivation of a scalar quantity (for example the performance index  $\varphi$ ) with respect to a column vector  $\mathbf{a}$  gives rise to a *row* vector whose components are the derivatives of  $\varphi$  with respect to the components of the original vector:

$$\frac{d\varphi}{d\mathbf{a}} = \left( \frac{d\varphi}{da_1}, \frac{d\varphi}{da_2}, \dots, \frac{d\varphi}{da_n} \right) \quad (\text{C.4})$$

Finally, in similarity to what was seen above, the derivation of a vector  $\mathbf{a}$  ( $n$  components) with respect to a second vector  $\mathbf{b}$  ( $m$  components) creates a matrix, indicated by square

brackets, with  $n$  rows and  $m$  columns: each column is in fact given by derivatives of the components of  $\mathbf{a}$  with respect to a single component of  $\mathbf{b}$  (treating the latter as a scalar quantity, this case is analogous to the derivation of a vector with respect to a scalar), while each row is given by the derivatives of a single component of  $\mathbf{a}$  (seen as scalar, in analogy to the derivation of a scalar with respect to a vector) with respect to the components of  $\mathbf{b}$ :

$$\left[ \frac{d\mathbf{a}}{d\mathbf{b}} \right] = \begin{bmatrix} da_1/db_1 & \dots & da_1/db_m \\ \vdots & \ddots & \vdots \\ da_n/db_1 & \dots & da_n/db_m \end{bmatrix} \quad (\text{C.5})$$

It should be emphasized that the subscripts used in this Appendix (which identify the vector component) should not be confused with those used in the rest of the work (where they generally indicate the point at which the vector is to be calculated).

# Bibliography

- [1] L. Casalino and M.Vavrina, *Optimal Power Partitioning for Electric Thrusters*, paper AAS 17-749.
- [2] Roger R. Bate, Donald D. Mueller, Jerry E. White, *Fundamentals of Astrodynamics*.
- [3] JPL Small-Body Database Browser, 27 April 2019 (last observation).
- [4] A. E. Bryson and Y.-C. Ho, *Applied Optimal Control*. New York, NY: Hemisphere, 1975. Revised printing.
- [5] N. Marmo, "Optimization of low-thrust Trajectory for a mission to the asteroid 433 Eros with Earth gravity assist", *Aerotecnica, The Journal of Aerospace Science, Technology and Systems*, Vol. 97, No. 3, pp. 163-174, July-September 2018
- [6] <https://en.wikipedia.org/wiki/Solar-electric-propulsion>
- [7] <https://www1.grc.nasa.gov/space/sep/>
- [8] <https://www.nasa.gov/offices/oct/home/feature-sas.html>
- [9] <https://en.wikipedia.org/wiki/433-Eros>
- [10] [https://en.wikipedia.org/wiki/\(341843\)-2008-EV5](https://en.wikipedia.org/wiki/(341843)-2008-EV5)